WL-TR-97-3105

DEVELOPMENT OF STRUCTURAL INTEGRITY ANALYSIS TECHNOLOGIES FOR AGING AIRCRAFT STRUCTURES:

BONDED COMPOSITE PATCH REPAIR & WEIGHT FUNCTION METHODS

K.L. Boyd, S. Krishnan, A. Litvinov, J. H. Elsner
Analytical Services & Materials, Inc.
107 Research Drive
Hampton, Virginia

Dr. M.M. Ratwani
R-Tec
4 Latigo Lane
Rolling Hills Estates, CA

Mr. James A. Harter
WL/FIBEC, BLDG 65
2790 St. Room 504
Wright–Patterson AFB, OH

Dr. Grzegorz Glinka
SaFDD, Inc.
RR #2, Petersburg
Ontario, Canada

Final Report for Period November 1995 – July 1996

July 1997

FLIGHT DYNAMICS DIRECTORATE
WRIGHT LABORATORY
AIR FORCE MATERIEL COMMAND
WRIGHT-PATTERSON AFB, OHIO 45433-7562
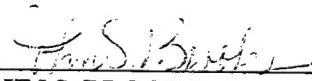
DTIC QUALITY INSPECTED 4

19980311 167

NOTICE

USING GOVERNMENT DRAWINGS, SPECIFICATIONS, OR OTHER DATA INCLUDED IN THIS DOCUMENT FOR ANY PURPOSE OTHER THAN GOVERNMENT PROCUREMENT DOES NOT IN ANY WAY OBLIGATE THE US GOVERENMENT. THE FACT THAT THE GOVERNMENT FORMULATED OR SUPPLIED THE DRAWINGS, SPECIFICATIONS, OR THER DATA DOES NOT LICENSE THE HOLDER OR ANY OTHER PERSON OR CORPORATION; OR CONVEY ANY RIGHTS OR PERMISSION TO MANUFACTURE, USE, OR SELL ANY PATENTED INVENTION THAT MAY RELATE TO THEM.

THIS REPORT IS RELEASABLE TO THE NATIONAL TECHNICAL INFORMATION SERVICE (NTIS). AT NTIS, IT WILL BE AVAILABLE TO THE GENERAL PUBLIC, INCLUDING FOREIGN NATIONS.
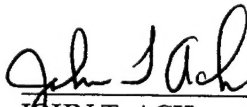
THIS TECHNICAL REPORT HAS BEEN REVIEWED AND IS APPROVED FOR PUBLICATION.

JOHN S. BROOKS
TEAM LEADER
STRUCTURAL INTEGRITY BRANCH

JAMES A. HARTER
AEROSPACE ENGINEER
STRUCTURAL INTEGRITY BRANCH

JOHN T. ACH
BRANCH CHIEF
STRUCTURAL INTEGRITY BRANCH

IF YOUR ADDRESS HAS CHANGED, IF YOU WISH TO BE REMOVED FROM OUR MAILING LIST, OR IF THE ADDRESSEE IS NO LONGER EMPLOYED BY YOUR ORGANIZATION, PLEASE NOTIFY WL/FIBE, BLDG 65, 2790 D ST., ROOM 504, WRIGHT-PATTERSON AFB OH 45433-7402 TO HELP MAINTAIN A CURRENT MAILING LIST.

Do not return copies of this report unless contractual obligations or notice on a specific document requires its return.

REPORT DOCUMENTATION PAGE

Public reporting burden for this collection of information is estimated to average 1 hour per response, including the time for reviewing instructions, searching existing data sources, gathering and maintaining the data needed, and completing and reviewing the collection of information. Send comments regarding this burden estimate or any other aspect of this collection of information, including suggestions for reducing this burden, to Washington Headquarters Services, Directorate for Information Operations and Reports, 1215 Jefferson Davis Highway, Suite 1204, Arlington, VA 22202-4302, and to the Office of Management and Budget, Paperwork Reduction Project (0704-0188), Washington, DC 20503.

1. AGENCY USE ONLY *(Leave blank)*	2. REPORT DATE	3. REPORT TYPE AND DATES COVERED
	July 1997	FINAL, Nov 95 - July 96

4. TITLE AND SUBTITLE

Development of Structural Integrity Analysis Technologies for Aging Aircraft Structures: Bonded Composite Patch Repair and Weight Function Methods

5. FUNDING NUMBERS

C - F33615-94-D-3212
PE - 62201
PR - 2401
TA - 01
WU-01

6. AUTHOR(S)

K.L. Boyd, S. Krishnan, A. Litvinov, & J.H. Elsner - Analytical Services & Materials, Inc
J. A. Harter - WL/FIBE; M.M. Ratwani - R-Tee; G. Glinka - SaFDD, Inc.

7. PERFORMING ORGANIZATION NAME(S) AND ADDRESS(ES)

ANALYTICAL SERVICES AND MATERIALS, INC.
107 RESEARCH DRIVE
HAMPTON VA 23666

FLIGHT DYNAMICS DIRECTORATE
WRIGHT LABORATORY
AIR FORCE MATERIEL COMMAND
WPAFB, OH 45433-7402

8. PERFORMING ORGANIZATION REPORT NUMBER

9. SPONSORING/MONITORING AGENCY NAME(S) AND ADDRESS(ES)

FLIGHT DYNAMICS DIRECTORATE
WRIGHT LABORATORY
AIR FORCE MATERIEL COMMAND
WRIGHT-PATTERSON AFB OH 45433-7562
POC: JOHN BROOKS, WL/FIBE, 937-255-6104 X 233

10. SPONSORING/MONITORING AGENCY REPORT NUMBER

WL-TR-97-3105

11. SUPPLEMENTARY NOTES

12a. DISTRIBUTION AVAILABILITY STATEMENT

APPROVED FOR PUBLIC RELEASE;
DISTRIBUTION UNLIMITED

12b. DISTRIBUTION CODE

13. ABSTRACT *(Maximum 200 words)*

The purpose of this research was to develop advanced structural integrity analysis methods for aging aircraft structures. The primary focus of this study was to develop a method for performing fatigue crack growth analyses under a composite (repair patch) on a metallic structure. Also, it was envisioned that these methods would be incorporated into the fatigue crack growth software, AFGROW, so that this promising technology can be transitioned to U.S. Air Force Logistic Centers, U.S. Air Force contractors and other government agencies as quickly as possible.

Fatigue cracks growing from fastener holes, or multiple fastener holes, also are common problems found in aging aircraft. To address these problems, analytical methods (weight functions) were developed to assist engineers in the analysis of fatigue cracks growing in arbitrary stress fields, commonly found around cold-worked fastener holes and stop-drilled cracks. Furthermore, an approach to evaluate multiple cracking, or multiple-site damage (MSD), was developed as a future enhancement to the AFGROW program.

14. SUBJECT TERMS

AFGROW, fatigue cracks, aging aircraft, repair, adhesive bonding, metallic aircraft structure, crack growth, composite repair patch, multiple site damage, MSD, damage tolerance

15. NUMBER OF PAGES

163

16. PRICE CODE

17. SECURITY CLASSIFICATION OF REPORT	18. SECURITY CLASSIFICATION OF THIS PAGE	19. SECURITY CLASSIFICATION OF ABSTRACT	20. LIMITATION OF ABSTRACT
UNCLASSIFIED	UNCLASSIFIED	UNCLASSIFIED	UL

TABLE OF CONTENTS

LIST OF FIGURES

FOREWORD

This report was prepared by Analytical Services & Materials, Inc., Hampton Virginia for WL/FIBEC, Wright-Patterson Air Force Base, Ohio under contract F33615-94-D-3212, "Structural Integrity Analysis and Verification for Aircraft Structures." The U.S. Air Force project engineer was Mr. James A. Harter, WL/FIBEC. The government contract manager was Lt. Davis S. Conley. The period of performance for this report was November 1995 through July 1996.

The work performed under report (Delivery Order 0006) was performed by Analytical Services & Materials, Inc. personnel located at the WL/FIBE Fatigue & Fracture Test Facility, Bldg. 65, Area B, Wright-Patterson AFB, OH and their subcontractors. The Principal Investigator of this research was Mr. Kevin L. Boyd. The authors of this report were Mr. Kevin L. Boyd, Mr. Srinivas Krishnan, Mr. Alex Litvinov, Dr. Mohan Ratwani (R-Tec; Sections 2.0 & 3.0) and Dr. Gregory Glinka (SaFFD; Sections 4.0, 5.0 and Appendix A). Additional technical input and assistance was provided by Mr. James A. Harter.

1. INTRODUCTION

This purpose of this research was to develop advanced structural integrity analysis methods for aging aircraft structures. The primary focus of this study was to develop a method for performing fatigue crack growth analyses under a composite (repair patch) on a metallic structure. Also, it was envisioned that these methods would be incorporated into the fatigue crack growth software, AFGROW, so that this promising technology can be transitioned to U.S. Air Force Logistic Centers, U.S. Air Force contractors and other government agencies as quickly as possible.

Fatigue cracks growing from fastener holes, or multiple fastener holes, also are common problems found in aging aircraft. To address these problems, analytical methods (weight functions) were developed to assist engineers in the analysis of fatigue cracks growing in arbitrary stress fields, commonly found around cold-worked fastener holes and stop-drilled cracks. Furthermore, an approach to evaluate multiple cracking, or multiple-site damage (MSD), was developed as a future enhancement to the AFGROW program.

The development of enhanced damage tolerance methods are necessary to accurately determine the inspection intervals and safety of flight of repaired, aging aircraft structures. Current methods used to evaluate the structural integrity of repaired structures include time consuming (and limited) finite element analyses and/or static strength design criteria. While these methods are often adequate for estimating the equivalent stiffness and state of stress of a repaired structure, they do not include load interaction effects, cyclic debonding, or give an adequate estimation of the remaining life (or inspection intervals) of a repaired structure. The primary questions regarding bonded composite repair patches based on comments from ASIP managers at USAF Air Logistics Centers [1] are: (1) is the composite repair viable?; if so, (2) how long can I keep the aircraft flying with this repair?, and (3) how often should I inspect the repair? The statements are not necessarily made to underestimate the importance of finding qualified personnel to perform repairs and trained personnel with proven NDE methods to evaluate the structural integrity of the patch. In most cases, the decision to repair or replace structural components must be made quickly so that the aircraft may be returned to service as soon as possible. This requirement precludes the use of time consuming, detailed finite element analyses or rigorous testing programs.

Presently, engineers at the ALCs do not have integrated analysis tools to assist in the design of repairs and subsequently perform Damage Tolerance Analyses (DTA) to assign inspection intervals to repaired structures [1]. Therefore, it is important that advanced analysis methods be developed and implemented to assess the structural integrity of repairs being performed at various US Air Force Air Logistic Centers (ALCs). It is also important that analysis methods are user friendly, accurate, fast, economical, upgradable, well documented, and be supported by knowledgeable USAF personnel.

This research does not intend to discourage the use of finite element methods, static strength analysis methods or rigorous testing programs to accurately characterize the structural integrity of a patched, repaired structure. What this research wants to emphasize is that composite-patched repaired structures should be analyzed with methods capable of characterizing the dynamic aspects of a crack growing under a composite patch in a repaired structure. The USAF Aircraft Structural Integrity Program (MIL-STD-1530A) calls for aircraft to meet the damage tolerance criteria found in MIL-A-83444 (Airplane Damage Tolerance Requirements). It is the belief of the author that the design of repairs made to aging aircraft should also be evaluated under damage tolerance requirements to whatever extent possible.

With regard to composite repaired structures, the potential of repairing cracked metallic structures with composite patches for cost reduction and improved structural efficiency is becoming evident from the studies of various investigations [2-9]. The in-service application of the repair concept are found in the repair of C-141 weep hole cracks, C-5 fuselage skin, F-16 fuel access hole in lower wing skin and T-38 lower wing skin at 'D' panel. In the majority of cases where damage metallic structures have been repaired with composite patches, conventional mechanically-fastened repairs could not be used due to either non-availability of space to drill holes or detrimental effect of these holes on the structural integrity of the repaired structure. The composite patch repair concept offers an excellent potential to repair structures which cannot be repaired with conventional methods and thereby reduce the operational cost of in-service fleet.

This repair process essentially involves bonding of fiber-reinforced composite material over the cracked metallic material, thereby reducing the stress intensity of the crack. This results in a slowing of crack growth in cracked metal parts or even complete retardation in certain cases [4]. The use of composite patch repair has several advantages over conventional repair, namely:

1. More efficient load transfer from the cracked part to the repair patch, resulting in more reduction in stress intensity factors at crack tips as compared to conventional mechanically fastened repairs.

2. No additional stress concentrations due to drilling of holes for fasteners as in the case of conventional repairs.

3. Good durability under cyclic loading.

4. High directional stiffness of a patch allows use of thin patches.

5. Can be used to repair curved surfaces and complex geometries.

In order to assure the flight safety of structures repaired with composite patches, it is necessary to develop analysis methods to predict the life of repaired structures. Also, the

analysis techniques should be easily used by the engineers involved in designing repairs without causing any delay in aircraft down time.

This report has been broken down into three sections; development of composite repair design criteria, development of damage tolerance methods for repaired structures, and development of weight functions and approach to MSD. The development of composite repair design criteria is described in Section 2 and development of damage tolerance methods for composite patch repaired structures is described in Section 3. The development of weight functions is described in Section 4 and approach to MSD is reported in Section 5.

2. REPAIR DESIGN CONSIDERATIONS

A number of factors need to be considered in designing composite patch repairs for metallic structures. From the point of a structural designer the following factors need to be considered:

1) Repair patch material and thickness
2) Repair patch ply orientation and stacking sequence
3) Patch configuration
4) Adhesive material and thickness
5) Adhesive disbonding
6) Effect of moisture
7) Metallic material thickness
8) Effect of thermal stresses

Consideration should be given to the location of the repair when selecting the patch material, configuration, taper. External aircraft surfaces, particularly in areas critical to aerodynamic smoothness requirements (such as wing leading edges) require coordination with the proper authority for changes to external aerodynamic surfaces. A repair to a substructure will be dictated by the proximity of adjacent structural components. Some of the important factors influencing a composite patch repair will be discussed in the following sections.

2.1. Repair Patch Material & Thickness

A number of composite materials are available for bonded repair applications; however, the most commonly used materials are boron, graphite, and sometimes GLARE. Each of these materials has an application in composite patch repair depending on the metallic material thickness, type of load spectrum, and the stress level in the spectrum. For lightly loaded and thin structures such as in fuselage structures GLARE may be suitable. It has the advantage that it is relatively cheap compared to boron and graphite. Also, from the design point of view GLARE has nearly the same coefficient of expansion of the aluminum base material and produces no residual compressive stresses during the in-service operational environment of the aircraft. This can be an advantage in certain cases. However, for highly loaded structures and structures experiencing severe spectrum loading it is desirable to use materials such as boron or graphite. Both of these materials provide greater stiffness when compared to GLARE. Boron patches are generally thinner than graphite because boron has a modulus which is about 50% higher than that of graphite. However, the cost of Boron is about 20 times that of graphite.

It is desirable to keep patch thickness to a minimum, as thicker patches will result in out-of-plane bending when the repair patch is applied to one side only. The out-of-plane bending causes additional tensile stresses in the metal sheet and increases the stress

intensity factors, thereby reducing the effectiveness of the patch. In most cases, there is an optimum patch thickness which reduces the state of stress at the damage in the metal. Increasing the thickness beyond the optimum can result in significant out-of-plane bending and reduce the effectiveness of the patch.

In Reference 10, guidelines have been provided for repair patch thickness for two sided and one sided repairs shown in Figure 1. In the reference the repair patch thickness t_2 is recommended as follows:

For a two sided repair patch (Figure 1a), thickness t_2 of patch on each side is given by;

$$\left(E_1 t_1 / 2E_y\right) < t_2 < \left(1.2 E_1 t_1 / 2E_y\right)$$

For a one sided repair patch (Figure 1b), thickness t_2 of the patch is given by:

$$\left(E_1 t_1 / E_y\right) < t_2 < \left(1.2 E_1 t_1 / E_y\right)$$

The patch thickness is intended to restore original stiffness over the defect. It is desirable to provide a patch thickness to restore original stiffness of the structure being repaired. However, a stiffness of up to 20% higher than that of base metal is considered acceptable.

Repair Patch Thickness t_2, Modulus in Loading Direction E_y

Crack

Adhesive

Metal Thickness t_1, Modulus E_1
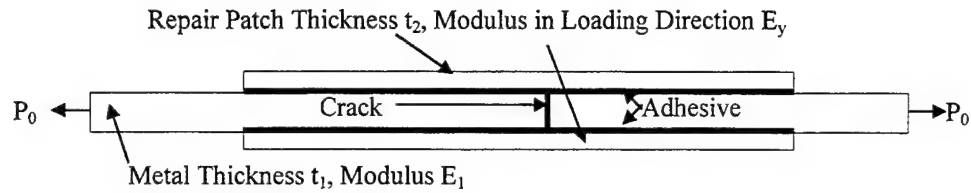
(a) Cracked Metal Sheet with Repair Patch on Both Sides

Repair Patch Thickness t2, Modulus in Loading Direction Ey

Crack

Adhesive

Metal Thickness t_1, Modulus E_1
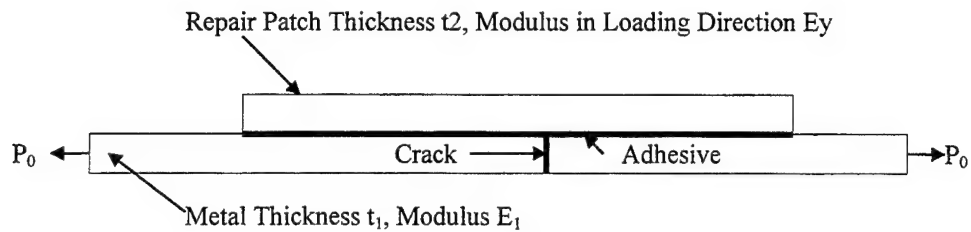
(b) Cracked Metal Sheet with Repair Patch on One Side

Figure 1. Repair Configurations

2.2.   Repair Patch Ply Orientations and Stacking Sequence

It is desirable to use highly orthotropic patches having a high stiffness in the direction normal to the crack, but with some fibers in directions at 45^0 and 90^0 to the primary direction. This configuration has been found to prevent matrix cracking under bi-axial loading and in-plane shear loads which exist for typical applications. A good design practice is to use about 70% 0^0, plies 20% $45^0/-45^0$ plies and 10% 90^0 plies. A typical repair patch is shown in Figure 2. When graphite/epoxy is used as a repair material, a barrier ply of 'S' glass is used between aluminum substrate and graphite patch to prevent galvanic corrosion. A wrap of 181 woven glass is sometimes applied on the patch surface as shown in Figure 2 to provide a smooth ply transition on exterior surface repairs. This has additional advantage that during any in-service damage woven glass is damaged and the repair may still be intact.

6
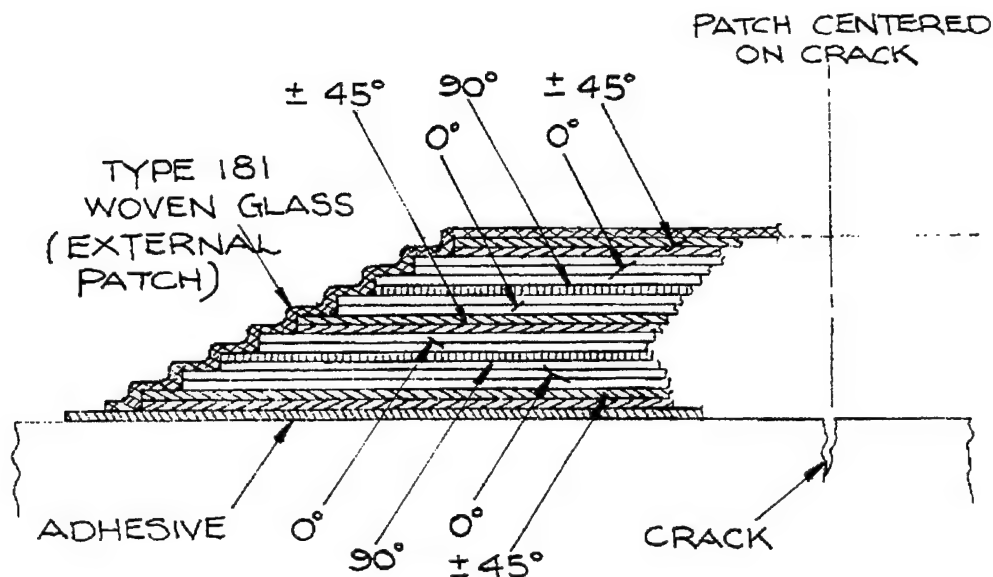
Figure 2. Typical Ply Orientations

The stacking sequence in a repair patch is also an important consideration in repair patch design. It is desirable to put +/-45 degree plies on the outside surface not in contact with damage area and zero degree plies within the patch laminate. This has two advantages; 1) during any in-service impact damage +/-45 degree plies will get damaged and the structural integrity of the patch is not significantly reduced, and 2) the presence of +/- 45 degree plies reduces the inter-laminar stresses at the edges of the patch and thereby reduces the tendency of the patch to delaminate at the edges during in-service cyclic environment. For thin patches, the stacking sequence may not have any significant influence on load transfer to the patch. While this may often be true for thin patches, it may not apply to thick patches, therefore, it is desirable to place 0 degree plies closer to the metal surface for thick repair patches. However, consideration must also be given to maintaining balanced laminate symmetry to avoid warpage in the pre-cure of the patch.

2.3.   Repair Patch Configuration

The repair patch configuration may vary and is primarily dependent on the structure's repair location and loading direction. Composite patch repairs to the external skin are a function of geometry and may take on the appearance of a circular or elliptical shape with circumferentially tapered edges (Figure 3), and are dictated by the aerodynamic smoothness criteria. Where geometry dictates, the prestaging of the patch is recommended.

7
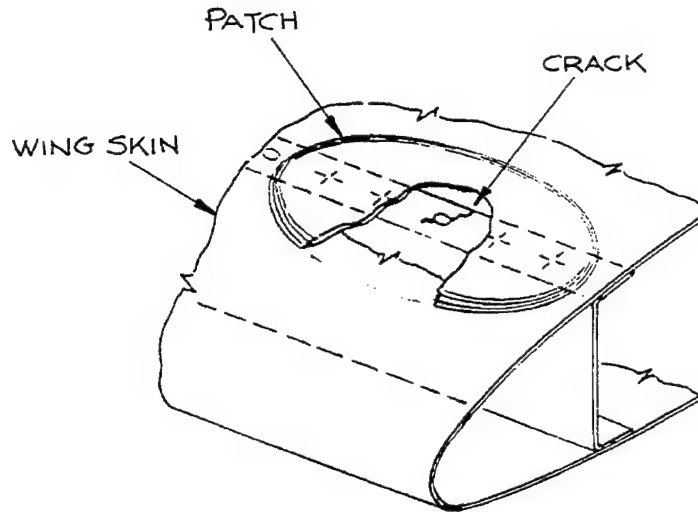
Figure 3. External Skin Repair

Repairs made to substructural components, such as spar caps and rib flanges with cracking at fastener hole locations, may require a staged or precured patch as shown in Figure 4. The ends of the patch are tapered for smooth load introduction and to reduce the peel stresses at the ends.

To efficiently transition the load into the repair patch, plies should be stepped at 0.1 inch for every 0.010 inch thick stacking of plies. This taper rate applies to both boron/epoxy and graphite/epoxy patches.
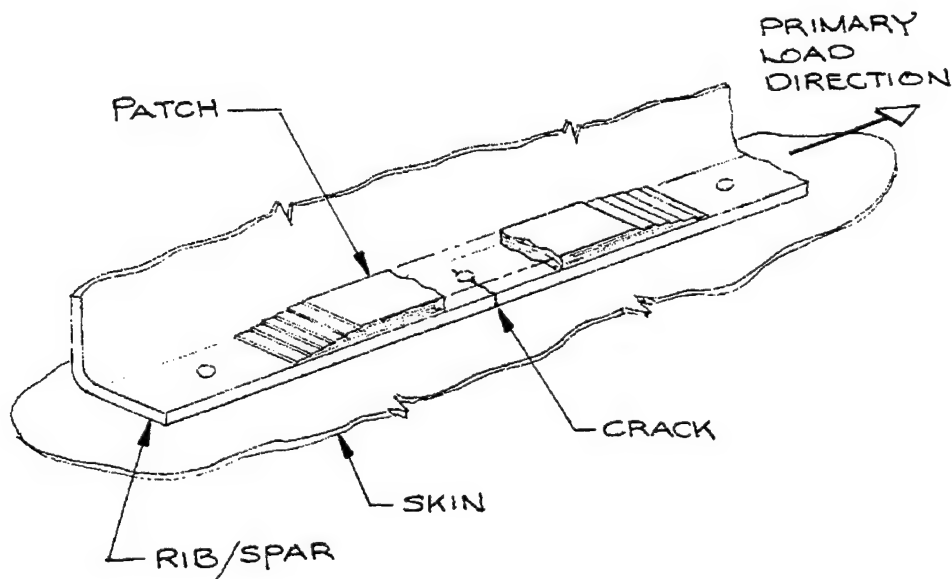
Figure 4. Substructure Repair

2.4. Adhesive Material & Thickness

Room temperature cure adhesives are not considered suitable due to service temperature requirements of 180°F in major aircraft repair applications and long-term durability needed for repairs. Room temperature cure adhesives are paste adhesives and generally do not result in uniform bond line thickness in the repair, thus, affecting the load transfer to composite patch. Hence, high temperature cure adhesives are preferred. A 350°F cure film adhesive is not considered desirable as the curing at such a high temperature is likely to cause undesirably high thermal stresses. Also, an aluminum structure exposed to 350°F temperature will experience a degradation in mechanical properties. A 250°F cure temperature film adhesive is considered suitable for the composite patch repairs of aluminum structure.

Ductile adhesives such as FM-73 are preferred over brittle adhesives such as FM-400 due to the greater tendency of the brittle adhesives to disbond around the damage area during flight loading. This adhesive disbonding reduces the load transfer effectiveness to the patch.

Adhesive thickness should be kept as small as possible so in order to develop full bond strength. A thick adhesive bondline causes less load transfer to the repair patch and increases the stress intensity factors in the cracked metallic structure and crack growth rate. Successful bonds are achieved using one ply of 0.01-inch thick adhesive. First, the adhesive is allowed to thaw to room temperature after removing it from the refrigerator. Next, the adhesive is cut to the size of the patch and installed on the base material bond surface in the prescribed location. Lastly, the appropriate procedure for applying pressure and following the recommended cure cycle must be followed to achieve the desired bond-line thickness. A desirable bond-line thickness ranges from 0.004-inches to 0.007-inches.

2.5. Adhesive Disbonding

Disbonding in the adhesive layer can occur during the fabrication of the repair patch, during the in-service spectrum loading as the damage in the metallic propagates due to fatigue, or due to in-service impact damage. The overall effect of the adhesive disbonding is to reduce the load transfer to the repair patch and reduce the effectiveness of the patch. The disbonding in the adhesive layer due to in-service fatigue loading is generally elliptical in shape for through the thickness cracks and the leading edge of the disbond generally coincides with the leading edge of the crack. The ratio of major to minor axis of the disbond depends on the type of adhesive being used. The effect of disbonding, caused by crack propagation due to in-service loads, should be taken into consideration during the design process. However, if the disbonding occurs due to in-service impact damage or fabrication process, it's effect on structural integrity will depend on the location of the disbond with respect to the crack plane.

2.6.   Effect of Moisture

Composite materials have the propensity to absorb moisture from the environment during in-service usage. The presence of moisture in the repair can influence the damage growth in the repaired structure. The effect of moisture must be taken into consideration in designing composite patch repair and life prediction. The maximum moisture content in composite patch under typical environment is generally about 1%. The presence of moisture can cause increase in crack growth rate due to two reasons: 1) The presence of moisture increases crack growth rate in the metal compared to room temperature environment, and 2) the presence of moisture affects the load transfer to the patch. The repair patch design should be verified by testing with repair patches that are moisture conditioned to represent realistic environments.

2.7.   Effect of Metallic Material Thickness

The effectiveness of composite patch repair concept depends on the thickness of the metallic structure being repaired. In thin metallic structures (thickness less than 0.12 inch) repaired with composite patches on one face or both the faces the crack growth in the metal during subsequent flight loads is fairly uniform. However, in thick metallic structures (thickness greater than 0.12 inch) repaired with composite patch on one side only, the crack growth is not uniform through the thickness. Fatigue crack growth is retarded on the repair patch side as compared to the side with no repair patch. The non-uniform crack growth is due to the out-of-plane bending and the load transfer to the patch on the repaired side of the structure.

In thick metallic structures with repair patches on both the faces, the crack growth may not be uniform through the thickness. The crack gets retarded more on the surface than in the central portion of the specimen. This is because there is more load transfer into the patch in the surface region as compared to the central portion of the plate. In such cases the crack may exhibit tunneling behavior. The effect of the nonuniform crack growth should be taken into consideration when designing composite patch repairs for thick structures. The existing analytical techniques do not account for this effect and need to be modified before yielding realistic results.

10

2.8.   Effect of Thermal Stresses

The operating temperatures of typical transport and fighter/trainer aircraft generally do not cause significant thermal stresses to warrant thermal stress analyses. However, the mismatch in thermal expansion properties between a composite patch and repaired metallic structure can cause residual thermal stresses, which may accelerate crack growth in aluminum structure. The residual stresses are greater in a graphite repair than a boron repair because of a larger thermal mismatch between graphite and aluminum (as compared to aluminum and boron). These thermal stresses are produced; (1) during the bonding of composite repair patches to aluminum and (2) during in-service operation. The residual stresses produced in aluminum during the bonding process are compressive and hence have a beneficial effect. This effect is generally neglected. In operating environments, at temperatures above room temperature, the aluminum is subjected to compressive stresses and the "closure" effect is beneficial. However, in operating temperatures below room temperature, the aluminum is subjected to tensile stresses, which will reduce the crack closure effect and accelerate damage growth. Therefore, if an aircraft is operating at -65°F for long durations, damage growth will be accelerated and should be taken into consideration.

In the mathematical formulation of the problem, ΔT is the temperature difference that produces thermal stresses as outlined in Section 3.4 of the analysis. The temperature difference can be defined by:

$$\Delta T = T_{ref} - T_{op}$$

where:
T_{ref}= "Effective" temperature of repair system
T_{op}= Temperature of current operating environment

T_{ref} is a temperature necessary to quantify the thermal residual stresses inherent in the metal due to the composite bonding process. The choice of reference temperature is highly subjective (difficult to measure experimentally) and must be selected with caution. The estimation of T_{ref} is often debated within the repair community and is often used as a "correction factor" used to fit test results. For example, one analyst may recommend using T_{ref} = 250°F (a typical cure temperature for film adhesives used in composite repairs), and estimate the T_{ref} at room temperature to be approximately, 250-70°F= 180°F. A second analyst may estimate that the actual temperature at which the adhesive stops flowing and "locks in" the residual stresses to be approximately 120°F, yielding a T_{ref} of 120-70°F= 50°F. At present, there is no definitive answer to this question. The estimation of T_{ref}, is discussed more detail in the following paragraphs.

In summary, temperature differences due to either the composite bonding process and/or in-service loading can produce tensile or compressive stresses depending on the situation.

To illustrate the thermal effects of a composite patch on a metallic structure, the two cases specified are outlined below:

CASE 1: Effect of Thermal Stresses due to Composite Repair Bonding Process

Thermal stresses are produced during the bonding process when the coefficients of expansion of two materials are different. If boron or graphite is used as repair materials, thermal stresses will be produced during bonding process. All of the repairs on test specimens have shown that the test specimens are bent with repair patch on the outside and metal on inside. This indicates that the metal is under compression and the patch is under tension. Therefore, the stresses produced in metal are compressive and will tend to reduce stress intensity factor to some degree. This effect is generally neglected.

CASE 2: Effect of Thermal Stresses due to In-Service Loading

This case considers a composite patch repair that has already been performed on a structure and the structure is subjected to in-service temperature changes. If a structure is subjected to a operating temperature T_{op} which is higher than T_{ref}, then metallic structure will try to expand more than the composite repair, and will be restrained by the composite repair as shown in Figure 5. This will cause compressive stresses in the metallic structure and tensile stresses in the repair patch as shown in Figure 5. Thus, the stress intensity factor due to thermal stresses (caused by a temperature increase) should be subtracted from the stress intensity factor due to mechanical loading.
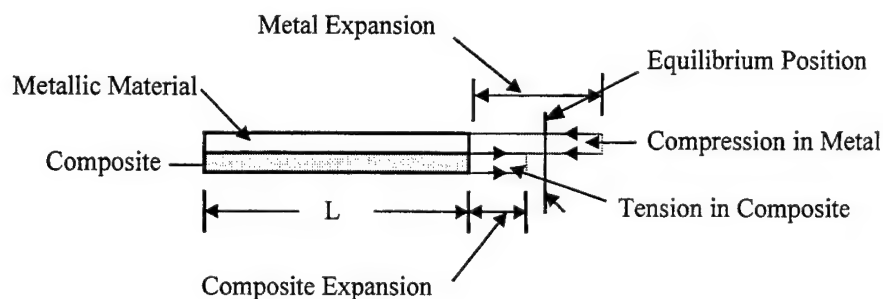
Figure 5. Repaired Structure Subjected to Temperature Increase

In the case where a structure is subjected to temperatures lower than the reference temperature, T_{ref} (e.g. an aircraft flying at -65°F), the metallic material will tend to contract more than the repair patch (Figure 6) but will be restrained by the composite patch. This will cause tensile stresses in metal and compressive stresses in the composite as shown in Figure 6. Thus, the stress intensity factors due to temperature decrease should be added to the stress intensity factors due to mechanical loading.
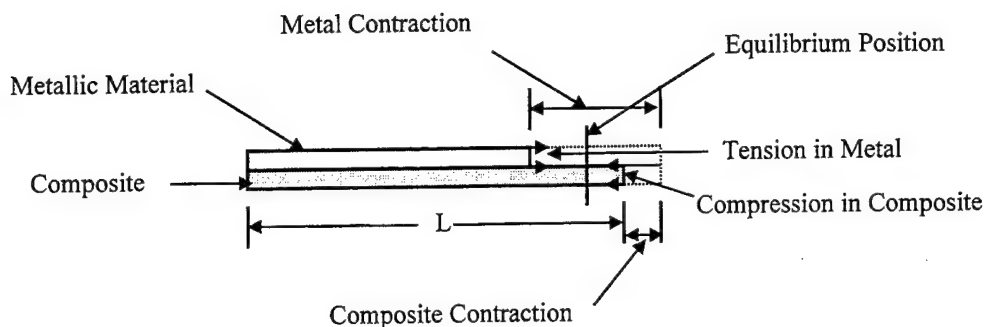
Figure 6. Repaired Structure Subjected to Temperature Decrease

It should be noted that the increase or decrease in stress intensity factors, due to thermal stresses, may not occur at the same time as the maximum stress in the spectrum. For example, in a fighter aircraft, the maximum stress occurs during combat and the temperature is not likely to be -65°F. When this temperature occurs the maximum stress in the spectrum is likely to be corresponding to 1g or 2g load, which is likely to be much less than design limit load or maximum spectrum load. Therefore, the superposition of the thermal and mechanical stress intensity factors must be carefully considered in order to obtain accurate stress intensity factors used in life prediction analyses.

In conclusion, these idealized models are not always representative of the situation encountered in real structures. In real aircraft structure, the deformations producing thermal stresses are local to the vicinity of the repair. Therefore, the influence of the substructure's constraint will depend on the proximity of the substructure, relative stiffness of the substructure, type of fastening, etc. Within the present scope of this program, it was impossible to develop and verify the analytical techniques used to determine the effect of these constraints.

3. METHOD TO ANALYZE CRACKED METALLIC STRUCTURES REPAIRED WITH COMPOSITE PATCHES

The analysis of a cracked metallic sheet with a bonded repair patch has been studied by various investigators [11-21]. In References 17-19, finite element techniques have been developed to analyze a cracked metallic sheet with a bonded composite repair patch. The finite element method is not a very convenient tool for use by engineers who are not experts in modeling and requires special training. Therefore, there is a need to develop simple methods to analyze cracked metallic structures repaired with composite patches. These techniques should be easy to use and not require expert knowledge.

In the following sections, a mathematical method of analysis is described. The details of the approach are discussed in the following paragraphs.

3.1. Formulation of the Problem

The problem of an adhesively bonded composite repair patch to a cracked metallic sheet is shown in Figure 7. A fatigue crack of length 2a is assumed in the metallic sheet. During fatigue cycling, a debond may develop in the adhesive layer. The debond is assumed to be elliptical in shape, with major axis along the crack direction and the leading edge of the debond coinciding with the crack tip.
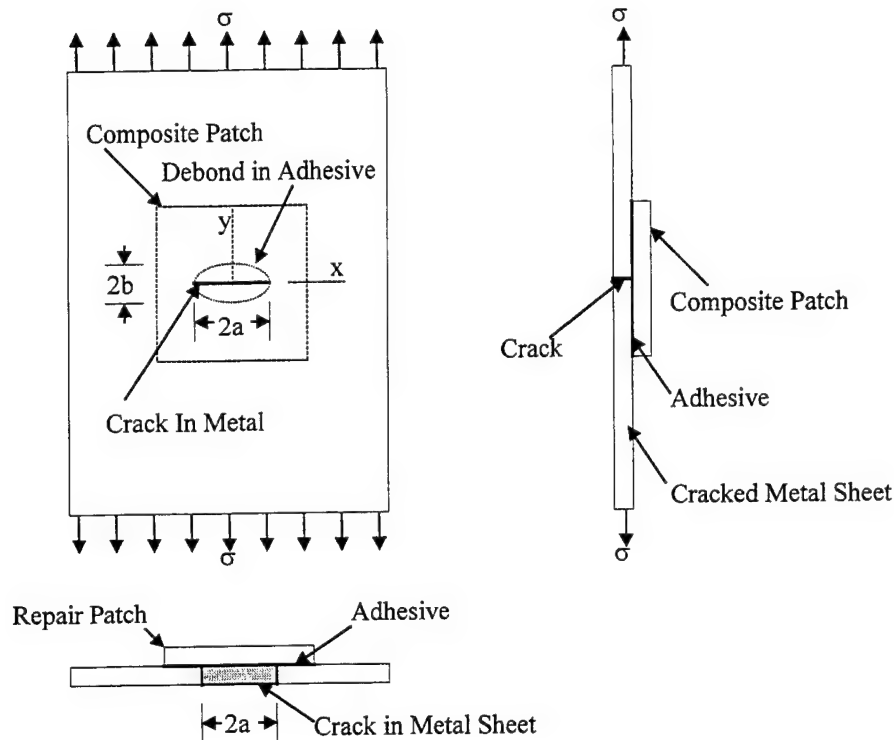
Figure 7. Cracked Metal Sheet with Composite Repair Patch

The analysis of the cracked metallic structure repaired with a composite patch, shown in Figure 7, is based on the following assumptions:

1. Composite repair patch is considered as an orthotropic material with principal directions along the crack plane and at right angles.

2. The thickness of the metallic sheet and composite patch are small compared to the in-plane dimensions so the structure may be considered under plane stress.

3. The variation of the stress through the thickness of the metal sheet and composite patch is neglected.

4. Metal sheet, composite patch, and adhesive layer are linearly elastic materials.

5. The adhesive thickness is small compared to the metal and patch thickness so that the adhesive may be treated as a shear spring.

6. The surface shear transmitted through the adhesive acts as a body force.

7. The dimensions of the plate and patch are sufficiently large so that infinite plate solutions for Green's functions may be used.

15

For the purpose of analysis, the structure in Figure 7 can be represented by the structure shown in Figure 8; where the structure in Figure 8a has no crack and the structure in Figure 8b has a crack with loading applied to the crack surface. The solution to the problem of Figure 7 is given by the perturbation problem of Figure 8b, as the structure of Figure 8a has no crack and hence no stress intensity factor.

(a) Bonded Sheet with No Crack   (b) Perturbation Problem
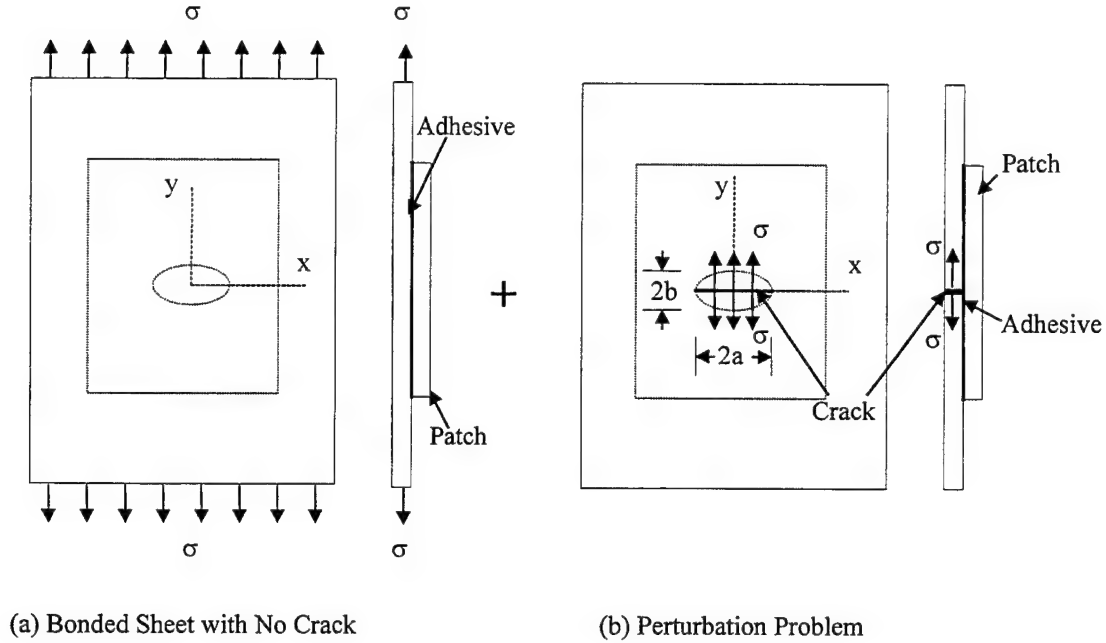
Figure 8. Superposition Technique for Cracked Sheet with Patch

In the perturbation problem of Figure 8b, let u_1, v_1 and u_2, v_2 be the x, and y components of the in-plane displacements in metal sheet and composite patch, respectively,. The shear stresses τ_x and τ_y are the components of shear stresses in the adhesive. The continuity conditions in the displacements of sheet and patch give:

$$u_1 - u_2 = \left(h_a/\mu_a\right)\tau_x$$
$$v_1 - v_2 = \left(h_a/\mu_a\right)\tau_y \tag{1}$$

where, μ_a is the shear modulus of adhesive and h_a is adhesive thickness.

The perturbation problem of Figure 8b may be considered as a metallic sheet with body forces and crack surface loading as shown in Figure 9a and composite patch with body forces as shown in Figure 9b. The body forces acting on the cracked sheet are X_1 and Y_1 at z_o (x_o, y_o) in x and y directions, respectively. The body forces acting in the composite patch are X_2, Y_2 at z_o (x_o, y_o) acting in x and y directions, respectively.

16

Figure 9. Loading on Metal Sheet and Composite Patch in Perturbation Problem

The body forces between the sheet and composite patch are transferred through the adhesive shear stresses. The relationship between the body forces and shear stresses is given by:

$$X_1 = -(\tau_x/h_1), \quad Y_1 = -(\tau_y/h_1)$$
$$X_2 = -(\tau_x/h_2), \quad Y_2 = -(\tau_y/h_2) \tag{2}$$

The stresses and displacements in terms of complex functions ϕ and ψ are given by Reference 22:

$$\sigma_x + \sigma_y = 2\left[\phi(z) + \overline{\phi(z)}\right] \tag{3a}$$

$$\sigma_y - \sigma_x + 2i\tau_{xy} = 2\left[(\bar{z} - z)\phi'(z) - \phi(z) + \overline{\psi}(z)\right] \tag{3b}$$

$$2\mu(u + iv) = \kappa \int_0^z \phi(z) - \int_0^{\bar{z}} \psi(\bar{z})d\bar{z} - (z - \bar{z})\overline{\phi(z)} \tag{3c}$$

17

3.1.1. Displacements in Orthotropic Composite Repair Patches

In the perturbation problem in Figure 9b, the body forces X_2 and Y_2 are the only forces acting on the patch. The stresses and displacements in the patch can be obtained from the solution of the problem of concentrated body forces acting at any arbitrary location z_0. This solution is used as Green's function and integrated over the bonding region 'D' to obtain displacements and stresses due to forces acting in the entire bonded region. The Kolosov-Muskhelishvili functions for the orthotropic composite under concentrated loads, X_2 and Y_2 acting z_0, are given by [23]:

$$\phi_2(z_1) = (C_{11}X_2 + C_{12}Y_2)\log(z_1 - \xi_1)$$
$$\chi_2(z_2) = (C_{21}X_2 + C_{22}Y_2)\log(z_2 - \xi_2) \tag{4}$$

where,

$$z_k = x + s_k y, \qquad \xi_k = x_0 + s_k y_0, \qquad (k = 1,2)$$
$$z = x + iy, \qquad z_0 = x_0 + iy_0 \tag{5}$$

$$C_{11} = (1/2\pi i)\left[s_2 + \bar{s}_2 + \bar{s}_1 + \bar{s}_1 s_2 \bar{s}_2 (v_x E_y/E_x)\right]/\left[(s_1 - s_2)(s_1 - \bar{s}_1)(1 - \bar{s}_2/s_1)\right]$$
$$C_{12} = (1/2\pi i)\left[s_2 \bar{s}_2 + \bar{s}_1 s_2 + \bar{s}_1 \bar{s}_2 + v_x\right]/\left[(s_1 - s_2)(s_1 - \bar{s}_1)(1 - \bar{s}_2/s_1)\right]$$
$$C_{21} = (1/2\pi i)\left[s_1 + \bar{s}_1 + \bar{s}_2 + s_1 \bar{s}_1 \bar{s}_2 (v_x E_y/E_x)\right]/\left[(s_2 - s_1)(s_2 - \bar{s}_2)(1 - \bar{s}_1/s_2)\right]$$
$$C_{22} = (1/2\pi i)\left[s_1 \bar{s}_1 + \bar{s}_2 s_1 + \bar{s}_2 \bar{s}_1 + v_x\right]/\left[(s_2 - s_1)(s_2 - \bar{s}_2)(1 - \bar{s}_1/s_2)\right] \tag{6}$$

In Equation (6) s_1 and s_2 are roots of

$$s^4 + (E_x/G_{xy} - 2v_x)s^2 + E_x/E_y = 0 \tag{7}$$

for which $\text{Im}(s_k) > 0$.

The stresses and displacements in the plate may be expressed in terms of ϕ_2 and χ_2. Assuming that the body forces X_2 and Y_2 are continuous functions of $z_0(x_0,y_0)$ defined in bonded region 'D', the displacements at a point in the composite may be written as:

$$u_2(x,y) = \iint_D \left[K_{11}(x,y; x_0,y_0)X_2(x_0,y_0) + K_{12}(x,y; x_0,y_0)Y_2(x_0,y_0)\right]dx_0 dy_0$$
$$v_2(x,y) = \iint_D \left[K_{21}(x,y; x_0,y_0)X_2(x_0,y_0) + K_{22}(x,y; x_0,y_0)Y_2(x_0,y_0)\right]dx_0 dy_0 \tag{8}$$

where kernels K_{ij} (i,j = 1,2) are given by the Green's functions (4).

3.1.2. Displacements in Cracked Plate

The displacements in the cracked plate consist of two parts, one due to uniformly applied stress on the crack surface and the other due to the body forces acting on the cracked plate. The displacements due to uniform applied stress on the crack surface are given by:

$$u_{11}(x,y) = \sigma \left\{ (\kappa - 1) \operatorname{Re}\left[(z^2 - a^2)^{1/2} \right] - 2y \operatorname{Im}\left[z/(z^2 - a^2)^{1/2} \right] + (1 - \kappa)x \right\}/4\mu = \sigma f_1(x,y) \quad (9a)$$

$$v_{11}(x,y) = \sigma \left\{ (\kappa + 1) \operatorname{Im}\left[(z^2 - a^2)^{1/2} \right] - 2y \operatorname{Re}\left[z/(z^2 - a^2)^{1/2} \right] + (1 - \kappa)y \right\}/4\mu = \sigma f_2(x,y) \quad (9b)$$

where,

v_1 is Poisson Ratio of plate material
μ is the shear modulus of plate material

$$\kappa = (3 - v_1)/(1 + v_1)$$

The displacements u_{12} and v_{12} in the cracked plate due to body forces are given in Reference 21. These displacements are given by:

$$2\mu(u_{12} + v_{12}) = S\{-\kappa\left[\log(z - z_0) + \log(\bar{z} - \bar{z}_0)\right] + \kappa\left[\theta_1(z,z_0) + \theta_1(\bar{z},\bar{z}_0)\right]/2 - \left[\theta_1(\bar{z},z_0) + \kappa^2\theta_1(\bar{z},\bar{z}_0)\right]/2$$
$$+ (\kappa - 1)\left[\kappa\theta_2(z) - \theta_2(\bar{z})\right]/2 + (z - \bar{z}_0)\theta_5(z,z_0)/(\bar{z} - z_0)\}$$
$$+ \bar{S}\left[(z - z_0)/(\bar{z} - \bar{z}_0) - 1 + \kappa\theta_3(z,z_0) - \theta_3(\bar{z},z_0) - \theta_4(z,z_0) + \kappa\theta_4(\bar{z},\bar{z}_0)\right]$$
$$+ \text{Rigid Body Displacement} \quad (10)$$

where,

$$S = (X_1 + Y_1)/[2\pi(1+\kappa)]$$

$$\overline{S} = (X_1 - Y_1)/[2\pi(1+\kappa)]$$

$$\theta_1(z,z_o) = \log\left[zz_0 - a^2 + \left(z_0^2 - a^2\right)^{1/2}\left(z^2 - a^2\right)^{1/2}\right]$$

$$\theta_2(z) = \log\left[z + \left(z^2 - a^2\right)^{1/2}\right]$$

$$\theta_3(z,z_0) = \left[(\overline{z}_0 - z_0)/2(z - \overline{z}_0)\right]\left[1 + \left(z^2 - a^2\right)^{1/2}\left(\overline{z}_0^2 - a^2\right)^{1/2}/\left(a^2 - \overline{z}_0^2\right)\right]$$

$$\theta_4(z,z_0) = \left[(z - \overline{z})/2(\overline{z} - \overline{z}_0)\right]\left[I(\overline{z}) - I(\overline{z}_0)/\left(\overline{z}^2 - a^2\right)^{1/2}\right]$$

$$\theta_5(z,z_0) = \theta_4\left(z,\overline{z}_0\right) - (z - \overline{z})J(\overline{z}_0)/\left[2\left(\overline{z}^2 - a^2\right)^{1/2}\right]$$

$$I(z) = \pi\left[\left(z^2 - a^2\right)^{1/2} - z\right]$$

$$J(z) = \pi\left[z\left(z^2 - a^2\right)^{-1/2} - 1\right] \tag{11}$$

Assuming, the body forces X_1, and Y_1 are continuous functions of (x_0,y_0) defined in the bonded region 'D', and using equations 10 and 11 as the Green's functions, the displacements in the cracked plate due to body forces may be written as:

$$u_{12}(x,y) = \iint_D \left[h_{11}(x,y; x_0y_0)X_1(x_0,y_0) + h_{12}(x,y; x_0y_0)Y_1(x_0,y_0)\right]dx_0dy_0$$

$$v_{12}(x,y) = \iint_D \left[h_{21}(x,y; x_0y_0)X_1(x_0,y_0) + h_{22}(x,y; x_0y_0)Y_1(x_0,y_0)\right]dx_0dy_0 \tag{12}$$

The total displacement in the cracked plate may be written as:

$$u_1(x,y) = u_{11} + u_{12}, \qquad v_1(x,y) = v_{11} + v_{12} \tag{13}$$

3.1.3. Integral Equations for τ_x & τ_y

The τ_x and τ_y are the adhesive shear stresses in the x and y directions, respectively. The relationship between the body forces and shear stresses is given by Equation 2. Using displacements u_1, u_2 and v_1, v_2 in Equation 1 gives the following system of integral equations for the unknown shear stresses τ_x and τ_y:

$$(h_a/\mu_a)\tau_x(x,y) + \iint_D \left[k_{11}(x,y; x_0,y_0) + \tau_x(x_0,y_0) + k_{12}(x,y; x_0,y_0) + \tau_y(x_0,y_0)\right]dx_0dy_0 = \sigma f_1(x,y)$$

$$(h_a/\mu_a)\tau_y(x,y) + \iint_D \left[k_{21}(x,y; x_0,y_0) + \tau_x(x_0,y_0) + k_{22}(x,y; x_0,y_0) + \tau_y(x_0,y_0)\right]dx_0dy_0 = \sigma f_2(x,y)$$

$$\tag{14}$$

The functions f_1 and f_2 are given by Equation (9) and,

$$k_{11} = H_{11}/h_1 + K_{11}/h_2 \qquad\qquad k_{12} = H_{12}/h_1 + K_{12}/h_2$$
$$k_{21} = H_{21}/h_1 + K_{21}/h_2 \qquad\qquad k_{22} = H_{22}/h_1 + K_{22}/h_2 \qquad (15)$$

Kernels K_{ij} (i,j = 1,2) which have logarithmic singularities are known and are square integrable in region 'D'.

3.1.4. Stress Intensity Factors

The stress intensity factors in plane stress problems may be expressed in terms of Kolosov Muskhelishvili function $\phi(z)$ as follows [24]:

$$k_1 - ik_2 = \lim_{x \to a} [2(x-a)^{1/2}[\sigma_y(x,0) - i\tau_{xy}(x,0)]$$
$$= \lim_{z \to a} 2[2(z-a)]^{1/2} \phi(z) \qquad (16)$$

In the present problem, the shear component of the stress intensity factor is zero due to the symmetry in loading and geometry and only cleavage component k_1 is present. The cleavage component is obtained by adding the effects of crack surface loading p_0 and the body forces X_1 and Y_1. The stress intensity factor k_1 is given by:

$$k_1 = \sigma(a)^{1/2} + \iint_D [h_1(x_0,y_0) X_1(x_0,y_0) + h_2(x_0,y_0) Y_1(x_0,y_0)] dx_0 dy_0 \qquad (17)$$

where, $h_1(x_0,y_0)$ and $h_2(x_0,y_0)$ are the cleavage components of the stress intensity factor due to the concentrated body forces X_1 and Y_1, respectively. The stress intensity factors are given by:

$$k_1 - ik_2 = (1/a)^{1/2} \{-S[a + I(z_0)]/(a - z_0) + \chi \bar{S}[a + I(z_0)]/(a - z_0) - S(\bar{z}_0 - z_0)$$
$$[(a + I(z_0))/(a - z_0)^2 + J(z_0)/(a - z_0)] \qquad (18)$$

$h_1(x_0,y_0)$ and $h_2(x_0,y_0)$ are the coefficients of X_1 and Y_1 respectively in real part of Equation (18).

3.2. Solution of Integral Equations

The integral equations given by Equation (14) are the Fredholm type and may be solved by collocation. The region 'D' is divided into smaller cells and unknown shear stresses τ_x and τ_y are assumed to be constant in each cell. In the integral equations the integral is replaced by summation and using collocation a 2N X 2N system of equations are obtained. The equations are given by:

$$\left(h_a/\mu_a\right)\tau_x\left(x_i,y_j\right)+\sum_{p=1}^{N}\sum_{q=1}^{N}\left[k_{11}\left(x_i,y_j;x_{0p},y_{0q}\right)\tau_x\left(x_{0p},y_{0q}\right)+k_{12}\left(x_i,y_j;x_{0p},y_{0q}\right)\tau_y\left(x_{0p},y_{0q}\right)\right]\Delta_{xp}\Delta_{yq}$$

$$= \sigma f_1\left(x_i,y_j\right) \tag{19a}$$

$$\left(h_a/\mu_a\right)\tau_y\left(x_i,y_j\right)+\sum_{p=1}^{N}\sum_{q=1}^{N}\left[k_{21}\left(x_i,y_j;x_{0p},y_{0q}\right)\tau_x\left(x_{0p},y_{0q}\right)+k_{22}\left(x_i,y_j;x_{0p},y_{0q}\right)\tau_y\left(x_{0p},y_{0q}\right)\right]\Delta_{xp}\Delta_{yq}$$

$$= \sigma f_1\left(x_i,y_j\right) \tag{19b}$$

$$i = 1,.....N, \qquad j = 1,.....N$$

The kernels in Equation (19) have logarithmic singularities, hence the singular part of the kernels is evaluated separately in the closed form. In the actual integration a telescopic grid is used. A typical grid used in integration is shown in Figure 10, where only a quarter of the integration region is shown because of symmetry. The grid size is kept small above the crack plane for a distance of about half-crack length 'a', as the shear stresses are high in this region. The grid size is increased as the distance from the crack increases. Theoretically the integration region is infinite, however, in the perturbation problem the shear stresses in the adhesive decrease rapidly away from the crack plane. Hence, the integration region is kept finite as shown in Figure 10. The integration region is determined so that the stress intensity factors are not significantly affected. The convergence of the solution depends on the crack length and elastic properties of an adhesive, cracked sheet, and composite patch.
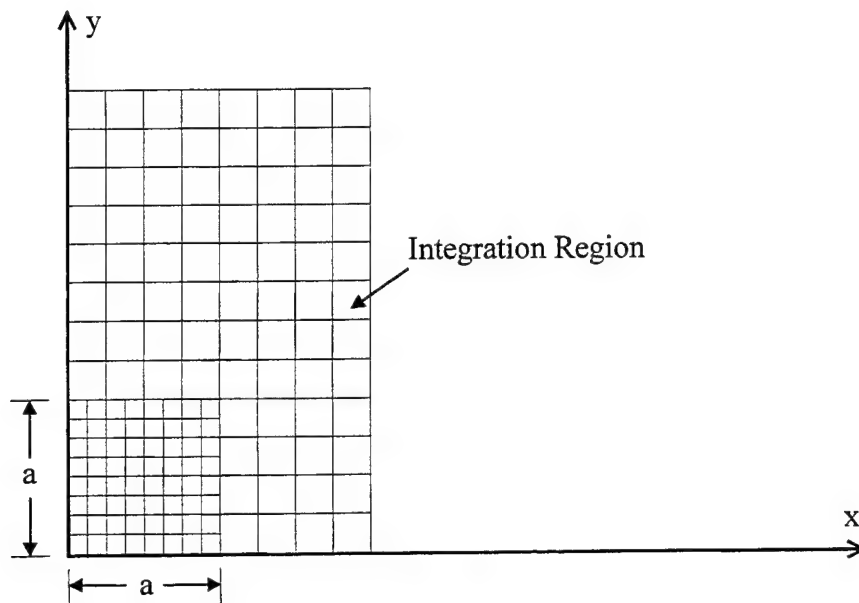
Figure 10. Grid Used in Numerical Integration (Due to Symmetry Only 1/4 of Panel Shown)

3.3. Effect of Bending

The analysis of a cracked sheet repaired with a composite patch (in Section 3.1) is for extension loading and it is assumed that the patch or sheet has no bending stiffness. It is applicable to cases where the repair patches are applied to both the surfaces of the cracked sheet as shown in Figure 11a. This type of repair is not always feasible, for in the majority of cases the access for repair is available on one side only, and therefore the repair patch may be applied on one surface only (Figure 11b). The presence of a patch on one side only will produce out-of-plane bending at the crack plane. This bending will produce tensile stresses in the sheet and compressive stresses in the repair patch. The tensile stresses due to bending in the sheet will produce stress intensity factors in addition to those produced by the applied membrane stress, σ. The stress intensity factors due to bending should be added to those produced by membrane stresses. A simple method of calculating stress intensity factors due to bending [11-12], is discussed in the following paragraphs for the composite repair patch geometry shown in Figure 11b.

(a) Cracked Sheet w/Repair on Both Surfaces   (b) Cracked Sheet w/Repair on One Surface
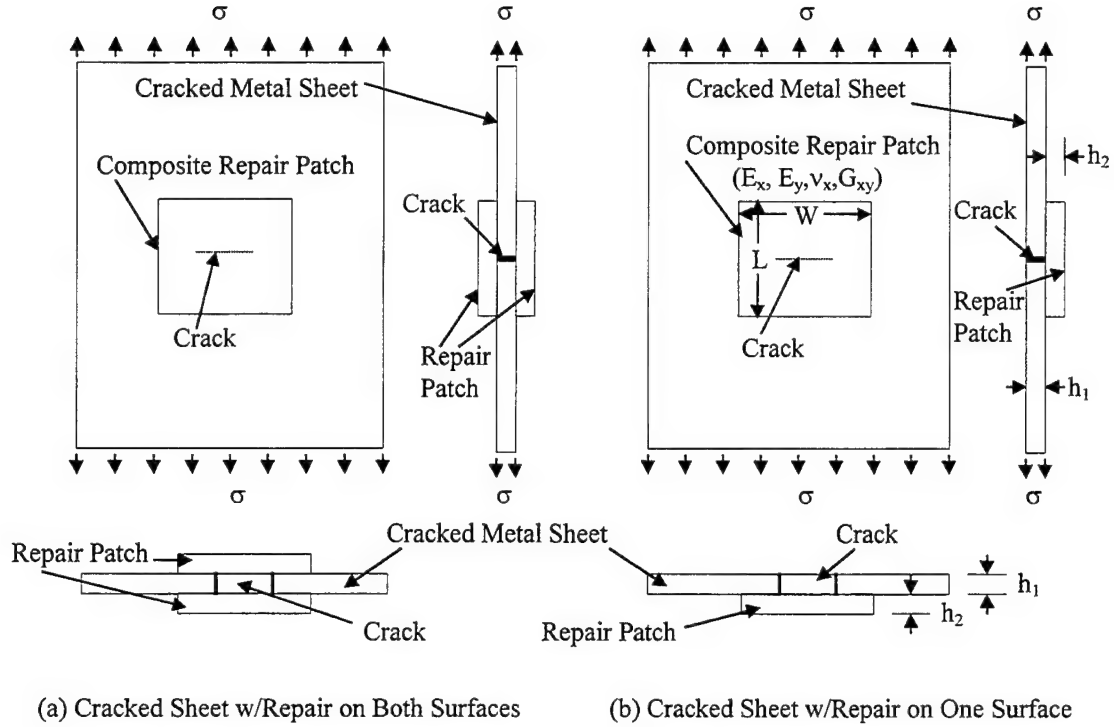
Figure 11. Repair Patch Configurations

In a cracked sheet with a central crack of 2a and far field applied stress of σ, the load released due to the presence of the crack at the crack plane is $(2ah_1)\sigma$ (area x stress). This load is entirely taken by the stress singularities produced ahead of the crack tips. In a cracked sheet repaired with a composite patch shown in Figure 11b, the same load released due to the presence of a crack $(2ah_1\sigma)$ at the crack plane is partly taken by the stress singularities ahead of the crack tips, as in the case of a single cracked sheet, and the remainder of the load is transferred to the repair patch through the adhesive. The load transferred to the patch produces bending. Let the load transmitted to the patch be $2ah_1\sigma_t$ (area x stress) where σ_t is equivalent stress transferred to the patch.

Assuming the thickness of the adhesive to be small compared to plate thickness, the moment produced by the load transfer between the cracked sheet and patch is given by:

$$M = 2ah_1\sigma_t\left[(h_1 + h_2)/2\right] \tag{20}$$

where $(h_1 + h_2)/2$ is the distance between the centerline of the metal sheet and repair patch.

or

$$M = ah_1(h_1 + h_2)\sigma_t \tag{21}$$

24

Assuming that the bending is resisted by the plate width equal to the patch width W, the maximum bending stress in the layer is given by:

$$\sigma_b = My_{max}/I \qquad (22)$$

where y_{max} is the distance of the outer sheet edge from neutral axis and I is the equivalent moment of inertia of the section. For computing the moment of inertia and y_{max} the thickness of the adhesive may be neglected and the section of the patch resisting bending moment (Figure 10a) may be represented by that shown in Figure 12b. For computing the moment of inertia and y_{max} the equivalent section is shown in Figure 12c, where it is assumed that E_y is greater than E_1 and the section is uncracked.

(a) Section of Cracked Sheet w/Patch (b) Idealized Section for Bending Analysis

(c) Equivalent Section for Bending Stress Analysis
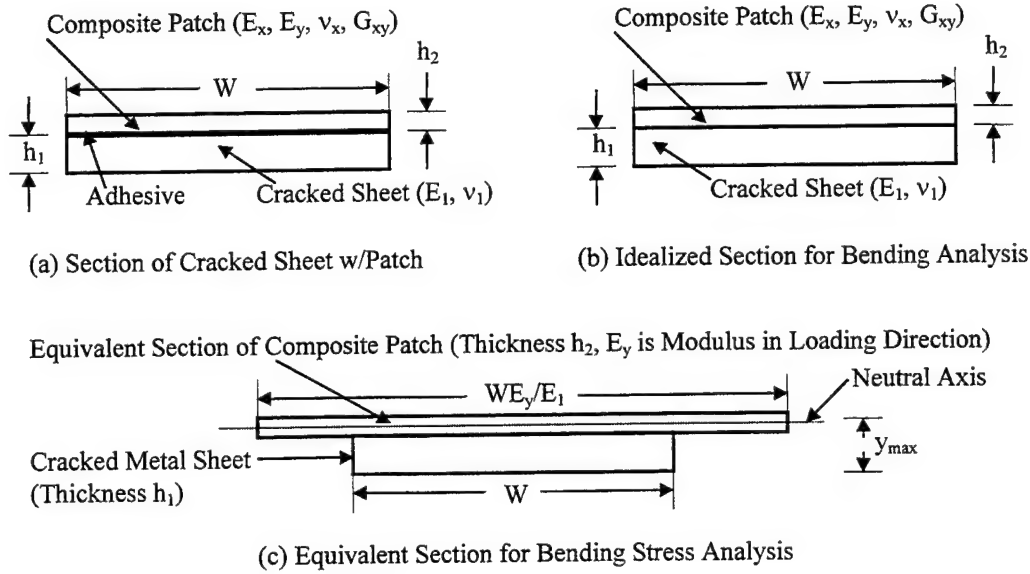
Figure 12. Equivalent Section for Bending Stress Analysis

Substituting Equation (22) in (21) gives:

$$\sigma_b = \left[ah_1(h_1 + h_2)\sigma_t y_{max}\right]/I \qquad (23)$$

3.3.1. Load Transfer Factor

The load transfer factor, L_f, is defined as the ratio of the load transferred (to the patch) to the load released due to the presence of a crack.

$$L_f = (2ah_1\sigma_t)/(2ah_1\sigma) = \sigma_t/\sigma \qquad (24)$$

25

Substituting Equation (24) in (23) gives:

$$\sigma_b = [ah_1(h_1 + h_2)L_f \sigma y_{max}]/I$$
$$\sigma_b/\sigma = [ah_1(h_1 + h_2)L_f y_{max}]/I \qquad (25)$$
$$= BC, \text{Bending Correction Factor}$$

Therefore the effective stress used in computing the stress intensity factors is increased by an amount σ_b.

3.3.2. Load Transfer Factor Computation

In a cracked structure with no repair patch the stress intensity factor may be written as:

$$K_s = \sigma(\pi a)^{1/2} f(a/W) \qquad (26a)$$

where, a is half crack length and f(a/W) is finite width correction.

K_a is the stress intensity factor in the cracked structure with repair patch and applied stress of σ. The equivalent stress σ_e acting on a sheet with no repair patch and giving stress intensity factor of K_a is given by:

$$K_a = \sigma_e(\pi a)^{1/2} f(a/W) \qquad (26b)$$

Using Equation (26), K_a may be expressed as:

$$K_a = \sigma_e K_s/\sigma \qquad (26c)$$

or

$$\sigma_e = K_a \sigma/K_s \qquad (27)$$

The stress transferred to the repair patch is the difference between the remotely applied stress in the repaired structure and the uniform in-plane stress that produces the same stress intensity factor in a single sheet as in the repaired structure. The stress transferred, σ_t, may be written as:

$$\sigma_t = \sigma - \sigma_e \qquad (28)$$

26

Using Equation (27),

$$\sigma_t = \sigma - K_a \sigma / K_s$$

The load transfer factor is given as:

$$L_f = \sigma_t / \sigma = 1 - K_a / K_s \tag{29}$$

K_a is the stress intensity factor in the adhesively bonded structure obtained from mathematical or finite element analysis. K_s is the stress intensity factor in a single layer structure having the same crack length as the repaired structure and can be obtained from any handbook on stress intensity factors. Substituting this value of load transfer factor in equation (25) gives the bending correction factor, BC:

$$BC = \sigma_b / \sigma = [ah_1(h_1 + h_2)(1 - K_a / K_s) y_{max}] / I \tag{30}$$

The moment of inertia I and y_{max} are obtained for the equivalent section shown in Figure 12c. In the equivalent section shown in the figure, E_y is the modulus of the repair patch in the loading direction.

3.4. Effect of Thermal Stresses

In a cracked metallic structure repaired with composite patches, the coefficients of linear expansion of the cracked metallic sheet and composite repair patch are different, and this difference in the coefficients of expansion gives rise to thermal stresses. These thermal stresses may be due to the residual stresses produced during the curing process or due to the in-service environment experienced by the repair. The fabrication of the panels with graphite or boron repairs have shown that residual stresses produced by fabrication processes are generally compressive, have beneficial effects on crack growth, and are generally neglected. However, the residual stresses produced by in-service change of temperature may produce tensile or compressive stresses. In general, an increase in in-service temperature compared to room temperature will produce compressive stresses and hence a reduction in stress intensity factors. While a reduction in in-service temperature will produce tensile stresses and an increase in stress intensity factors, it may be noted that no residual stresses are produced if the repair material is GLARE as the coefficients of expansion of aluminum and GLARE are about the same.

A simplified thermal stress analysis of a metallic structure bonded to composite was presented in Reference 25. This stress analysis was used in the present work to compute stress intensity factors due to thermal stresses. Consider the bonded structure shown in Figure 11b. Let,

27

α_1 = Coefficient of expansion of metallic material
α_y = Coefficient of expansion of composite repair patch in loading direction
ΔT = Temperature difference producing thermal stresses $(T_{ref}-T_{op})$
L = Dimension of the patch in loading direction at right angles to crack plane
E_1 = Modulus of elasticity of metallic material
E_y = Modulus of elasticity of composite material in loading direction

The thermal stresses are computed as follows:

Expansion of metallic material $= \alpha_1 T(L/2)$

Expansion of repair patch $= \sigma_y T(L/2)$

Differential deformation producing thermal stresses $= \alpha_1 T(L/2) - \alpha_y T(L/2)$

$$= (\alpha_1 - \alpha_y)\Delta T(L/2) \qquad (31)$$

Strain produced by thermal stresses $= (\alpha_1 - \alpha_y)\Delta T(L/2) = (\alpha_1 - \alpha_y)\Delta T \qquad (32)$

Residual stress in metallic sheet due to thermal mismatch is given by,

$$E_1(\alpha_1 - \alpha_y)\Delta T \qquad (33)$$

This far field stress is used to compute stress intensity factors in the structure with a repair patch. It may be noted that the thermal stress analysis, discussed here, is approximate and does not account for two factors namely; 1) effect of adhesive deformation in relieving strain and reducing the effect of thermal mismatch, and 2) the effect of relative differential expansion between composite and metal at right angles to the loading direction along the crack plane.

3.5. Effect of Disbonding in Adhesive Layer

Experimental results [11-12] have shown that as the crack propagates under fatigue loading, disbonding occurs in the adhesive. This disbonding cannot be predicted by a static analysis because it occurs due to cyclic loading at much lower stresses than those predicted by static analysis. The prediction of disbonding due to cyclic loading is rather complex and was not attempted in the present research. The disbonding in the adhesive layer influences the load transfer to the repair patch, and ultimately, the stress intensity factors in the cracked sheet. The presence of a disbond will cause less load transfer from the cracked sheet to the repair patch and thereby increase the stress intensity factors and hence crack growth rate. The presence of cyclic disbonding should be taken into consideration in making any life predictions.

The experimental studies were used to account for the disbond in the adhesive layer. These studies have shown that the disbonding in the adhesive layer tends to be elliptical in shape with the leading edge of the disbond coinciding with the leading edge of the crack (Figure 13). The minor axis of the disbond is along a direction that is at right angles to the crack plane and at the crack centerline. The ratio of minor to major axis of the disbond depends on a number of parameters such as the type of adhesive (ductile versus brittle), adhesive thickness and the properties of bonded (metal and composite) materials.

Location of Crack Tips in Cracked Sheet

2b

2a

Elliptical Shape Disbond in Adhesive
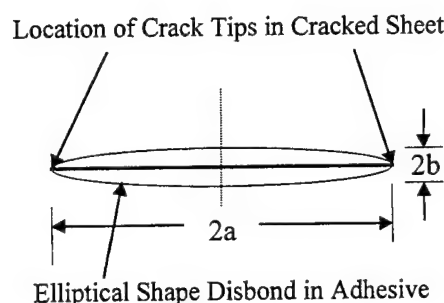
Figure 13. Schematic Representation of Adhesive Disbond Under Cyclic Loading

3.6. Development of Computer Program to Calculate Normalized SIF's

A computer program was written to compute shear stresses in the adhesive and stress intensity factors in the cracked sheet due to applied loading and thermal mismatch between the metallic sheet and composite repair patch. The stress intensity factors can be used in making crack growth and residual strength predictions.

The computer program is written to account for the elliptical disbond in the adhesive with major axis along the crack plane and leading edge of the disbond coinciding with the crack tip. The user has the option to input the minor to major axis ratio of the disbond b/a (Figure 13). The recommendation for the size of disbond to be used in the analysis is given in the section on design guidelines and in the AFGROW [26] software program further developed as part of the present research.

The normalized stress intensity factor is calculated based on a unit applied remote stress to an infinitely wide center-cracked panel. In AFGROW, this normalized stress intensity factor is equivalent to the ratio of the patched stress intensity factor to the unpatched stress intensity factor.

The computer program also accounts for the effect of bending in the structure. The bending correction discussed in Section 3.3 has been incorporated in the program. The computer program has the following inputs:

29

Cracked Sheet Parameters:

1) Elastic Modulus, E_1
2) Poisson ratio, ν_1
3) Coefficient of linear expansion, α_1
4) Thickness, h_1

Repair Patch Parameters:

1) Elastic modulus of the repair patch along the crack plane direction, E_x
2) Elastic modulus of the repair patch along loading direction at right angles to crack plane, E_y
3) Poisson ratio, ν_x
4) Shear Modulus G_{xy}
5) Coefficient of linear expansion of patch material α_y along loading direction
6) Patch width W
7) Patch Length L
8) Patch Thickness

Adhesive Parameters

1) Thickness, 'h_a'
2) Shear Modulus, 'μ_a'
3) Ratio of minor to major axis of debond, 'deb'

Crack Parameters

1) Half crack length, 'a'
2) Increment in half crack length, 'da', for computing stress intensity factors
3) Number of runs, 'nab'

Temperature Parameters

1) Temperature difference, ΔT, which causes thermal mismatch

3.7. Implementation of Composite Repair/Analysis into AFGROW

This section describes the implementation of a preliminary composite bonded repair design module into the AFGROW computer program. This feature has been integrated with the existing life prediction capability so that the effect of a repair patch may be included in crack growth analysis. A limited "knowledge base" has also been built into this system to aid the user in selecting an initial patch material and ply layup. The

following sections contain a description of the features, capabilities and limitations of this module.

3.8.   Repair Design Considerations

A number of factors need to be considered in designing composite repair patches for metallic structures. The following factors are taken into account in AFGROW:

1. Repair patch material and ply thickness.

2. Repair patch layup.

3. Substructure material properties and thickness.

4. Effect of thermal stresses.

5. Effect of bending.

6. Adhesive properties and thickness.

7. Local disbonding of adhesive around crack.

While there are several other important considerations such as repair location, repair geometry and dimensions, and edge taper, these are outside the scope of the current version of AFGROW (Version 3.85.6). The program is intended to provide preliminary solutions to repair design problems and to assess the effect of various parameters on the life of repaired substructures. More detailed analyses would require the use of tools capable of creating and analyzing detailed models of the repaired structure. Such tools may then be used in combination with AFGROW for life prediction purposes.

3.9.   Program Implementation

The bonded repair module was designed to work with the existing crack growth analysis capability so that a repair can be applied to the current analysis model at any time. The life prediction routine includes the effect of the repair in all subsequent analyses until the repair is deleted by the user. However, repairs are not applicable to all the crack configurations offered in AFGROW. The range of applicability is outlined in the section below.

3.9.1. Repair Application Bounds

Repairs are applicable to all the through-crack solutions in AFGROW with the exception of the solid circular shaft, pipe, and disc solutions. They may not be applied to any of the

part-through crack configurations. In addition, certain other limitations are placed on the dimensions of the model to be repaired. These are:

1. Minimum thickness of plate = 0.04"

2. Maximum thickness of plate = 0.125"

3. Maximum crack length = 2.00"

The minimum thickness and maximum crack length limitations are due to the range of applicability of the repair design solution module. The maximum thickness limitation is imposed because the current release of AFGROW (Version 3.85.6) can not model the variation in crack length (through the thickness) that occurs when repairs are applied to thicker specimens.

AFGROW prohibits the application of a repair if the model configuration and dimensions are not within the acceptable limits.

3.9.2. Design Parameters and Controls

It is recommended to set up all the model parameters and properties before designing a repair. AFGROW uses these parameters and the repair patch properties to compute a set of "beta correction factors" which are used to correct the stress intensity factors during crack propagation to account for the presence of the repair patch. These factors are stored in a tabular form as a function of crack length. If the model geometry, dimensions or material properties are changed after a repair has been applied, AFGROW automatically deletes the repair as the beta correction factors are no longer valid. In such a case, the repair must be redesigned.

Spectrum information is used by AFGROW to automatically design a repair. If the "auto-design" feature is to be used, then the correct spectrum must be opened and the stress multiplication factor must be specified prior to using this feature. The program determines the maximum stress level from the spectrum and uses this information to choose the most appropriate repair material for the application.

The repair design module is invoked by clicking on the "Design" option in the "Repair" pull-down menu. The repair design dialog, shown in Figure 14, appears on the screen.
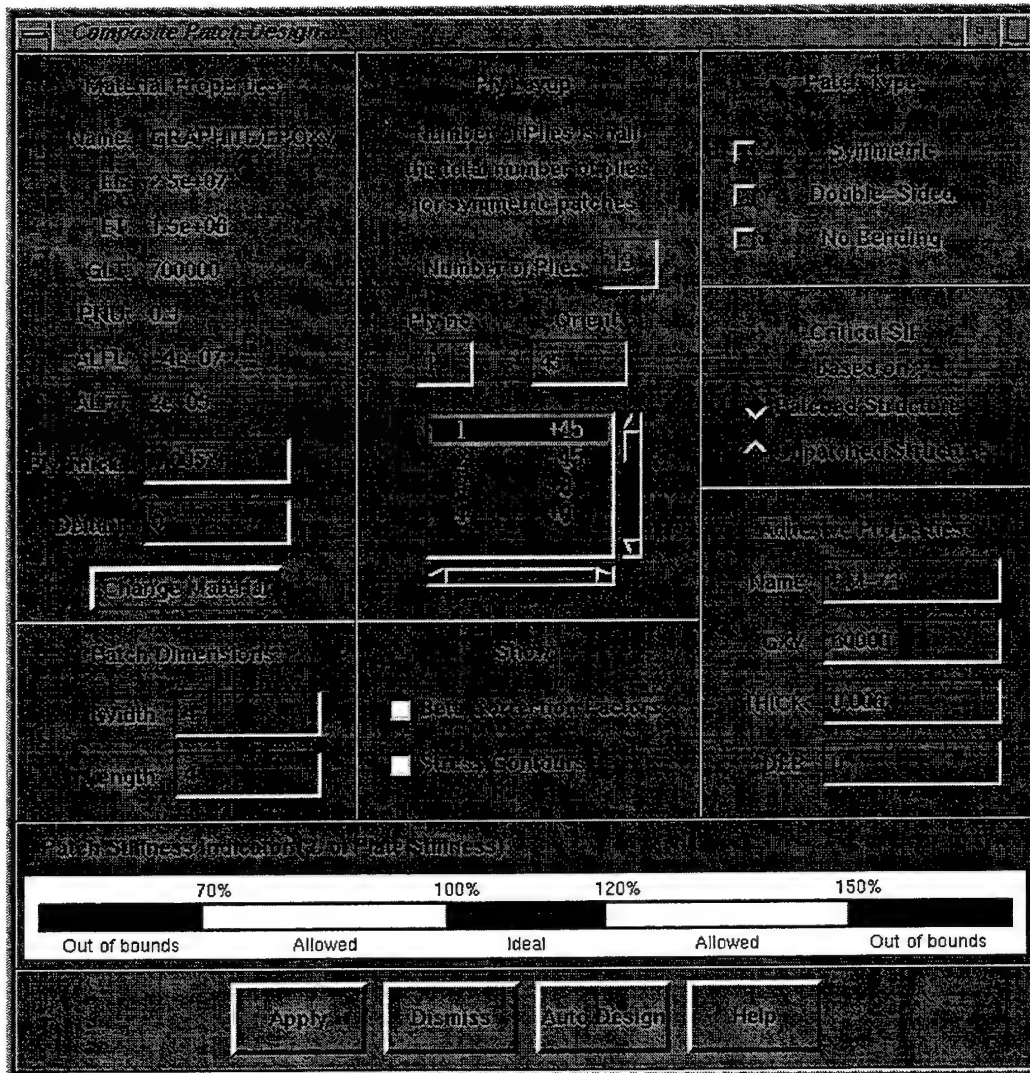
Figure 14. The Composite Patch Design Dialog

This dialog contains various controls that can be used to change the repair patch parameters. These parameters and the controls that are used to modify them are explained in the following sections.

3.9.2.1. Material Properties

The current patch material is displayed on the upper left portion of the dialog box. A new material may be specified by clicking the "Change Material" button. This causes a file browser containing patch material data files to pop up. This release of AFGROW includes one such file, called `patch.pch`, which contains material properties for boron, graphite, and GLARE. The user may then select one of these materials to be the new

33

patch material. If a material other than these is to be used, data for that material must be present in patch.pch or any other *.pch file.

The material properties are referred to on the dialog by means of abbreviations, as seen in Figure 14. The list of properties is:

EL:	Young's modulus in longitudinal direction
ET:	Young's modulus in transverse direction
GLT:	Shear modulus
PNU:	Poisson's ratio
ALFL:	Coefficient of thermal expansion in longitudinal direction
ALFT:	Coefficient of thermal expansion in transverse direction

It must be noted that the program does not allow the user to alter the values of the material properties directly. This is because the repair module relies on the material being orthotropic; unexpected results may occur if the properties do not satisfy the conditions of orthotropy. Since most repair applications utilize boron, graphite or GLARE, the material datafile included with AFGROW is sufficient in most cases. Other materials must be used only after ensuring that they are orthotropic.

A default ply thickness has been set for each of these materials. This value is editable, and may be set to any value. The other editable value is ΔT, which is used to account for thermal stresses due to differences in the curing temperature of the patch and the temperature of the plate.

3.9.2.2. Patch Dimensions

The patch dimensions (width and length) are used only for the purposes of calculating the effect of bending. The beta correction factors are based on the assumption of an infinite patch; the patch dimensions do not affect them unless bending is included in the solution.

3.9.2.3. Ply Layup

This release of AFGROW can model patches with up to 32 plies. The user may specify the orientation of each ply by selecting the ply from the scrollbox and entering its orientation in the textbox above it. If a symmetric patch with an even number of plies is to be modeled, then it is sufficient to enter the orientations for half the plies; AFGROW will automatically mirror the layup to construct the other half.

It is recommended to have 70% 0° plies, 20% ±45° plies, and 10% 90° plies. However, in most cases it is not possible to achieve this distribution and the closest distribution must be used. Also, it is desirable to place the ±45° plies on the surface as this will reduce the tendency of the patch to delaminate at the edges.

3.9.2.4. Patch Type

AFGROW allows the user to specify certain other options that are important from a design consideration. These are controlled by means of toggle buttons and include:

Symmetric patch

Specifying this option automatically mirrors the specified layup to create a symmetric patch. Consideration must be given to maintaining balanced laminate symmetry to avoid warpage in the precure of the patch.

Double-sided patch

This option applies the patch to both sides of the metallic substructure. Selection of this option may depend on factors such as location and accessibility of the repair.

An assumption is made in AFGROW that the effect of bending is negligible when patches are applied to both sides of the plate. The third toggle button, which controls whether bending is considered or not, is then automatically selected and "greyed out," or made inaccessible, to the user.

No Bending

The user may select this button to either include or neglect the effect of bending, depending on whether bending due to the presence of the patch is deemed to be significant at the repair location or not.

It may be turned on to assess the contribution of bending to the total stresses at the repair location, and to study the effect of bending on the fatigue life of the patched structure.

It must be noted that "bending" in this case refers only to the bending induced by the repair patch on the plate.

3.9.2.5. Adhesive Properties

The user may specify the adhesive that is used in the repair by entering the name, shear modulus (GXY), and thickness of the adhesive. In addition, a variable called DEB, which characterizes the extent of the disbond in the adhesive in the region of the crack, must be specified. The disbond is assumed to be elliptical in shape, with the crack lying along the major axis of the ellipse. DEB is the aspect ratio of this ellipse. The value of DEB must be between 0 and 1.

3.9.2.6. The Patch Stiffness Indicator

Near the bottom of the dialog box, and spanning its width, lies the patch stiffness indicator. A diamond-shaped marker indicates the equivalent stiffness of the current patch as a percentage of the stiffness of the plate to which the repair is to be applied.

It is desirable for a composite repair patch to have an equivalent stiffness between 100% and 120% of the stiffness of the metallic substructure. In AFGROW, this region is considered "ideal," with the 70% - 100% and 120% - 150% ranges being allowable, and any value outside these ranges considered unacceptable. If the stiffness indicator shows a stiffness that is not acceptable, the program will not allow that design to be applied.

Every time any of the parameters are changed, the equivalent properties of the patch are recomputed based on laminate theory, and the stiffness indicator moves to the position corresponding to the new equivalent stiffness of the patch.

The patch stiffness indicator is intended as an aid to the user in monitoring the relative stiffnesses of the patch and the plate.

3.9.2.7. The Auto Design Feature

Using this feature selects the most suitable patch configuration for the current problem definition and updates all the controls on the repair dialog box to reflect the new values. Auto Design selects the patch material based on the maximum stress in the spectrum (boron for 25 KSI and above, graphite for 20–25 KSI and GLARE for below 20 KSI) and the thickness of the metal plate (GLARE for t < 1/16", graphite or boron for t ≥ 1/16"). Auto Design then determines an optimum number of plies that satisfies the stiffness requirement while maintaining laminate symmetry and a reasonable level of orthotropy (% of ±45° and 90° plies as outlined in section 3.10.2.5).

36

3.9.2.8. Other Controls

The "Critical SIF" dialog allows the user to control whether the critical stress intensity factor will be based on the patched structure or the unpatched structure, by selecting the appropriate toggle button. While this has no bearing on the patch design itself, it is used during fatigue crack propagation to determine the failure criteria.

"Show" buttons are used to select the plots that are to be displayed after the beta correction factors are computed. These include "Beta Correction Factor" plots and Stress Contour plots of the stresses in the patch and the adhesive.

3.9.3. Patch Design

After all the design parameters have been specified, the "Apply" button may be clicked to compute the beta correction factors. At this point the main AFGROW window displays a color-coded schematic of the ply orientations, and a list of the equivalent properties of the composite patch, which are computed using laminate theory, Figure 15.
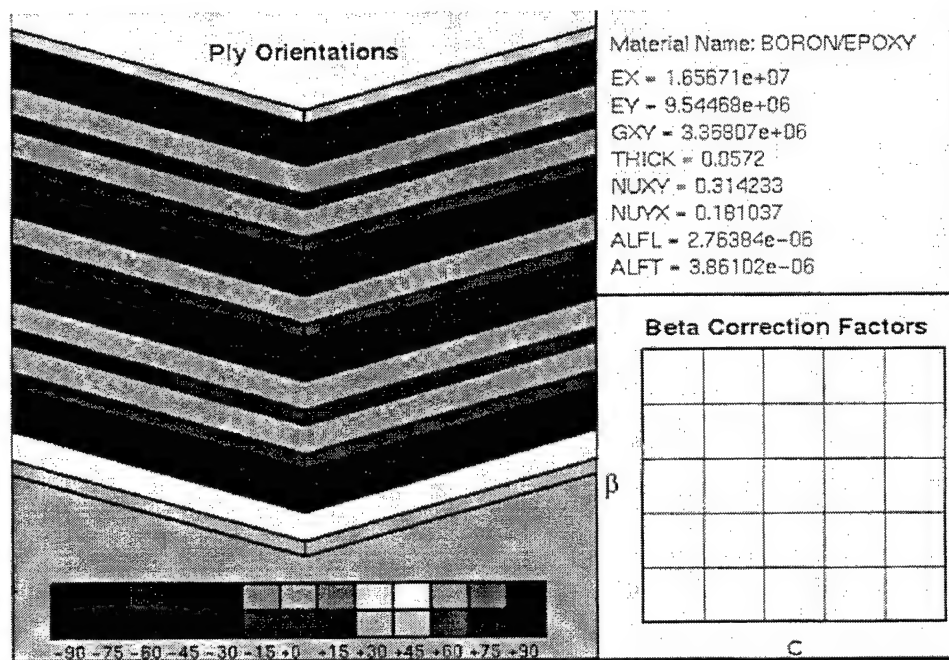
Figure 15. Ply Orientations and Equivalent Patch Properties

The beta correction factors are plotted on this screen as soon as they are computed. A bigger window that allows the user to overlay several beta correction factor plots is also displayed if the option is selected, Figure 16.
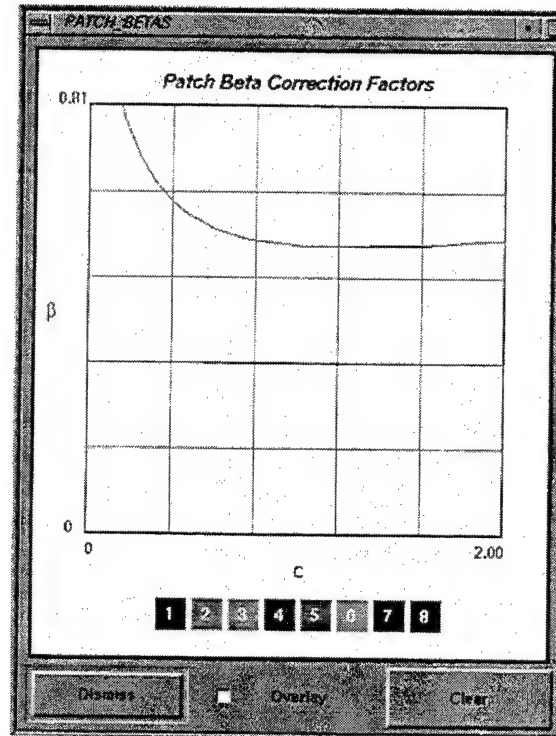
Figure 16. Beta Correction Factor Plot Window

The program also displays contours of the shear stresses in the adhesive and the stresses in the patch in a separate window, Figure 17:

38
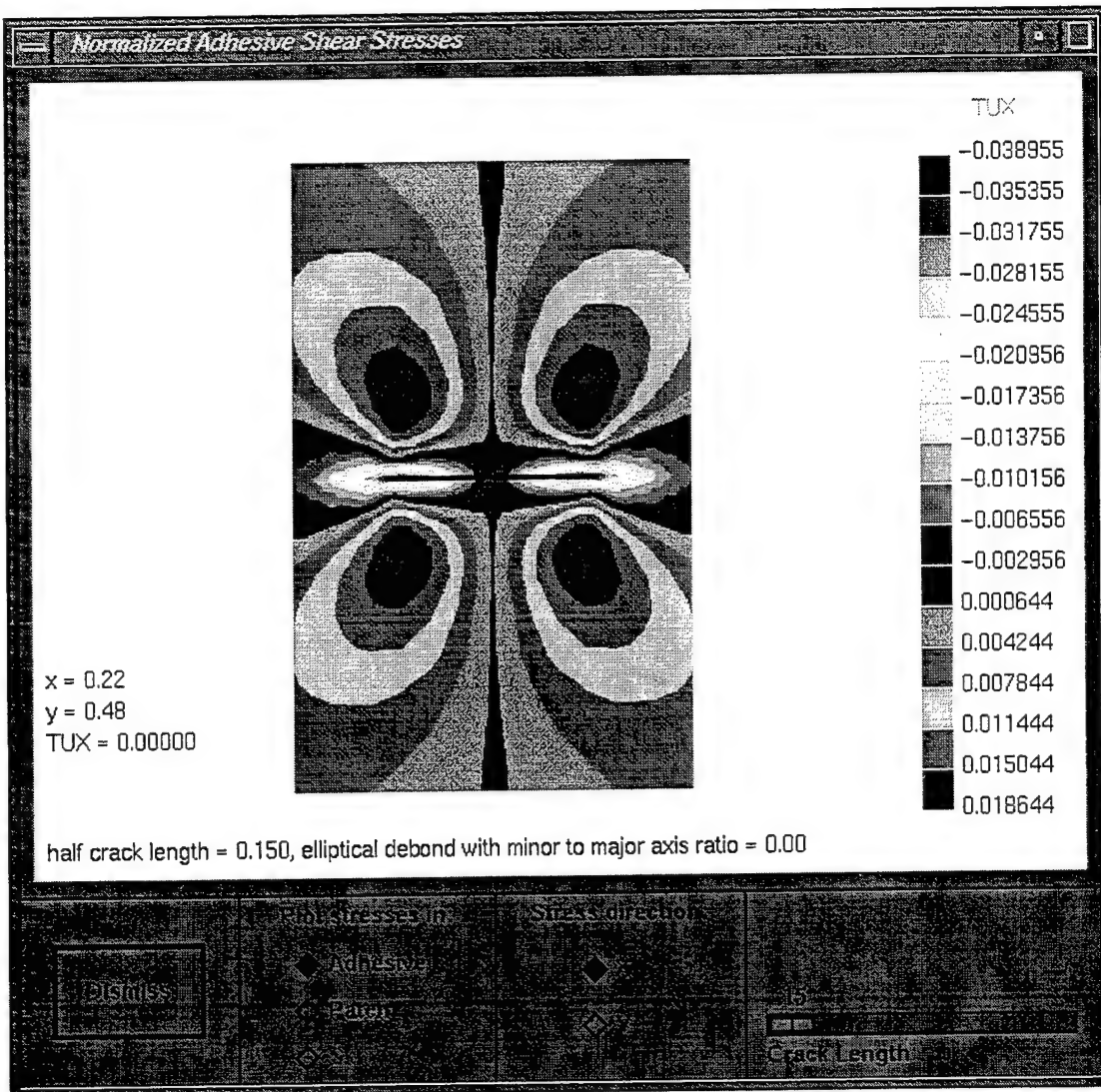
Figure 17. Stress Contour Window

This window includes toggle buttons to display either the adhesive or patch stresses. Currently, this release of AFGROW does not include the capability to display skin stresses and the toggle button is made inactive.

The slider bar at the lower right-hand corner controls the crack length. As the stresses in the patch and the adhesive redistribute continuously as the crack grows, this effect may be simulated by dragging the slider bar to the desired crack length.

It must be noted that the size of the plot area and the representation of the crack are kept constant when the crack length is changed using the slider bar. A display of the current coordinates and the stress at that point are provided to the left of the plot when the cursor is brought into the plot window. In addition, the stresses shown are for the center-cracked case and are not intended to reflect the actual stresses present for other

39

geometries. However, it is assumed that the Beta correction factors will provide a reasonable approximation of stress intensity for other geometries, especially if the cracks have grown a reasonable distance from the geometric configuration (notch, hole, etc.)

When a satisfactory patch design is achieved, the patch design dialog may be dismissed. At this point, a representation of the patch on the plate is displayed in the main window as shown in Figure 18.
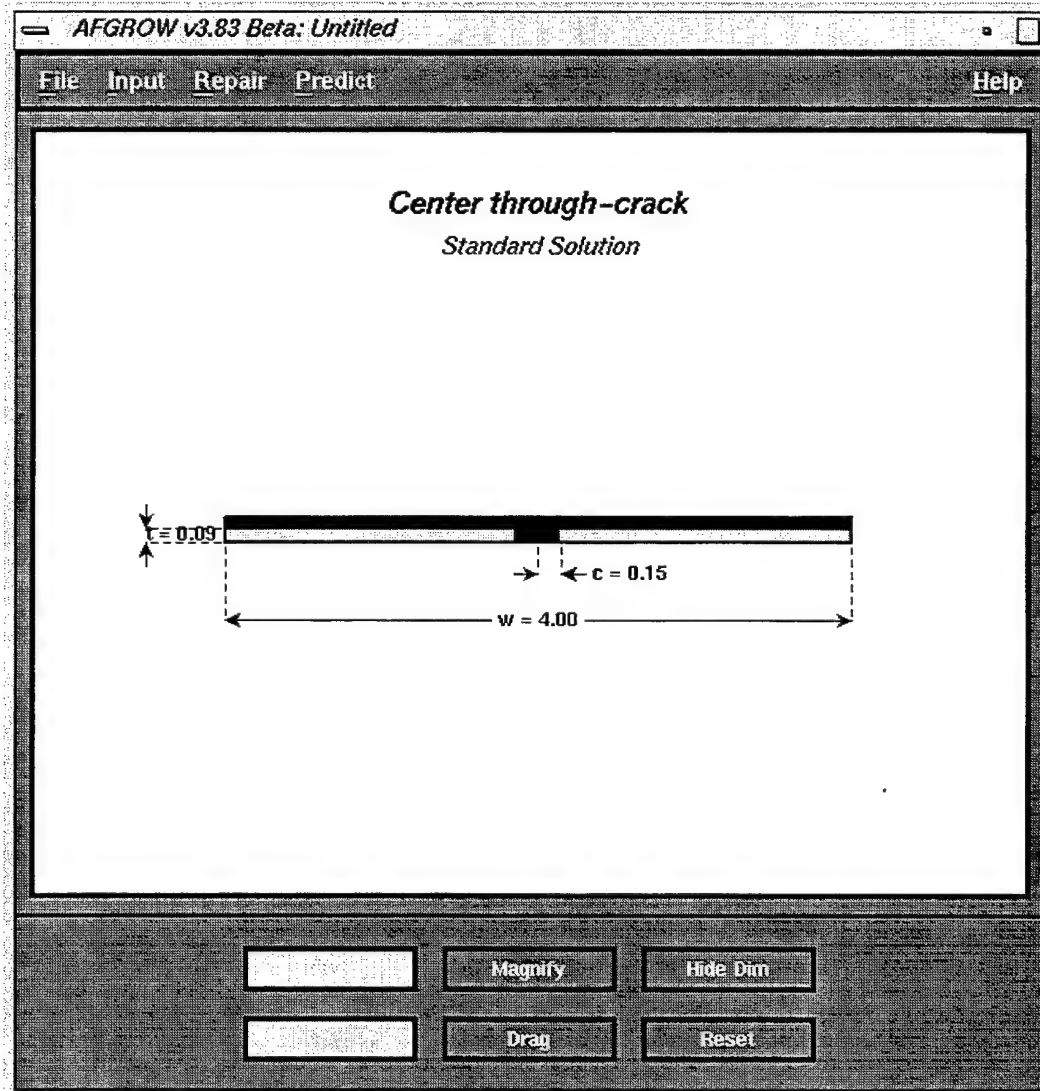
Figure 18. Main Window Showing Applied Patch

All subsequent crack growth analyses will include the effect of the patch until it is deleted using the "Dismiss" option in the Repair menu.

The patch is automatically deleted when the model configuration, dimensions, or material properties are changed. This is because the stored beta factors are design specific and no longer valid.

The effect of different patch designs on fatigue crack growth life may be observed by overlaying the crack growth plots. Other features of the code, such as retardation models, residual stress capability, and extreme environment effects may be used simultaneously with the composite repair capability.

4. WEIGHT FUNCTION DEVELOPMENT

Durability and strength evaluation of notched and cracked structural elements requires the calculation of stress intensity factors for cracks located in regions characterized by complex stress fields. This is particularly true for cracks emanating from notches and other stress concentration regions that might be frequently found in mechanical and structural components. In the case of engine components, complex stress distributions are often due to temperature effects. The existing stress intensity factor handbook solutions are not sufficient in such cases due to the fact that most of them have been derived for simple geometry and loading configurations. The variety of notch and crack configurations and the complexity of stress fields occurring in engineering practice require more efficient tools for calculating stress intensity factors than the large but nevertheless limited number of currently available ready made solutions obtained for a few specific geometry and load combinations.

Therefore, methods were developed for the efficient calculation of stress intensity factors for cracks in complex stress fields by using the weight function approach.

4.1. Technical Background

Most of the existing methods of calculating stress intensity factors require a separate analysis for each load and geometry configuration. The weight function method developed by Bueckner [27] and Rice [28] simplifies considerably the determination of stress intensity factors. If the weight function is known for a given cracked body, the stress intensity factor due to any load system applied to the body can be determined by using the same weight function. Therefore, there is no need to derive a ready made stress intensity factor for each load system and resulting internal stress distribution. The stress intensity factor can be obtained by multiplying the weight function, m(x,a), and the internal stress distribution $\sigma(x)$ in the prospective crack plane and integrating the product along the crack length 'a'.

The success of the weight function technique for calculating stress intensity factors lies in the possibility of using superposition. It can be shown [29] that the stress intensity factor for a crack body (Figure 19) subjected to the external loading, S, is the same as the stress intensity factor in a geometrically identical body with the local stress field, $\sigma(x)$, applied to the crack faces. The local stress field, $\sigma(x)$, in the prospective crack plane is due to the external load, S, and it is determined for the *uncracked* body by ignoring the presence of the crack.

42
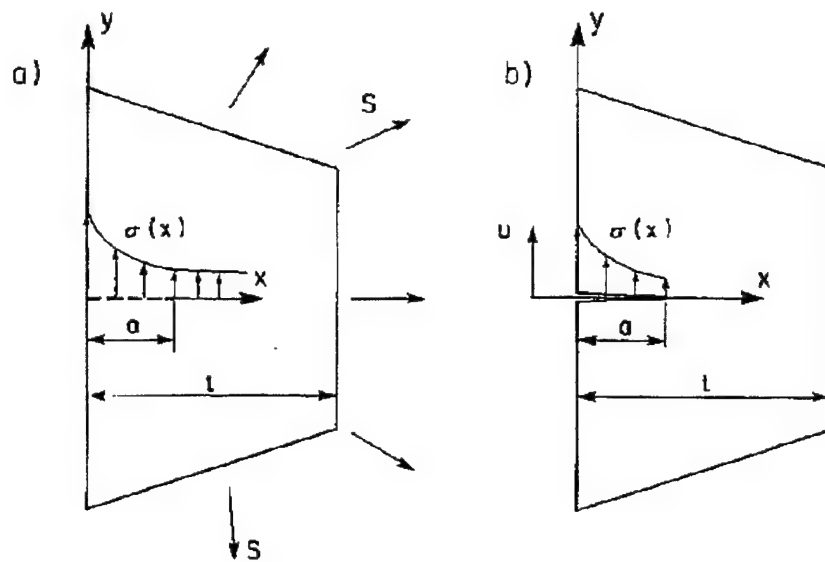
(a) Local stress field in an uncracked body subjected to external loading, S

(b) Geometrically identical body with local tractions, σ(x) applied to crack faces

Figure 19. Nomenclature and Concept of Superposition
(used with permission from G. Glinka)

The unique feature of the weight function method is that once the weight function for a particular cracked body is determined, the stress intensity factor for any loading system applied to the body can be calculated by simple integration of the product of the stress field, $\sigma(x)$, and the weight function, $m(x,a)$.

$$K = \int_0^a \sigma(x)\, m(x,a)\, dx \qquad (34)$$

The idea of using weight functions is illustrated in Figures 20a and 20b, where the through thickness crack is used as an example. The weight function, $m(x,a)$, can be interpreted as the stress intensity factor that results from a pair of splitting forces applied to the crack face at position x. Since the stress intensity factors are linearly dependent on the applied loads, the contributions from multiple splitting forces applied along the crack surface can be superposed and the resultant stress intensity factor can be calculated as the

43

sum of all individual load contributions. This results in the integral (34) of the product of the weight function, m(x,a), and the stress field, σ(x), for the case of continuously distributed stress field.

The Weight Function Approach to Calculation of Stress Intensity Factors

<u>Weight Function</u> - stress intensity factor, K, for a pair of splitting forces applied to crack surfaces
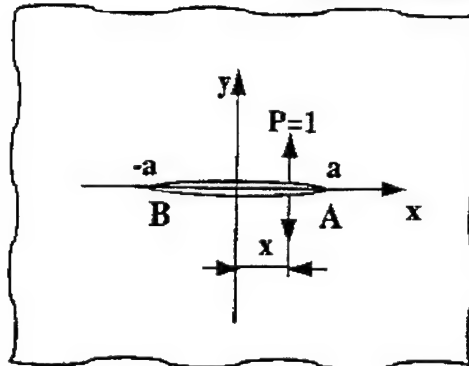
For a through crack in infinite plate:

$$m_A(x,a) = \frac{1}{\sqrt{\pi a}} \sqrt{\frac{a+x}{a-x}}$$

$$m_B(x,a) = -\frac{1}{\sqrt{\pi a}} \sqrt{\frac{a-x}{a+x}}$$

Stress intensity factors for crack crack tips A and B respectively:

$$K_A = m_A(x,a,P) = \frac{P}{\sqrt{\pi a}} \sqrt{\frac{a+x}{a-x}}$$

$$K_B = m_B(x,a,P) = \frac{P}{\sqrt{\pi a}} \sqrt{\frac{a-x}{a+x}}$$

Figure 20a. Weight Function and Stress Intensity Factors for a Through-Crack in an Infinite Plate
(used with permission from G.Glinka)

44

The Weight Function Approach to Calculation of Stress Intensity Factors
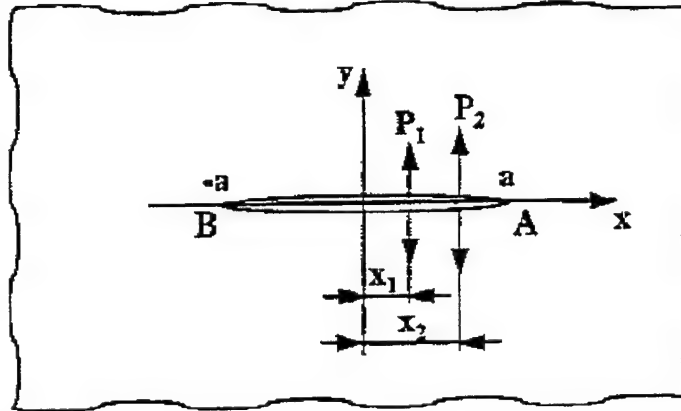
In the case of two forces, by using superposition

$$K_A = m_A(x_1, a, P_1) + m_A(x_2, a, P_2)$$

$$K_A = \frac{P_1}{\sqrt{\pi a}} \sqrt{\frac{x_1 + a}{a - x_1}} + \frac{P_2}{\sqrt{\pi a}} \sqrt{\frac{x_2 + a}{a - x_2}}$$

In the case of multiple forces

$$K_A = m(a, x_1, P_1) + m(a, x_2, P_2) + \ldots + m(a, x_i, P_i)$$

For the stress distribution σ(x)

$$K_A = \int_{-a}^{a} \sigma(x) m_A(x, a) dx$$

$$K_B = \int_{-a}^{a} \sigma(x) m_B(x, a) dx$$

Figure 20b. Weight Function and Stress Intensity Factors for a Through-Crack in an Infinite Plate Subjected to multiple Loads and/or Continuously Distributed Stress.
(used with permission from G. Glinka)

4.2. Universal Weight Functions for One-Dimensional Cracks

The weight function is dependent on the geometry only and in principle should be derived individually for each geometrical configuration. However, Glinka and Shen [30] have found that one general weight function expression can be used to approximate weight functions for a variety of geometrical configurations of cracked bodies with one dimensional cracks of Mode I:

$$m(x,a) = \frac{2}{\sqrt{2\pi(a-x)}}\left[1 + M_1\left(1-\frac{x}{a}\right)^{\frac{1}{2}} + M_2\left(1-\frac{x}{a}\right)^{1} + M_3\left(1-\frac{x}{a}\right)^{\frac{3}{2}}\right] \qquad (35)$$

The system of coordinates and the notation for through internal and edge cracks are given in Figure 21.
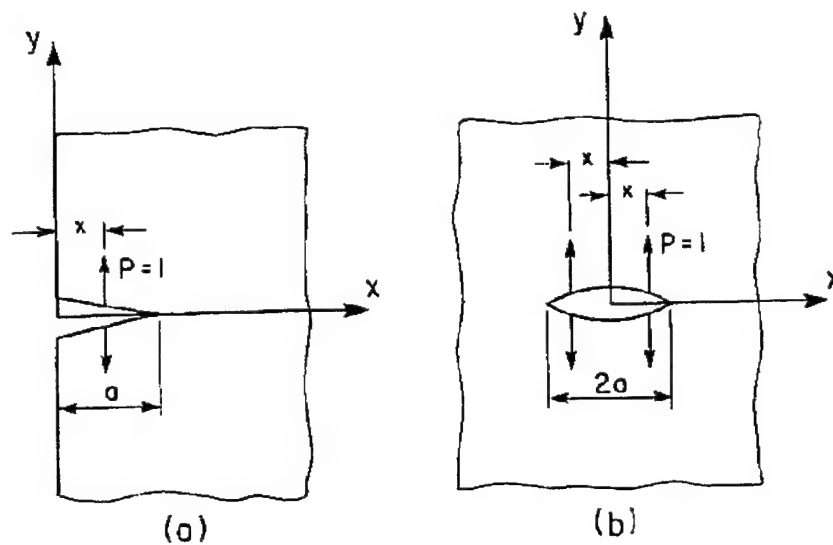
Figure 21. Single Edge Crack and Central Through-Crack Under Symmetrical Loading

In order to determine the weight function, m(x,a), of eq. (35) for a particular cracked body it is sufficient to determine [31] the three parameters M_1, M_2, and M_3. Because the weight function of eq. (35) is the same for all cracks then the same integration routine can be used for calculating stress intensity factors from eq. (34). Moreover, only a limited number of generic weight functions is needed to enable the determination of stress intensity factors for a large number of load and geometry configurations.

4.3. Universal Weight Functions for Two-Dimensional Part-Through Surface and Corner Cracks

In the case of 2-D cracks such as semielliptical and corner surface cracks in plates and cylinders, the stress intensity factor changes along the crack front. However, in most practical cases the deepest point A (Figure 22) and the surface point B are associated with the highest and the lowest value of the stress intensity factor along the crack front. Therefore, the weight functions for the points A and B have been derived [32] analogously to the universal weight function (35).

- For point A (Figure 22)

$$m_A(x,a,a/c,a/t) = \frac{2}{\sqrt{2\pi(a-x)}} \left[1 + M_{1A}\left(1 - \frac{x}{a}\right)^{\frac{1}{2}} + M_{2A}\left(1 - \frac{x}{a}\right)^{1} + M_{3A}\left(1 - \frac{x}{a}\right)^{\frac{3}{2}} \right] \quad (36)$$

- For point B (Figure 22)

$$m_B(x,a,a/c,a/t) = \frac{2}{\sqrt{\pi x}} \left[1 + M_{1B}\left(\frac{x}{a}\right)^{\frac{1}{2}} + M_{2B}\left(\frac{x}{a}\right)^{1} + M_{3B}\left(\frac{x}{a}\right)^{\frac{3}{2}} \right] \quad (37)$$

The weight functions $m_A(x,a)$ and $m_B(x,a)$ given above corresponding to the deepest and the surface points A and B, respectively, have been derived for one-dimensional stress fields (Figure 22), dependent on one variable , x, only.

48
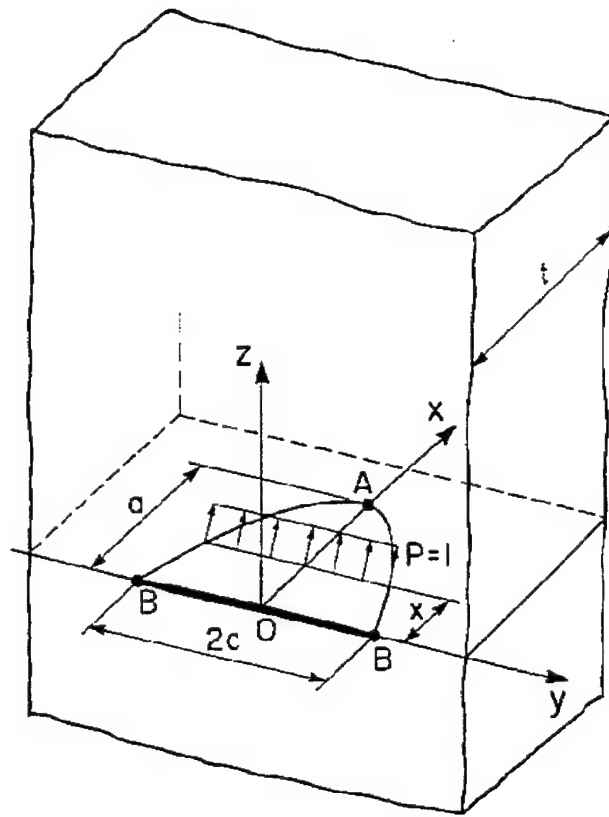
Figure 22. Semielliptical Surface Crack in an Infinite Plate of Finite Thickness, t

4.4. Sequence of Steps for Calculating Stress Intensity Factors Using Weight Functions

In order to calculate stress intensity factors using the weight function technique the following tasks need to be carried out:

- Determine stress distribution $\sigma(x)$ in the prospective crack plane using linear elastic analysis of uncracked body (Figure 19a), i.e., perform the stress analysis ignoring the crack and determine the stress distribution $\sigma(x) = \sigma_0\ f(S,x)$; where: σ_0 - nominal stress, x - coordinate, S - external load

- Apply the "uncracked" stress distribution, $\sigma(x)$, to the crack surfaces (Figure 19b) as tractions

49

- Choose appropriate generic weight function (i.e., choose appropriate M_1, M_2, and M_3 parameters).

- Integrate the product of the stress function $\sigma(x)$ and the weight function $m(x,a)$ over the entire crack length or crack surface, eq. (34).

4.5. Determination of Weight Functions

The derivation of the weight function of eq. (35) for a one-dimensional crack is essentially reduced to the determination of parameters M_1, M_2, and M_3. There are several methods available depending on the amount of information available as described in [31]. The most frequently used method based on two reference stress intensity factors is described below.

Supposing that two reference stress intensity solutions K_{r1} and K_{r2} for two different stress fields $\sigma_{r1}(x)$ and $\sigma_{r2}(x)$, respectively, are known, a set of two equations can be written by using eqs. (34) and (35). The third equation necessary to determine parameters M_1, M_2, and M_3 can be formulated based on the knowledge of the crack surface slope [31,32] at the crack center (central through cracks) or from the crack surface curvature at the crack mouth (edge cracks). The three pieces of information result in three independent equations which can be used for the determination of unknown parameters M_1, M_2, and M_3:

- **Central Through Cracks Under Symmetric Loading** (Figure 21a)

$$K_{r1} = \int_0^a \sigma_{r1}(x) \frac{2}{\sqrt{2\pi(a-x)}} \left[1 + M_1\left(1-\frac{x}{a}\right)^{\frac{1}{2}} + M_2\left(1-\frac{x}{a}\right)^1 + M_3\left(1-\frac{x}{a}\right)^{\frac{3}{2}} \right] dx \quad (38)$$

$$K_{r2} = \int_0^a \sigma_{r2}(x) \frac{2}{\sqrt{2\pi(a-x)}} \left[1 + M_1\left(1-\frac{x}{a}\right)^{\frac{1}{2}} + M_2\left(1-\frac{x}{a}\right)^1 + M_3\left(1-\frac{x}{a}\right)^{\frac{3}{2}} \right] dx \quad (39)$$

$$\frac{\partial}{\partial x} \left\{ \frac{2}{\sqrt{2\pi(a-x)}} \left[1 + M_1\left(1-\frac{x}{a}\right)^{\frac{1}{2}} + M_2\left(1-\frac{x}{a}\right)^1 + M_3\left(1-\frac{x}{a}\right)^{\frac{3}{2}} \right] \right\} \Bigg|_{x=0} = 0 \quad (40)$$

50

- **Edge Cracks**

$$K_{r1} = \int_0^a \sigma_{r1}(x) \frac{2}{\sqrt{2\pi(a-x)}} \left[1 + M_1 \left(1 - \frac{x}{a} \right)^{\frac{1}{2}} + M_2 \left(1 - \frac{x}{a} \right)^1 + M_3 \left(1 - \frac{x}{a} \right)^{\frac{3}{2}} \right] dx \qquad (41)$$

$$K_{r2} = \int_0^a \sigma_{r2}(x) \frac{2}{\sqrt{2\pi(a-x)}} \left[1 + M_1 \left(1 - \frac{x}{a} \right)^{\frac{1}{2}} + M_2 \left(1 - \frac{x}{a} \right)^1 + M_3 \left(1 - \frac{x}{a} \right)^{\frac{3}{2}} \right] dx \qquad (42)$$

$$\frac{\partial^2}{\partial x^2} \left\{ \frac{2}{\sqrt{2\pi(a-x)}} \left[1 + M_1 \left(1 - \frac{x}{a} \right)^{\frac{1}{2}} + M_2 \left(1 - \frac{x}{a} \right)^1 + M_3 \left(1 - \frac{x}{a} \right)^{\frac{3}{2}} \right] \right\} \Bigg|_{x=0} = 0 \qquad (43)$$

The two reference cases can be obtained from the literature or they can be derived using finite element method. Most often available are the solutions for the uniform and linear stress distributions induced by simple tension or bending load and those cases were predominantly used to derive the weight functions listed below.

- **Semielliptical Surface and Corner Cracks**

The set of equations necessary for deriving M_{iA} parameters for the weight function corresponding to the deepest point A on the crack front (Figure 21) was found to be identical to the set of equations derived for the edge crack.

$$K_{r1}^A = \int_0^a \sigma_{r1}(x) \frac{2}{\sqrt{2\pi(a-x)}} \left[1 + M_{1A} \left(1 - \frac{x}{a} \right)^{\frac{1}{2}} + M_{2A} \left(1 - \frac{x}{a} \right)^1 + M_{3A} \left(1 - \frac{x}{a} \right)^{\frac{3}{2}} \right] dx \qquad (44)$$

$$K_{r2}^A = \int_0^a \sigma_{r2}(x) \frac{2}{\sqrt{2\pi(a-x)}} \left[1 + M_{1A} \left(1 - \frac{x}{a} \right)^{\frac{1}{2}} + M_{2A} \left(1 - \frac{x}{a} \right)^1 + M_{3A} \left(1 - \frac{x}{a} \right)^{\frac{3}{2}} \right] dx \qquad (45)$$

$$\frac{\partial^2}{\partial x^2} \left\{ \frac{2}{\sqrt{2\pi(a-x)}} \left[1 + M_{1A} \left(1 - \frac{x}{a} \right)^{\frac{1}{2}} + M_{2A} \left(1 - \frac{x}{a} \right)^1 + M_{3A} \left(1 - \frac{x}{a} \right)^{\frac{3}{2}} \right] \right\} \Bigg|_{x=0} = 0 \qquad (46)$$

In the case of the surface point B the first two equations were the same as previously and the additional equation was derived [32] by satisfying the condition that the weight function must vanish for x=0.

51

$$K_{r1}^B = \int_0^a \sigma_{r1}(x) \frac{2}{\sqrt{\pi x}} \left[1 + M_{1B} \left(\frac{x}{a} \right)^{\frac{1}{2}} + M_{2B} \left(\frac{x}{a} \right)^1 + M_{3B} \left(\frac{x}{a} \right)^{\frac{3}{2}} \right] dx \qquad (47)$$

$$K_{r2}^B = \int_0^a \sigma_{r2}(x) \frac{2}{\sqrt{\pi x}} \left[1 + M_{1B} \left(\frac{x}{a} \right)^{\frac{1}{2}} + M_{2B} \left(\frac{x}{a} \right)^1 + M_{3B} \left(\frac{x}{a} \right)^{\frac{3}{2}} \right] dx \qquad (48)$$

$$0 = 1 + M_{1B} + M_{2B} + M_{3B} \qquad (49)$$

The three unknown parameters M_i can be determined by simultaneously solving one of the set of equations presented above.

4.6.   Numerical Integration of the Weight Function and Calculation of Stress Intensity Factors

The calculation of stress intensity factors from the weight function requires integration of of the product "s(x)m(x,a)" along the crack length according to eq. (34). The weight function can always be written in the general form of eq.(36) or eq.(37). However, the stress distribution "s(x)" can take any form depending on the problem of interest. If the stress distribution is given in the form of a mathematical expression, analytical integration can be performed and closed form integrals of eq. (1) are sometimes feasible. However, very often the stress distribution "s(x)" is obtained from finite element calculations and the results are given as a series of stress values corresponding to a range of point of coordinate "x." Therefore, a numerical integration technique is needed for the integration of equation (34) and the calculation of stress intensity factors. Two methods of efficient integration of eq. (34) are described below.

4.6.1. Integration Using Centroids of Areas Under the Weight Function Curve

The integration method using the area centroids is based on the following theorem:
If m(x,a) and $\sigma(x)$ are monotonic and linear function, respectively, and both depend on variable x only, (Figure 23), then the integral (34) can be calculated from expression (47), representing the product of the area S under the curve m(x,a) and the value of the function $\sigma(X)$ corresponding to the coordinate x=X of the centroid C.

$$K = S * \sigma(X) \qquad (50)$$

The weight functions, m(x,a), are monotonic and nonlinear. The stress functions, $\sigma(x)$,

are usually nonlinear as well. Therefore, in order to apply the theorem above to the integral (34), the integration interval is divided into "n" subintervals in such a way that, the stress function $\sigma(x)$ is approximated by the secant line drawn between the end points of each subinterval Figure 22. Thus, the stress function $\sigma(x)$ over the subinterval "I," may be written in the form of eq. (51),

$$\sigma_i(x) = A_i x + B_i \quad \text{for } (x_i - 1) \le x \le x_i \tag{51}$$

where :

$$A_i = \frac{\sigma(x_i) - \sigma(x_{i-1})}{x_i - x_{i-1}} \quad \text{and } B_i = \sigma(x_i) - A_i x_i \tag{51a}$$

After substitution of expression (51) into eq. (34) and summation over all subintervals the following expression for the stress intensity factor can be derived.

$$K = \sum_{i=1}^{n} \int_{x_{i-1}}^{x_i} (A_i x + B_i) m(x,a) dx \tag{52}$$

Each integral in eq. (52) can be computed by using the simplified (Figure 23) integration method given in the form of eq. (50). Thus, the stress intensity factor, K, can be finally written in the form of expression (53).

$$K = \sum_{i}^{n} S_i * \sigma(X_i), \quad \text{where } i = 1,2,\ldots n \tag{53}$$

In order to calculate the stress intensity factor given in the form of eq. (53), it is necessary to calculate the areas S_i under the weight function curve $m(x,a)$, and the coordinates of their centroids, X_i. Both the areas S_i and the centroid coordinates X_i for each sub-interval can be calculated once in a general form based on the generalized weight function (35). However, they appear to be too lengthy for an easy hand calculation. Fortunately, further simplification of the integration routine is possible due to the fact that the weight functions are smooth within their ranges of integration. Therefore the procedure can be reversed (Figure 25) by calculating first the areas S_i^* under the stress function $\sigma(x)$ and the coordinates X_i^* of their centroid. Then the appropriate values of the weight function $m(X^*,a)$ can be calculated from expression (35). It is worth noting that in the case of the piece-wise approximation of the stress function, $\sigma(x)$, the areas S_i^* and the coordinates of their centroids, X_i^*, can be easily calculated from relations (54) and (55), respectively.

$$S_i^* = \frac{1}{2}\left[\sigma(x_i) + \sigma(x_{i-1})\right](x_i - x_{i-1}) \qquad (54)$$

$$X_i^* = x_i - \frac{(x_i - x_{i-1})\left[2\sigma(x_{i-1}) + \sigma(x_i)\right]}{3\left[\sigma(x_i) + \sigma(x_{i-1})\right]} \qquad (55)$$

Finally the stress intensity factor, K, is calculated from expression (56).

$$K = \sum_{i=1}^{n} S_i^* m(X_i^*, a) \qquad (56)$$

Thus, the numerical procedure for calculating the stress intensity factor using the integration method described above requires the calculation of appropriate parameters using equations (35) and (54-56). The method described above is recommended for quick approximate calculations with the help of a hand calculator.
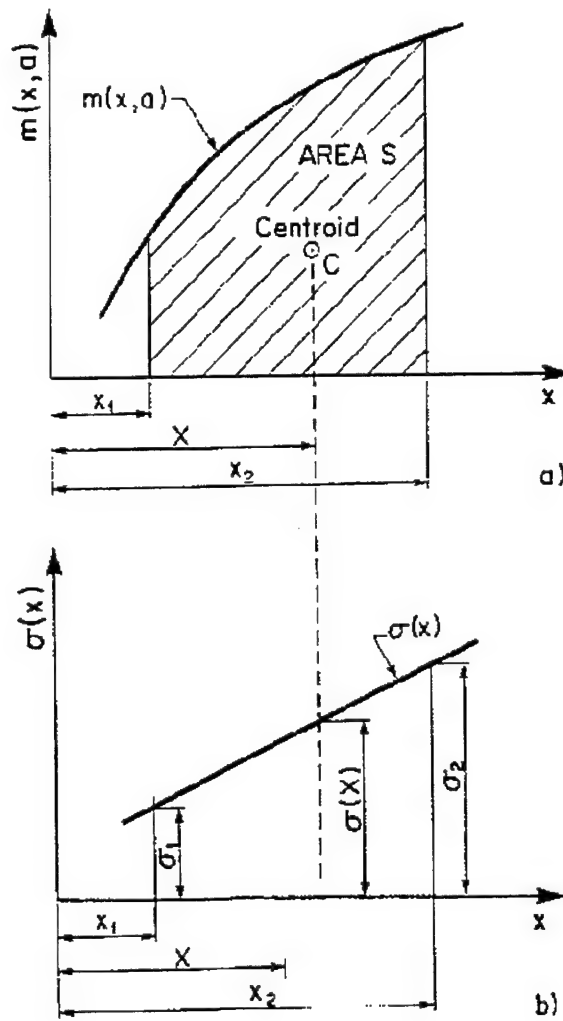
Figure 23. Graphical Representation of Simplified Integration of the Product of Two One-Dimensional Functions, a) Monotonic Nonlinear Weight Function m(x,a), b) Linear Stress Function, S(x)
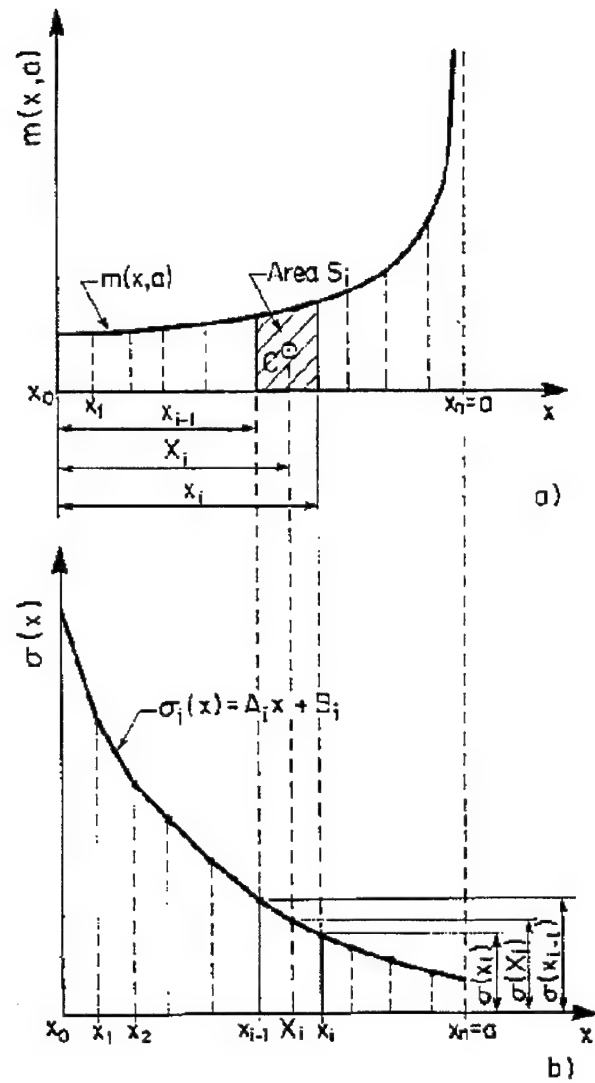
Figure 24. Application of the Simplified Integration Method to the Case of Nonlinear Stress Distribution; a) Weight Function m(x,a), b) Linearized Stress Function

56
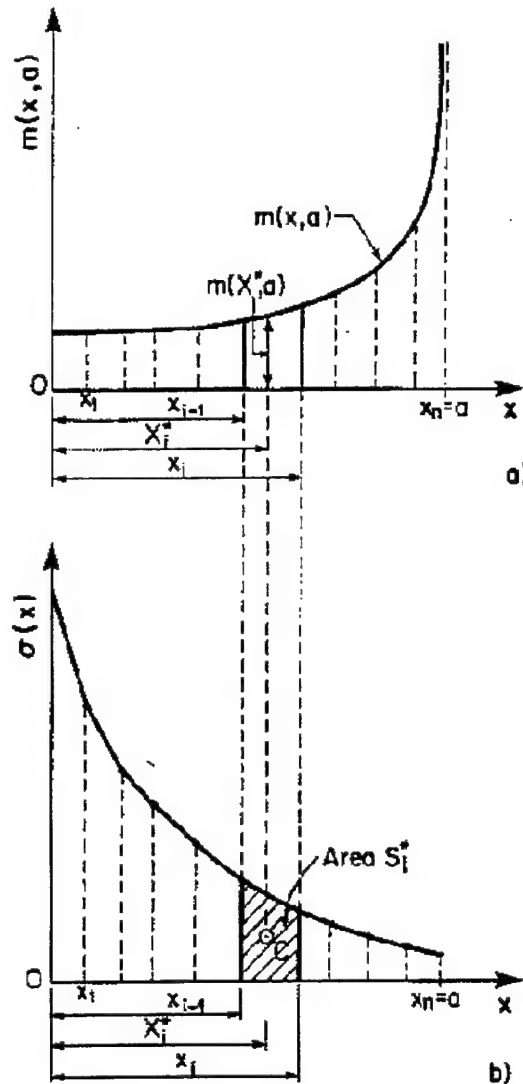
Figure 25. Integration Method Based on the Subareas and Centroids of the Linearized Piecewise Stress Function, a) Weight Function m(x,a), Linearized Piecewise Stress Function

4.6.2. Analytical Integration of the Linearized Piecewise Stress Distribution and the Weight Function

The integration technique described in Section 4.6.1 is convenient for hand calculator calculation when the stress distribution can be approximated by a few linear segments. However, the segments adjacent to the crack tip can not be large because the weight function tends to infinity near the crack tip and if the stress is the highest near the crack tip the method described above might be sometimes inaccurate. Moreover, in the case of stress distributions characterized by high gradients accurate approximation of the stress distribution requires relatively large number of linear pieces and the integration has to be

57

carried out with the help of a computer. However, the computer integration routine can also be significantly simplified because closed form solution to the integral (52) can be derived analytically for each linear piece (Figure 25) of the stress function s(x).

The stress function s(x) over the linear segment "i" can be given in the form of the linear equation (51). Thus the contribution to the stress intensity factor associated with the stress segment "i" can be calculated from eq. (34) after substituting appropriate expressions for the stress and the weight function. The solutions given below have been derived for the deepest and for the surface point of semielliptical crack using the weight function (36) and (37), respectively. The solution to one-dimensional cracks is the same as for the deepest point of semielliptical cracks.

- Deepest Point A (Figure 22)

$$K_i^A = \int_{x_{i-1}}^{x_i} (A_i x + B_i) \frac{2}{\sqrt{2\pi a\left(1 - \dfrac{x}{a}\right)}} \left[1 + M_{1A}\left(1 - \frac{x}{a}\right)^{\frac{1}{2}} + M_{2A}\left(1 - \frac{x}{a}\right)^{1} + M_{3A}\left(1 - \frac{x}{a}\right)^{\frac{3}{2}}\right] dx \quad (57)$$

- Surface Point B (Figure 22)

$$K_i^B = \int_{x_{i-1}}^{x_i} (A_i x + B_i) \frac{2}{\sqrt{2\pi x}} \left[1 + M_{1B}\left(\frac{x}{a}\right)^{\frac{1}{2}} + M_{2B}\left(\frac{x}{a}\right)^{1} + M_{3B}\left(\frac{x}{a}\right)^{\frac{3}{2}}\right] dx \quad (58)$$

The closed form expressions resulting from the integration of eq. (57) and eq. (58) are given below.

- Deepest Point A (Figure 22)

$$K_i^A = \sqrt{\frac{2}{\pi a}} \left[\begin{array}{l} \alpha_i \left(C_{i1} + M_{1A} C_{i2} + M_{2A} C_{i3} + M_{3A} C_{i4} \right) \\ \qquad\qquad + \beta_i \left(C_{i3} + M_{1A} C_{i4} + M_{2A} C_{i5} + M_{3A} C_{i6} \right) \end{array} \right] \quad (59)$$

where :

$$\alpha_i = B_i + a A_i \qquad \text{and} \qquad \beta_i = -a A_i$$

$$C_{i1} = 2a \left[\left(1 - \frac{x_{i-1}}{a} \right)^{\frac{1}{2}} - \left(1 - \frac{x_i}{a} \right)^{\frac{1}{2}} \right] \qquad C_{i2} = a \left[\left(1 - \frac{x_{i-1}}{a} \right)^{1} - \left(1 - \frac{x_i}{a} \right)^{1} \right]$$

$$C_{i3} = \frac{2a}{3} \left[\left(1 - \frac{x_{i-1}}{a} \right)^{\frac{3}{2}} - \left(1 - \frac{x_i}{a} \right)^{\frac{3}{2}} \right] \qquad C_{i4} = \frac{a}{2} \left[\left(1 - \frac{x_{i-1}}{a} \right)^{2} - \left(1 - \frac{x_i}{a} \right)^{2} \right]$$

$$C_{i5} = \frac{2a}{5} \left[\left(1 - \frac{x_{i-1}}{a} \right)^{\frac{5}{2}} - \left(1 - \frac{x_i}{a} \right)^{\frac{5}{2}} \right] \qquad C_{i6} = \frac{a}{3} \left[\left(1 - \frac{x_{i-1}}{a} \right)^{3} - \left(1 - \frac{x_i}{a} \right)^{3} \right]$$

Surface Point B (Figure 22)

$$K_i^B = \sqrt{\frac{2}{\pi a}}\left[\begin{array}{l}(\alpha_i + \beta_i)(D_{i1} + M_{1B}D_{i2} + M_{2B}D_{i3} + M_{3B}D_{i4}) \\ \qquad\qquad - \beta_i(D_{i3} + M_{1B}D_{i4} + M_{2B}D_{i5} + M_{3B}D_{i6})\end{array}\right] \quad (60)$$

where :

$$\alpha_i = B_i + aA_i \qquad \text{and} \qquad \beta_i = -aA_i$$

$$D_{i1} = 2a\left[\left(\frac{x_i}{a}\right)^{\frac{1}{2}} - \left(\frac{x_{i-1}}{a}\right)^{\frac{1}{2}}\right] \qquad D_{i2} = a\left[\left(\frac{x_i}{a}\right)^{1} - \left(\frac{x_{i-1}}{a}\right)^{1}\right]$$

$$D_{i3} = \frac{2a}{3}\left[\left(\frac{x_i}{a}\right)^{\frac{3}{2}} - \left(\frac{x_{i-1}}{a}\right)^{\frac{3}{2}}\right] \qquad D_{i4} = \frac{a}{2}\left[\left(\frac{x_i}{a}\right)^{2} - \left(\frac{x_{i-1}}{a}\right)^{2}\right]$$

$$D_{i5} = \frac{2a}{5}\left[\left(\frac{x_i}{a}\right)^{\frac{5}{2}} - \left(\frac{x_{i-1}}{a}\right)^{\frac{5}{2}}\right] \qquad D_{i6} = \frac{a}{3}\left[\left(\frac{x_i}{a}\right)^{3} - \left(\frac{x_{i-1}}{a}\right)^{3}\right]$$

Equations (59) and (60) can be used for calculating stress intensity contributions due to each linear piece of the stress distribution function by substituting appropriate values for a, x_{i-1}, x_i, A_i and B_i. The stress intensity factor K can be finally calculated as the sum of all contributions K_i associated with the linear pieces within the range of $0 = x = a$.

$$K = \sum_{i}^{n} K_i \qquad\qquad\qquad (61)$$

Thus, the integration can be reduced to the substitution of appropriate parameters into equations (59-60) and summation according to eq. (61). This makes it possible to develop very efficient numerical integration routines, which is important in the case of lengthy fatigue crack growth analyses.

4.7.   Implementation of Weight Function Methods into AFGROW

This section describes the adaptation of the Weight Function Solutions into the AFGROW program. It also describes the procedure required to apply a stress distribution to a weight function model configuration in the AFGROW program.

4.7.1. Selecting a Weight Function Stress Intensity Solution Model

To select a Weight Function Stress Intensity Solution model; go to the **Insert** menu; select **Model;** and then select **Weight Function Solutions** menu item. This will cause a **Model Configuration Dialog Box** (Figure 26) to appear on the screen.
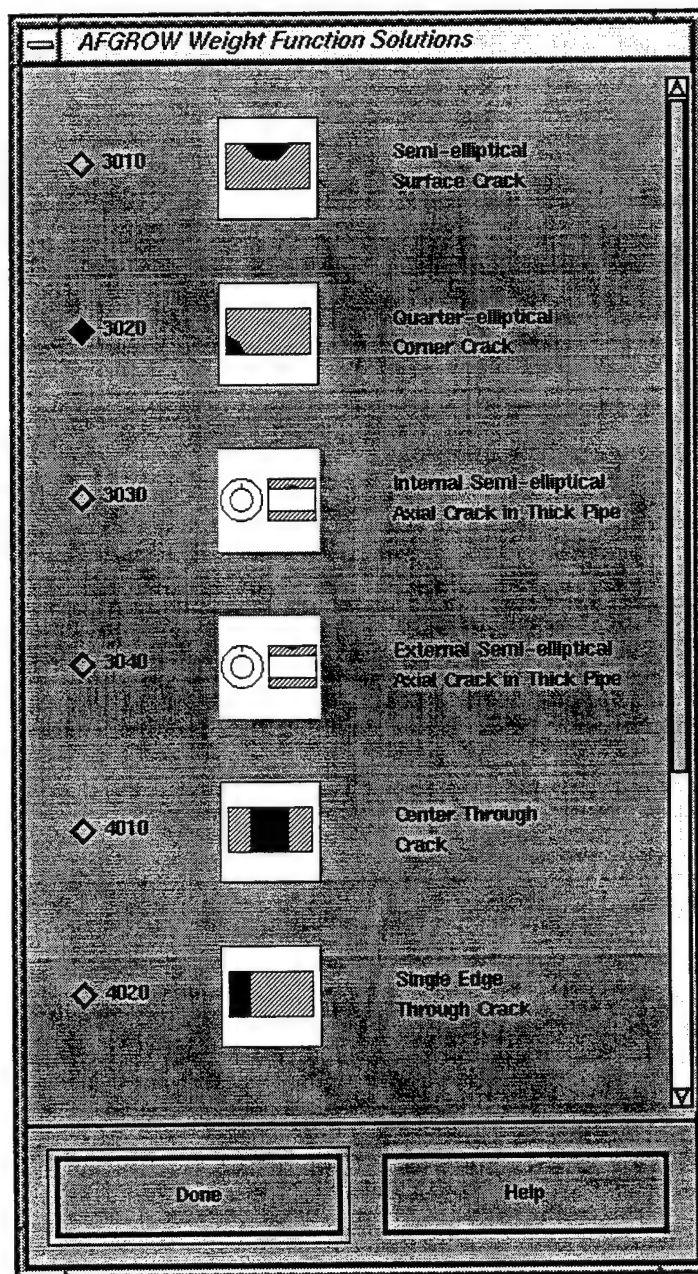
Figure 26. Weight Function Model Configuration Dialog

This dialog consists of a scrolled window that displays iconic representations of the nine Weight Function model configurations currently available in the AFGROW program. To

the right of each of these icons is a brief description of the corresponding model configuration. You may select any of the weight function solutions in this dialog by selecting the toggle button to the left of the model of interest. Depressing any toggle button causes any toggle button that is already depressed to pop out, ensuring that only one configuration is selected.

After selecting the desired configuration, the user must click the **DONE** button at the bottom of the dialog to choose that configuration for further analysis.

When a Weight Function Stress Intensity Solution model has been chosen, the title of the specimen configuration in the **Main Display Area** will include a "Weight Function Solution" statement (Figure 27).
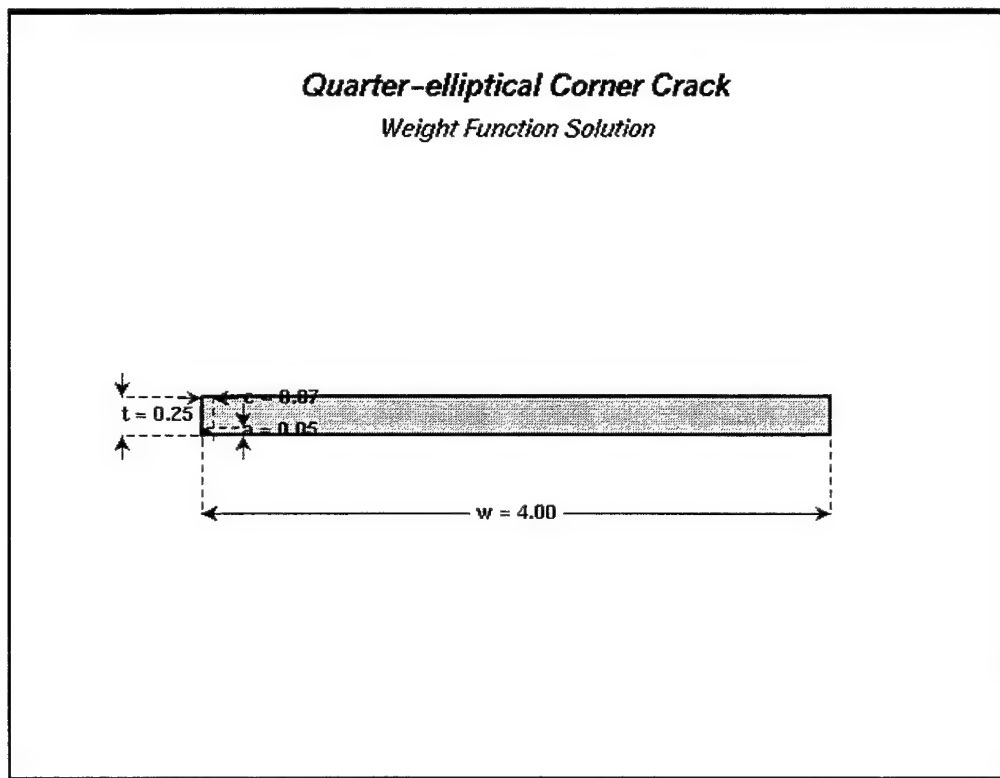
Figure 27. AFGROW Model Configuration Display

4.7.2. Entering a Stress Distribution

Each Weight Function Stress Intensity Solution Model requires an "uncracked" stress distribution along crack plane.

The AFGROW program uses a normalized stress distribution in the prospective 'a' crack plane (S_y) to calculate Stress Intensity Factors (SIF) for the part-through cracks (2-D

solutions); and a normalized stress distribution in prospective '*c*' crack plane (S_x) to calculate SIF for the through-cracks (1-D solutions).

Note that both solutions currently allow the input stress field to vary in the one direction only. When a part-through crack transitions into a through-the-thickness crack, the model is automatically converted into the appropriate 1-D case, and the applicable stress distribution is used to continue the life prediction.

It is recommended that the weight function stress distribution(s) should be normalized according to the stress value at the crack origin. However, it is important to remember that the load spectra are <u>also</u> normalized with respect to the maximum spectrum stress (usually maximum stress=1.0). Therefore, *it may be necessary to adjust the Stress Multiplication Factor (SMF) to account for the additional normalization of the weight function stress distribution.* The goal is to ensure that the proper stresses are being applied to the crack face.

To enter a stress distribution; first go to the **Insert** menu; click **Model,** and then select **Geometry & Parameters**. When the **Model Geometry & Parameters Dialog Box** appears, click on the **Stress Distribution** button. This action calls the **Weight Function Stress Distribution Dialog Box** (Figure 28), which contains several control groups.

A user may enter stress distributions along both '*a*' and '*c*' crack planes through a table of editable text fields in the scrolled window. The default assumes that only two sets of data are used. If the user wishes to use more than two sets, the desired number of the sets in the 'Y' and 'X' directions must be entered. In cases where the input stress distribution does not cover the extent of the specimen dimensions, the last input stress value is assumed for the remaining model's geometry. When a 1-D problem is active, the 'S_y' part of the stress distribution table is "grayed out."

At the bottom of the dialog, a **Preview Window** has been placed in order for a user to visualize the entered, tabular stress distribution. In order to plot the inputted stress distribution press the **Apply** button.

The two toggle buttons near the left side of the **Preview Window** are used to switch between plots of the 'S_x' and 'S_y' stress distributions.

Figure 28. Weight Function Stress Distribution Dialog

The functionality of other controls in **Weight Function Stress Distribution Dialog Box** are:

1. **NORMALIZE** button: Normalize stress distribution with respect to the stress value in the crack origin row.
2. **APPLY** button: Apply the current stress distribution to the chosen model.

64

3. **READ** button: Read files with a ".wfs" extension , which contain stress distribution information.

4. **SAVE** button: Save the current stress distribution to a file.

5. **DISMISS** button: Dismiss the dialog box.

5.   MODELING OF FATIGUE GROWTH OF MULTIPLE CRACKS

There are several ways of modeling the fatigue growth of multiple cracks. The two methods described briefly below are concerned with multiple cracks growing in the same plane.

Method 1:
The simplest method is to neglect the interference between cracks and to model only the coalescence of cracks as they approach each other. The coalescence of cracks is often model assuming the resultant dimensions of the final crack as a sum of all cracks joining each other as shown in Figure 29.
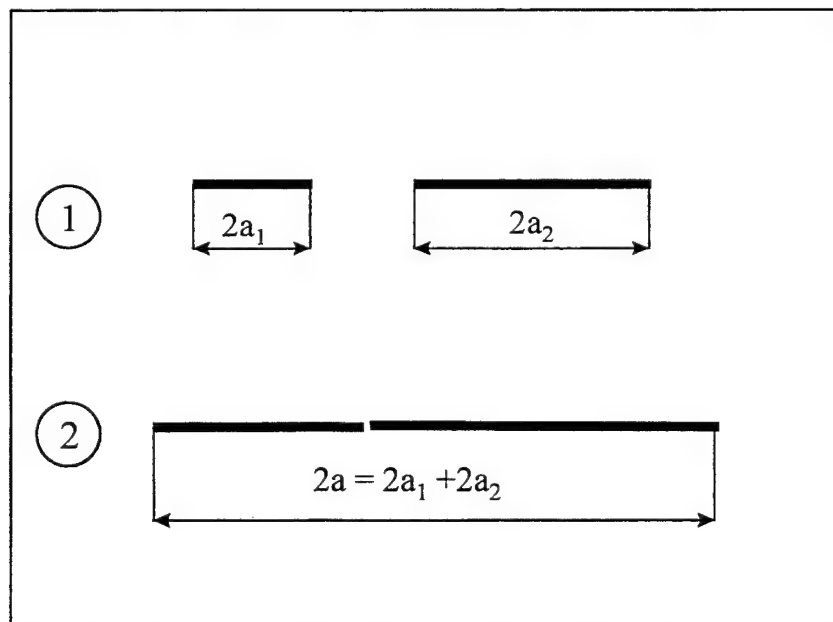
Figure 29. Coalescence of Two Through-Cracks in a Finite Width Plate

It is assumed in that type of fatigue crack growth modeling that cracks grow as they were single cracks with stress intensities at each tip calculated as for a single crack (stage 1). They subsequently join each other as soon as their tips come to contact with each other and from that point on the two cracks are considered to be transformed into one crack, with the dimension being the sum of appropriate lengths of all cracks in contact (stage 2). In the case of semielliptical surface cracks it is assumed that two or more cracks form one resultant crack as soon as their surface tips come into contact with each other (Figure 30). The resultant length is the sum of the surface lengths of all cracks in contact. The depth is assumed to be equal to the depth of the deepest crack among all cracks forming at a given moment, the single resultant crack.

66
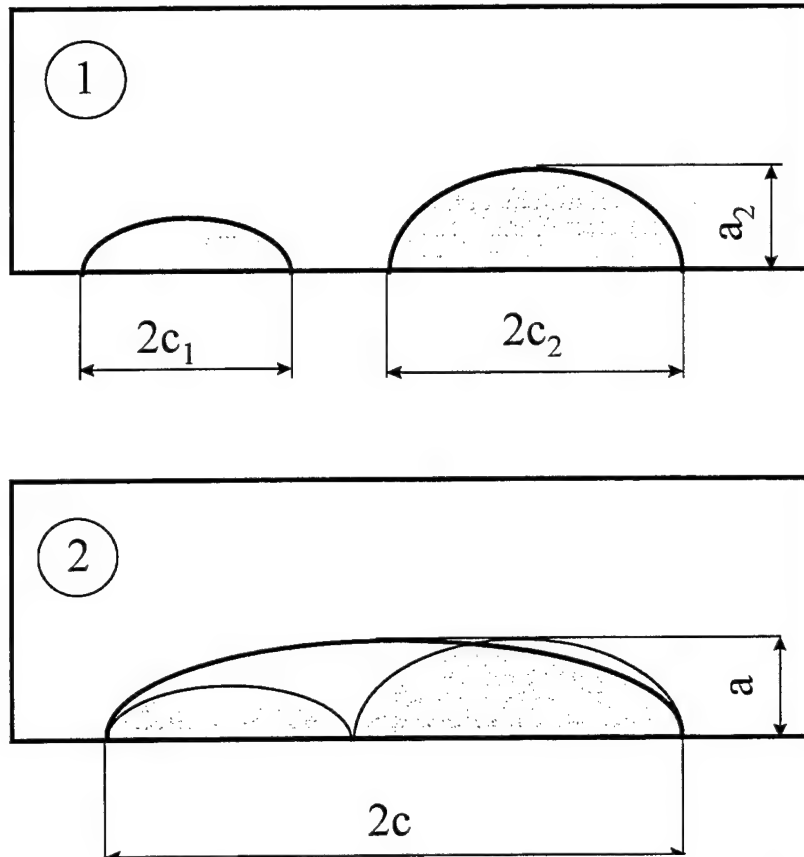
Figure 30. Coalescence of Two Semielliptical Surface Cracks in a Finite Thickness Plate.

Method 2:

The second method is based on the observation that fatigue cracks join each other very fast as soon as their cyclic plastic zones at the adjacent tips come into contact. It is assumed that the cracks grow independently of each other but they join immediately when the notch tip plastic zones come in contact as shown in Figure 31.
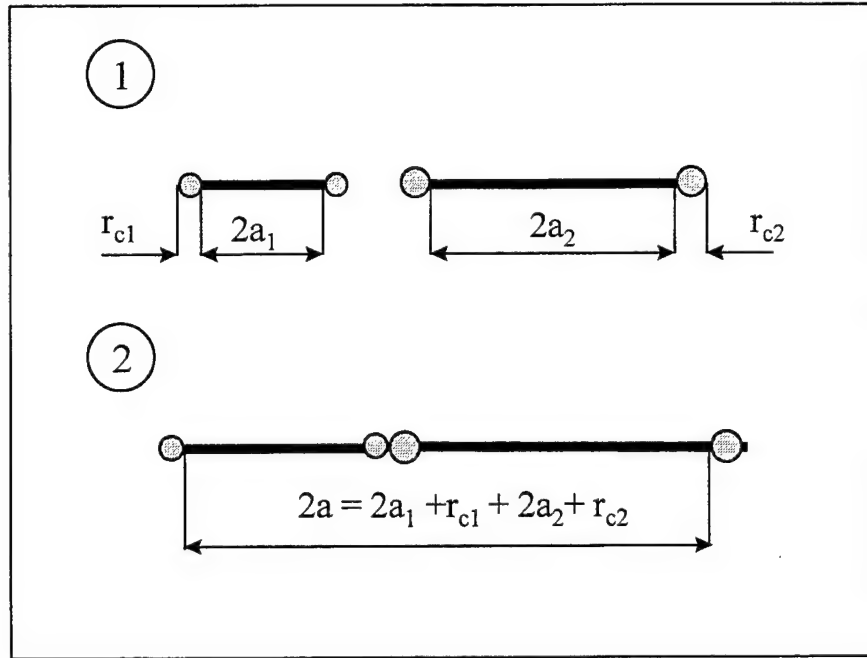
Figure 31. Coalescence of Fatigue Cracks Due to Sudden Jump Over the Cyclic Plastic Zones Coming in Contact with Each Other

Because the plastic zones contain highly damaged material it is assumed that the crack tips suddenly jump over the plastic zones as soon as they touch each other. Method #2 is more conservative because it assumes that the fatigue crack growth over the touching plastic zones occurs in one cycle. The resultant crack size is determined as the sum of the physical crack length of each crack plus the diameter of the cyclic plastic zone of each crack in contact. The diameter of the cyclic plastic zone in plane stress is calculated as:

$$r_c = \frac{1}{4\pi}\left(\frac{\Delta K}{\sigma_{ys}}\right)^2$$

The stress range and the plastic zone size are well defined in the case of constant amplitude loading. However, in the case of variable amplitude loading the stress range have to be defined by the user depending on the problem being analyzed. It may be the largest range in the loading history or it can be the average value determined at given crack size.

In the case of the surface semielliptical cracks it is assumed that the crack join each other as soon as their plastic cones on the surface come into contact. The resultant length on the surface is the sum of the length of each crack in contact plus the diameter of each cyclic plastic zone coming into contact with each other (Figure 32).

The cracks are considered to be "unaware" of each other until their plastic cyclic zones come into contact with each other. However, in order to model the coalescence of fatigue cracks, not only their growth has to be monitored continuously but their positions with respect to each other as well. Therefore, modeling of the growth of multiple fatigue cracks requires simultaneous monitoring of the growth and position of several cracks with respect to a chosen global system of coordinates. The task is intellectually not difficult but it may pose a labor intensive programming task and lengthy numerical calculations.
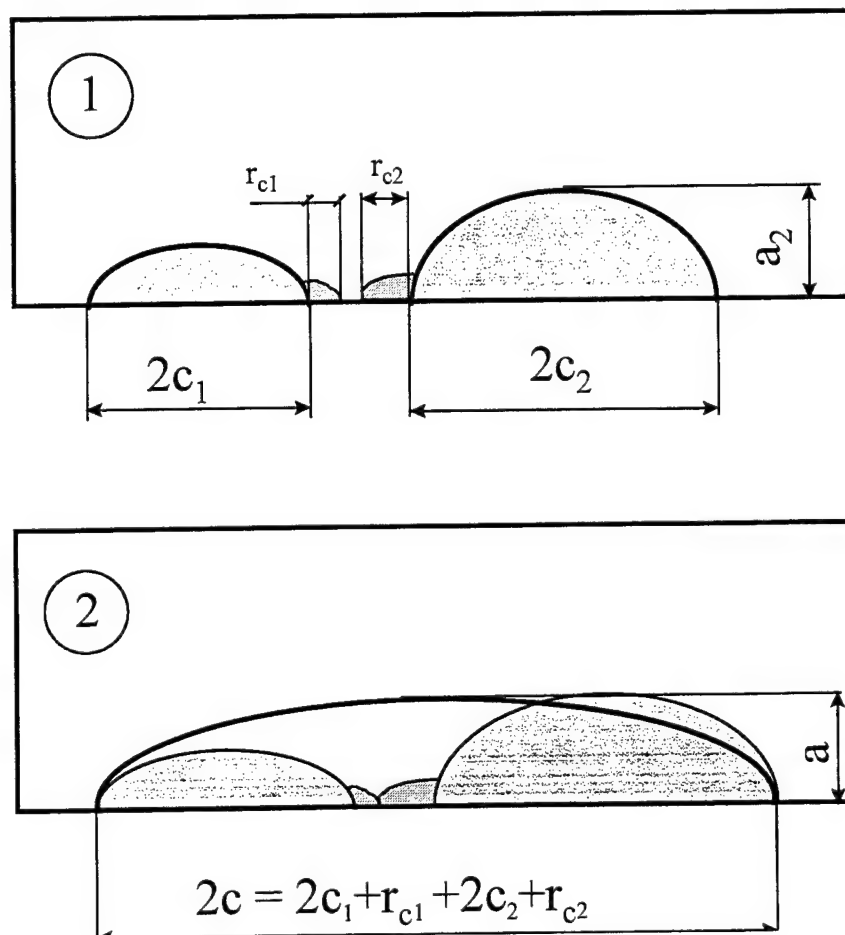
Figure 32. Coalescence of Two Semielliptical Cracks Over the Contacting Cyclic Plastic Zones

6. REFERENCES

[1] Boyd, K.L., Krishnan, S., "Evaluation of Aircraft Structural Repair/Analysis Codes," *WL-TR-97-?*, Flight Dynamics Directorate, Wright-Patterson Air Force Base, OH, November 1996.

[2] Ratwani, M. M., "Development of Bonded Composite Patch Repairs for Cracked Metal Structure," *Proceedings of the International Workshop on Defense Applications of Advanced Repair Technology for Metal And Composite Structures*, July 1981.

[3] Labor, J. D. and Ratwani, M. M., "Composite Patch Repair of Cracked Metal Structure," *Final Contract Report, Volumes I and II*, prepared for the U. S. Navy by Northrop Corporation, November 1980.

[4] Ratwani, M. M. and Kan, H. P., "Composite Patch Repair of Complex Structures," *Final Technical Report, Volumes I and II*, prepared for the U. S. Navy by Northrop, 1982.

[5] Kan, H. P., and Ratwani, M. M., "Composite Patch Repair of Thick Aluminum Structures," *Final Contract Report*, prepared for the U. S. Navy by Northrop, 1983.

[6] Baker , A.N., "Bonded Composite Repair of Metallic Aircraft Components," *AGARD Proceedings- Composite Repair of Military Aircraft Structures*, January 1995.

[7] Belason, E.B., "Status of Bonded Boron/Epoxy Doublers for Military and Commercial Aircraft," *AGARD Proceedings- Composite Repair of Military Aircraft Structures*, January 1995.

[8] Poole, P.,Young, A, and Ball, A.S., "Adhesively Bonded Composite Patch Repair of Cracked Aluminum Alloy Structures," *AGARD Proceedings- Composite Repair of Military Aircraft Structures*, January 1995.

[9] Cochran, J.B., Christian, T., and Hammond, D.O., "C-141 Repair of Metal Structures by Use of Composites," *Proceedings of ASIP Meeting*, 1988.

[10] "Repair Design Procedures," *RAAF Composite Materials and Adhesive Bonded Repairs Design Guide*.

[11]   Ratwani, M. M., "Characterization of Fatigue Crack Growth in Bonded Structures -Crack Growth Prediction in Bonded Structures," *AFFDL-TR-77-31, Volume I,* Air Force Flight Dynamics Laboratory, July 1977.

[12]   Ratwani, M. M., "Characterization of Fatigue Crack Growth in Bonded Structures -Analysis of Cracked Bonded Structures," *AFFDL-TR-77-31, Volume II,* Air Force Flight Dynamics Laboratory, July 1977.

[13]   Ratwani, M. M., and Kan,H. P., "Analysis of a Cracked Metallic Layer Bonded to an Orthotropic Composites Layer," *Report NOR 78-32,* Northrop Corporation, 1978.

[14]   Ratwani, M. M., and Kan, H. P., "Influence of Nonlinear Adhesive Behavior on Analysis of Cracked Adhesively Bonded Structures," *AIAA Journal,* Volume 18, pp. 1275-1278, 1980.

[15]   Keer, L. M., Lin, C. T., and Mura T.," Fracture Analysis of Adhesively Bonded Sheets," *Journal of Applied Mechanics,* Paper No. 76-WA/APM-12.

[16]   Rose, L. R. F., "A Cracked Plate Repaired by Bonded Reinforcement," *International Journal of Fracture,* 1981.

[17]   Jones, R., and Callinan, R. J., "Finite Element Analysis of Patched Cracks," *Journalof Structural Mechanics,* 1979.

[18]   "FRANC2D: A Two-Dimensional Crack Propagation Simulator," *NASA Contractor Report 4572,* March 1994.

[19]   "COMPAT-3D" Knowledge Systems Inc., May 1995.

[20]   Fredell R. S., "Damage Tolerance Repair Techniques for Pressurized Fuselage," *WL-TR-94-3134,* Flight Dynamics Directorate, Wright-Patterson Air Force Base, OH, June 1994.

[21]   Erdogan F. and Arin K., "A Sandwich Plate with a Part-Through and Debonding Crack," *Engineering Fracture Mechanics,* Vol. 4, 1972.

[22]   Muskhelishvilli, N. I., "Some Basic Problems of the Mathematical Theory of Elasticity," *Nordhoff Publication,* 1951.

[23]   Lekhnitskii, S. G., "Anisotropic Plates," *Gordon and Breach,* New York, 1968.

[24]   Erdogan F, "On the Stress Distribution in Plates with collinear cuts Under Arbitrary Loading," *Proceedings of the 4th U.S. National Congress of Applied Mechanics ASME,* pp. 547-553, 1962.

[25]   Roderick G. L, Everett Jr. R. A and Crews J. H, "Cyclic Debonding of Unidirectional Composite Bonded to Aluminum Sheet for Constant Amplitude Loading," *NASA Technical Note NASA TN D-8126*, January 1976.

[26]   Krishnan, S., Boyd, K.L., Harter, J.A."AFGROW User's Manual: Version 3.0.4," *WL-TM-96-3096*, Air Force Flight Dynamics Directorate, Wright-Patterson Air Force Base, OH, July 1995.

[27]   Bueckner, H.F., "A Novel Principle for the Computation of Stress Intensity Factors," *Zeitschrift fur Angewandte Mathematik und Mechanik*, 50, pp. 529-546, 1970.

[27]   Rice, J.R., "Some Remarks on Elastic Crack-Tip Stress Field," *International Journal of Solids and Structures,* 8, pp. 751-758, 1972.

[28]   Broek, D., *The Practical Use of Fracture Mechanics*, Kluwer, 1988.

[29]   Glinka G. and Shen, G., "Universal Features of Weight Functions for Cracks in Mode I," *Engineering Fracture Mechanics*, 40, pp. 1135-1146, 1991.

[30]   Shen, G. and Glinka, G., "Determination of Weight Functions from Reference Stress Intensity Factors," *Theoretical and Applied Fracture Mechanics*, 15, pp. 237-245, 1991.

[31]   Shen G., Glinka G., 1991, "Weight Functions for a Surface Semielliptical Crack in a Finite Thickness Plate," *Theor. Appl. Fract. Mech.*, Vol. 15, No. 2, pp. 247-255.

[32]   Fett, T., Mattheck C.and Munz, D., "On the Evaluation of Crack Opening Displacement from the Stress Intensity Factor," *Engineering Fracture Mechanics*, Vol. 27, No. 6, pp. 697-715, 1987.

[33]   Moftakhar, A. and Glinka, G., "Calculation of Stress Intensity Factors by Efficient Integration of Weight Functions", *Engineering Fracture Mechanics*, Vol. 43, No. 5, pp. 749–756, 1992.

APPENDIX A

NOTATION FOR WEIGHT FUNCTIONS

A   - crack length for one-dimensional cracks or crack depth (minor semi-axis) for semielliptical cracks

A_i, B_I - coefficients of the linearized stress function in the subinterval "i"

c   - crack length (major semiaxis) for semielliptical crack

C_{ij} - coefficients of the integrated weight function $m_A(x,a)$ in association with the linearized stress field s(x)

D_{ij} - coefficients of the integrated weight function $m_B(x,a)$ in association with the linearized stress field s(x)

K   - stress intensity factor

K_I - mode I stress intensity factor (general)

K_0^A - mode I reference stress intensity factor for the deepest point A of a crack under the uniform stress field

K_0^B - mode I reference stress intensity factor for the surface point B of a crack under the uniform stress field

K^A - mode I stress intensity factor for the deepest point A on the crack front

K^B - mode I reference stress intensity factor for the surface point B on the crack front

M_i - parameters of the weight function (i = 1, 2, 3)

M_{iA} - coefficients of the weight functions for the deepest point A (i= 1,2,3)

M_{iB} - coefficients of the weight functions for the surface point B (i= 1,2,3)

m(x,a)   - weight function

$m_A(x,a)$ - weight function for the deepest point A of a crack

$m_B(x,a)$ - weight function for the surface point B of a crack

S   - area under a monotonic curve m(x,a)

S_i^* - area under the linearized stress function s(x) corresponding to the subinterval "i"

S_i - area under the weight function curve m(x,a) corresponding to the sub-interval "i"

Q   - the semielliptical crack shape factor: $Q = 1 + 1.464(a/c)^{1.65}$ for a/c < 1

t   - wall thickness of a cylinder or plate thickness

x   - the local, through the thickness coordinate along the crack depth

X   - coordinate x of the centroid of the area S

X_i - coordinate x of the centroid of the area S_i corresponding the sub-interval "i"

X_i^* - coordinate x of the centroid of the area S_i^* corresponding to the sub-interval "i"

$\sigma(x)$ - stress distribution

$\sigma(x_i)$ - value of stress function at $x = x_i$

$\sigma(X)$ - value of stress function at $x = X$

$\sigma_\rho(x)$ - a reference stress distribution

Y_{nA} - the geometric stress intensity correction factor for the deepest point A

Y_{nB} - the geometric stress intensity correction factor for the surface point B

WEIGHT FUNCTIONS FOR CRACKS IN PLATES & DISKS

The weight functions are given in the form of expressions describing the M_i parameters as functions of crack dimensions and geometry of the cracked body. Given are the range of application, the accuracy and the source of the reference stress intensity factors for each set of parameters M_i including the generic geometry of the crack body.

Through-Crack in an Infinite Plate Subjected to Symmetrical Loading.

WEIGHT FUNCTION (Figure 33a):

$$m(x,a) = \frac{2}{\sqrt{2\pi(a-x)}}\left[1 + M_1\left(1-\frac{x}{a}\right)^{\frac{1}{2}} + M_2\left(1-\frac{x}{a}\right)^1 + M_3\left(1-\frac{x}{a}\right)^{\frac{3}{2}}\right]$$

PARAMETERS:

$M_1 = 0.0698747$

$M_2 = -0.0904839$

$M_3 = 0.427203$

ACCURACY: Max. error less than 1% when compared to exact solution
REFERENCES:

- weight function:
Glinka G., Shen G., 1991, "Universal Features of Weight Functions for Cracks in Mode I," *Engng. Fract. Mech,* Vol. 40, No. 6, pp. 1135-1146.

- reference data:
Tada H., Paris P. C., Irwin G.R., 1985, *The Stress Analysis of Cracks Handbook,* 2nd ed., Paris Productions Inc., St. Louis, Missouri, pp. 5.11-5.11a.
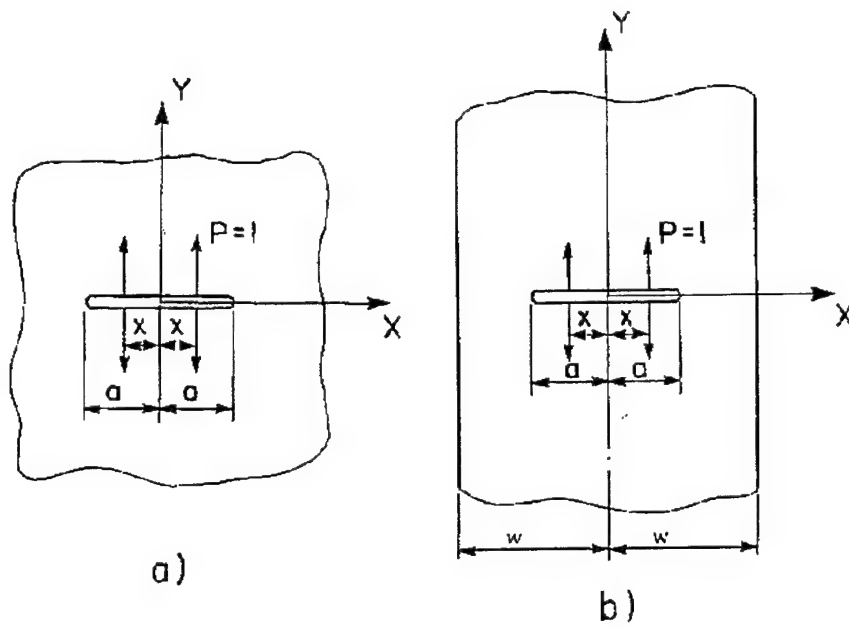
Figure 33. a) Through-Crack in an Infinite Plate Subjected to Symmetrical Loading; b) Central Through-Crack in a Finite Width Plate Subjected to Symmetrical Loading

Central Through-Crack in a Finite Width Plate Subjected to Symmetric Loading

WEIGHT FUNCTION (Figure 33b):

$$m(x,a) = \frac{2}{\sqrt{2\pi(a-x)}}\left[1 + M_1\left(1-\frac{x}{a}\right)^{\frac{1}{2}} + M_2\left(1-\frac{x}{a}\right)^{1} + M_3\left(1-\frac{x}{a}\right)^{\frac{3}{2}}\right]$$

PARAMETERS:

$$M_1 = 0.06987 + 0.40117\left(\frac{a}{w}\right) - 5.5407\left(\frac{a}{w}\right)^2 + 50.0886\left(\frac{a}{w}\right)^3 - 200.699\left(\frac{a}{w}\right)^4$$

$$+ 395.552\left(\frac{a}{w}\right)^5 - 377.939\left(\frac{a}{w}\right)^6 + 140.218\left(\frac{a}{w}\right)^7$$

$$M_2 = -0.09049 - 2.14886\left(\frac{a}{w}\right) + 22.5325\left(\frac{a}{w}\right)^2 - 89.6553\left(\frac{a}{w}\right)^3 + 210.599\left(\frac{a}{w}\right)^4$$

$$- 239.445\left(\frac{a}{w}\right)^5 + 111.128\left(\frac{a}{w}\right)^6$$

$$M_3 = 0.427216 + 2.56001\left(\frac{a}{w}\right) - 29.6349\left(\frac{a}{w}\right)^2 + 138.40\left(\frac{a}{w}\right)^3 - 347.255\left(\frac{a}{w}\right)^4$$

$$+ 457.128\left(\frac{a}{w}\right)^5 - 295.882\left(\frac{a}{w}\right)^6 + 68.1575\left(\frac{a}{w}\right)^7$$

RANGE OF APPLICATION: $0 < a/w < 0.9$.
ACCURACY: Better than 1% when compared to the reference solution.
REFERENCES:

- weight function:
Moftakhar A., Glinka G., 1992, "Calculation of Stress Intensity Factors by Efficient Integration of Weight Functions," *Engng. Fract. Mech.*, Vol. 43, No. 5, pp. 749-756.

Glinka G., Shen G., 1991, "Universal Features of Weight Functions for Cracks in Mode I," *Engng. Fract. Mech.*, Vol. 40, No. 6, pp. 1135-1146.

- reference data:
Tada H., Paris P. C., Irwin G.R., 1985, *The Stress Analysis of Cracks Handbook*, 2nd ed., Paris Productions Inc., St. Louis, Missouri, pp. 2.1-2.2, 2.34.

Sih G., 1973, *Handbook of Stress Intensity Factors*, Institute of Fracture and Solid Mechanics, Lehigh University, Bethlehem, P.A.

Edge Crack in a Semi-Infinite Plate

WEIGHT FUNCTION (Figure 34a):

$$m(x,a) = \frac{2}{\sqrt{2\pi(a-x)}}\left[1 + M_1\left(1 - \frac{x}{a}\right)^{\frac{1}{2}} + M_2\left(1 - \frac{x}{a}\right)^{1} + M_3\left(1 - \frac{x}{a}\right)^{\frac{3}{2}}\right]$$

PARAMETERS:

$M_1 = 0.0719768$

$M_2 = 0.246984$

$M_3 = 0.514465$

ACCURACY: Max. error less than 1% when compared to the reference solution

REFERENCES:

- weight function:
Glinka G., Shen G., 1991, "Universal Features of Weight Functions for Cracks in Mode I," *Engng. Fract. Mech.*, Vol. 40, No. 6, pp. 1135-1146.

- reference data:
Tada H., Paris P. C., Irwin G.R., 1985, *The Stress Analysis of Cracks Handbook*, 2nd ed., Paris Productions Inc., St. Louis, Missouri, pp. 8.3-8.3a.

Sih G., 1973, *Handbook of Stress Intensity Factors*, Institute of Fracture and Solid Mechanics, Lehigh University, Bethlehem, P.A.
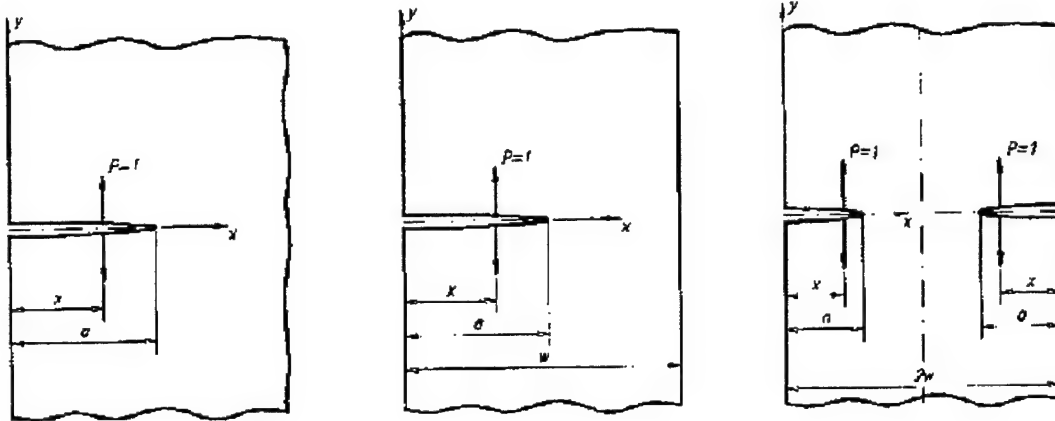
Figure 34. a) Edge Crack in a Semi-Infintite Plate; b) Edge Crack in a Finite Width Plate; c) Two Symmetrical Edge Cracks in a Finite Width Plate Subjected to Symmetrical Loading

Edge Crack in a Finite Width Plate

WEIGHT FUNCTION (Figure 34b):

$$m(x,a) = \frac{2}{\sqrt{2\pi(a-x)}}\left[1 + M_1\left(1-\frac{x}{a}\right)^{\frac{1}{2}} + M_2\left(1-\frac{x}{a}\right)^{1} + M_3\left(1-\frac{x}{a}\right)^{\frac{3}{2}}\right]$$

PARAMETERS:

$$M_1 = 0.0719768 - 1.51346\left(\frac{a}{w}\right) - 61.1001\left(\frac{a}{w}\right)^2 + 1554.95\left(\frac{a}{w}\right)^3 - 14583.8\left(\frac{a}{w}\right)^4 + 71590.7\left(\frac{a}{w}\right)^5$$

$$- 205384\left(\frac{a}{w}\right)^6 + +356469\left(\frac{a}{w}\right)^7 - 368270\left(\frac{a}{w}\right)^8 + 208233\left(\frac{a}{w}\right)^9 - 49544\left(\frac{a}{w}\right)^{10}$$

$$M_2 = 0.246984 + 6.47583\left(\frac{a}{w}\right) + 176.456\left(\frac{a}{w}\right)^2 - 4058.76\left(\frac{a}{w}\right)^3 + 37303.8\left(\frac{a}{w}\right)^4 - 181755\left(\frac{a}{w}\right)^5$$

$$+ 520551\left(\frac{a}{w}\right)^6 - 904370\left(\frac{a}{w}\right)^7 + 936863\left(\frac{a}{w}\right)^8 - 531940\left(\frac{a}{w}\right)^9 + 127291\left(\frac{a}{w}\right)^{10}$$

$$M_3 = 0.529659 - 22.3235\left(\frac{a}{w}\right) + 532.074\left(\frac{a}{w}\right)^2 - 5479.53\left(\frac{a}{w}\right)^3 + 28592.2\left(\frac{a}{w}\right)^4$$

$$- 81388.6\left(\frac{a}{w}\right)^5 + 128746\left(\frac{a}{w}\right)^6 - 106246\left(\frac{a}{w}\right)^7 + 35780.7\left(\frac{a}{w}\right)^8$$

RANGE OF APPLICATION: $0 < a/w < 0.9$.
ACCURACY: Better than 1% when compared to the reference solution.
REFERENCES:

- weight function:
Moftakhar A., Glinka G., 1992, "Calculation of Stress Intensity Factors by Efficient Integration of Weight Functions," *Engng. Fract. Mech.*, Vol. 43, No. 5, pp. 749-756.

Glinka G., Shen G., 1991, "Universal Features of Weight Functions for Cracks in Mode I," *Engng. Fract. Mech.*, Vol. 40, No. 6, pp. 1135-1146.

- reference data:
Tada H., Paris P. C., Irwin G.R., 1985, *The Stress Analysis of Cracks Handbook*, 2nd ed., Paris Productions Inc., St. Louis, Missouri, p. 2.27.

Kaya A. C.. Erdogan F., 1980, "Stress Intensity Factors and COD in an Orthotropic Strip," *Int. J. Fracture*, Vol. 16, pp. 171-190.

Two Symmetrical Edge Cracks in a Finite Width Plate Subjected to Symmetrical Loading

WEIGHT FUNCTION (Figure 34c):

$$m(x,a) = \frac{2}{\sqrt{2\pi(a-x)}}\left[1 + M_1\left(1-\frac{x}{a}\right)^{\frac{1}{2}} + M_2\left(1-\frac{x}{a}\right)^{1} + M_3\left(1-\frac{x}{a}\right)^{\frac{3}{2}}\right]$$

PARAMETERS:

$$M_1 = 0.08502 - 0.02230\left(\frac{a}{w}\right) - 1.41028\left(\frac{a}{w}\right)^3 + 4.64559\left(\frac{a}{w}\right)^3 + 19.6924\left(\frac{a}{w}\right)^4$$

$$-148.266\left(\frac{a}{w}\right)^5 + 336.837\left(\frac{a}{w}\right)^6 - 336.591\left(\frac{a}{w}\right)^7 + 127.009\left(\frac{a}{w}\right)^8$$

$$M_2 = 0.2234 - 0.6146\left(\frac{a}{w}\right) + 11.1687\left(\frac{a}{w}\right)^2 - 56.5326\left(\frac{a}{w}\right)^3 + 151.937\left(\frac{a}{w}\right)^4$$

$$-182.634\left(\frac{a}{w}\right)^5 + 86.4731\left(\frac{a}{w}\right)^6$$

$$M_3 = 0.4983 + 0.7512\left(\frac{a}{w}\right) - 10.5597\left(\frac{a}{w}\right)^2 + 47.9251\left(\frac{a}{w}\right)^3 - 115.933\left(\frac{a}{w}\right)^4$$

$$+131.976\left(\frac{a}{w}\right)^5 - 59.8893\left(\frac{a}{w}\right)^6$$

RANGE OF APPLICATION: $0 < a/w < 0.9$.
ACCURACY: Better than 1% when compared to the reference solution.
REFERENCES:

- weight function:
Moftakhar A., Glinka G., 1992, "Calculation of Stress Intensity Factors by Efficient Integration of Weight Functions," *Engng. Fract. Mech.*, Vol. 43, No. 5, pp. 749-756.

Glinka G., Shen G., 1991, "Universal Features of Weight Functions for Cracks in Mode I," *Engng. Fract. Mech.*, Vol. 40, No. 6, pp. 1135-1146.

- reference data:
Tada H., Paris P. C., Irwin G.R., 1985, *The Stress Analysis of Cracks Handbook*, 2nd ed., Paris Productions Inc., St. Louis, Missouri, p. 2.31.

Shallow Semielliptical Surface Crack in a Finite Thickness Plate (a/c < 1)

WEIGHT FUNCTION (Figure 35) - Deepest Point A:

$$m_A(x,a) = \frac{2}{\sqrt{2\pi(a-x)}}\left[1 + M_{1A}\left(1-\frac{x}{a}\right)^{\frac{1}{2}} + M_{2A}\left(1-\frac{x}{a}\right)^{1} + M_{3A}\left(1-\frac{x}{a}\right)^{\frac{3}{2}}\right]$$

PARAMETERS:

$$M_{1A} = \frac{2\pi}{\sqrt{2Q}}(2Y_0 - 3Y_1) - \frac{24}{5}$$

$$M_{2A} = 3$$

$$M_{3A} = \frac{6\pi}{\sqrt{2Q}}(2Y_1 - Y_0) + \frac{8}{5}$$

where:

$$Q = 1 + 1.464\left(\frac{a}{c}\right)^{1.65}$$

$$Y_0 = A_0 + A_1\left(\frac{a}{t}\right)^2 + A_2\left(\frac{a}{t}\right)^4 + A_3\left(\frac{a}{t}\right)^6$$

$$A_0 = 1.0929 + 0.2581\left(\frac{a}{c}\right) - 0.7703\left(\frac{a}{c}\right)^2 + 0.4394\left(\frac{a}{c}\right)^3$$

$$A_1 = 0.456 - 3.045\left(\frac{a}{c}\right) - 2.007\left(\frac{a}{c}\right)^2 + \frac{1}{0.147 + \left(\frac{a}{c}\right)^{0.688}}$$

$$A_2 = 0.995 - \frac{1}{0.027 + \left(\frac{a}{c}\right)} + 22.0\left[1 - \left(\frac{a}{c}\right)\right]^{9.953}$$

$$A_3 = -1.459 + \frac{1}{0.014 + \left(\frac{a}{c}\right)} - 24.211\left[1 - \left(\frac{a}{c}\right)\right]^{8.071}$$

and

$$Y_1 = B_0 + B_1\left(\frac{a}{t}\right)^2 + B_2\left(\frac{a}{t}\right)^4 + B_3\left(\frac{a}{t}\right)^6$$

$$B_0 = 0.4537 + 0.1231\left(\frac{a}{c}\right) - 0.7412\left(\frac{a}{c}\right)^2 + 0.460\left(\frac{a}{c}\right)^3$$

$$B_1 = -1.652 + 1.665\left(\frac{a}{c}\right) - 0.534\left(\frac{a}{c}\right)^2 + \frac{1}{0.198 + \left(\frac{a}{c}\right)^{0.846}}$$

$$B_2 = 3.148 - 3.126\left(\frac{a}{c}\right) - \frac{1}{0.041 + \left(\frac{a}{c}\right)} + 17.259\left[1 - \left(\frac{a}{c}\right)\right]^{9.286}$$

$$B_3 = -4.228 + 3.643\left(\frac{a}{c}\right) + \frac{1}{0.020 + \left(\frac{a}{c}\right)} - 21.924\left[1 - \left(\frac{a}{c}\right)\right]^{9.203}$$

WEIGHT FUNCTION (Figure 35) - Surface Point B

$$m_B(x,a) = \frac{2}{\sqrt{2\pi(a-x)}}\left[1 + M_{1B}\left(\frac{x}{a}\right)^{\frac{1}{2}} + M_{2B}\left(\frac{x}{a}\right)^{1} + M_{3B}\left(\frac{x}{a}\right)^{\frac{3}{2}}\right]$$

PARAMETERS:

$$M_{1B} = \frac{3\pi}{\sqrt{Q}}(5F_1 - 3F_0) - 8$$

$$M_{2B} = \frac{15\pi}{\sqrt{Q}}(2F_0 - 3F_1) + 15$$

$$M_{3B} = \frac{3\pi}{\sqrt{Q}}(10F_1 - 7F_0) - 8$$

where:

$$Q = 1 + 1.464\left(\frac{a}{c}\right)^{1.65}$$

$$F_0 = \left[C_0 + C_1\left(\frac{a}{t}\right)^2 + C_2\left(\frac{a}{t}\right)^4\right]\sqrt{\frac{a}{c}}$$

$$C_0 = 1.2972 - 0.1548\left(\frac{a}{c}\right) - 0.0185\left(\frac{a}{c}\right)^2$$

$$C_1 = 1.5083 - 1.3219\left(\frac{a}{c}\right) + 0.5128\left(\frac{a}{c}\right)^2$$

$$C_2 = -1.101 - \frac{0.879}{0.157 + \left(\frac{a}{c}\right)}$$

and

$$F_1 = \left[D_0 + D_1\left(\frac{a}{t}\right)^2 + D_2\left(\frac{a}{t}\right)^4\right]\sqrt{\frac{a}{c}}$$

$$D_0 = 1.2687 - 1.0642\left(\frac{a}{c}\right) + 1.4646\left(\frac{a}{c}\right)^2 - 0.7250\left(\frac{a}{c}\right)^3$$

$$D_1 = 1.1207 - 1.2289\left(\frac{a}{c}\right) + 0.5876\left(\frac{a}{c}\right)^2$$

$$D_2 = 0.190 - 0.608\left(\frac{a}{c}\right) + \frac{0.199}{0.035 + \left(\frac{a}{c}\right)}$$

RANGE OF APPLICATION: $0 = a/t = 0.8$ and $0 = a/c = 1.0$
ACCURACY: Better than 3% when compared to the FEM data.
REFERENCES:

- weight function:
Wang X., Lambert S. B., 1995, "Stress Intensity Factors for Low Aspect Ratio Semielliptical Surface Cracks in Finite-Thickness Plates Subjected to Non-uniform Stresses," *Engng. Fract. Mech.*, Vol. 51, No. 4, pp. 517-532.

Shen G., Glinka G., 1991, "Weight Functions for a Surface Semi-Elliptical Crack in a Finite Thickness Plate," *Theor. Appl. Fract. Mech.*, Vol. 15, No. 2, pp. 247-255 (this paper contains the older version of the weight function).

Shen G., Plumtree A., Glinka G., 1991, "Weight Function for the Surface Point of Semi-Elliptical Surface Crack in a Finite Thickness Plate," *Engng. Fract. Mech.*, Vol. 40, No. 1, pp. 167-176 (this paper contains the older version of the weight function).

- reference data:

Shiratori M., Miyoshi T., Tanikawa K., 1986, "Analysis of Stress Intensity Factors for Surface Cracks Subjected to Arbitrarily Distributed Surface Stress (2nd Report, Analysis and Application of Influence Coefficients for Flat Plates with a Semielliptical Surface Crack)," *Trans. JSME*, Vol. 52, pp. 390-398.

Gross B., Srawley J. E., 1965, "Stress Intensity Factor for Single-Edge-Notch Specimens in Bending or Combined Bending and Tension by Boundary Collocation of a Stress Function," *NASA TN, D-2603.*

Gross B., Srawley J. E., 1966, *Plane Strain Crack Toughness Testing of High Strength Metallic Materials, ASTM STP 410.*

Raju I. S., Newman J. C., 1979, "Stress Intensity Factors for a Wide Range of Semielliptical Surface Cracks in Finite Thickness Plate," *Engng. Fracture Mech.*, Vol. 11, pp. 817-829.

Newman J. C., Raju I. S., 1981, "An Empirical Stress Intensity Factor Equation for the Surface Crack," *Engng. Fracture Mech.*, Vol. 15, pp. 185-192.
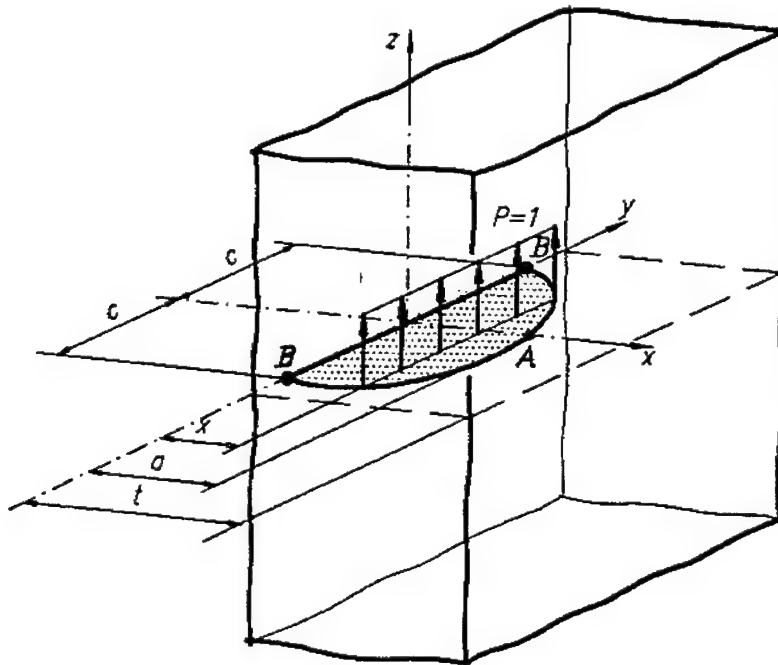
Figure 35. Shallow Semielliptical Surface Crack in a Finite Thickness Plate

Deep Semielliptical Surface Crack in a Finite Thickness Plate (a/c > 1)

WEIGHT FUNCTION (Figure 36) - Deepest Point A:

$$m_A(x,a) = \frac{2}{\sqrt{2\pi(a-x)}}\left[1 + M_{1A}\left(1-\frac{x}{a}\right)^{\frac{1}{2}} + M_{2A}\left(1-\frac{x}{a}\right)^{1} + M_{3A}\left(1-\frac{x}{a}\right)^{\frac{3}{2}}\right]$$

PARAMETERS:

$$M_{1A} = \frac{2\pi}{\sqrt{2Q}}(2Y_0 - 3Y_1) - \frac{24}{5}$$

$$M_{2A} = 3$$

$$M_{3A} = \frac{6\pi}{\sqrt{2Q}}(2Y_1 - Y_0) + \frac{8}{5}$$

where:

$$Q = \begin{cases} 1 + 1.464\left(\dfrac{a}{c}\right)^{1.65} & \text{for } 0 \le \dfrac{a}{c} \le 1.0 \\[4mm] \left[1 + 1.464\left(\dfrac{c}{a}\right)^{1.65}\right]\left(\dfrac{a}{c}\right)^{2} & \text{for } \dfrac{a}{c} > 1.0 \end{cases}$$

$$Y_0 = A_0 + A_1\left(\frac{a}{t}\right)^2 + A_2\left(\frac{a}{t}\right)^4$$

$$A_0 = 1.13047 - 0.12945\left(\frac{a}{c}\right) + 0.03526\left(\frac{a}{c}\right)^2$$

$$A_1 = 1.08461 - 1.01106\left(\frac{a}{c}\right) + 0.2454\left(\frac{a}{c}\right)^2$$

$$A_2 = 0.7855 + 0.5517\left(\frac{a}{c}\right) - 0.0934\left(\frac{a}{c}\right)^2$$

and

$$Y_1 = B_0 + B_1\left(\frac{a}{t}\right)^2 + B_2\left(\frac{a}{t}\right)^4$$

$$B_0 = 0.5044 - 0.2609\left(\frac{a}{c}\right) + 0.0529\left(\frac{a}{c}\right)^2$$

$$B_1 = 0.7259 - 0.6352\left(\frac{a}{c}\right) + 0.1492\left(\frac{a}{c}\right)^2$$

$$B_2 = -0.6459 + 0.4177\left(\frac{a}{c}\right) - 0.0731\left(\frac{a}{c}\right)^2$$

WEIGHT FUNCTION (Figure 36) - Surface Point B

$$m_B(x,a) = \frac{2}{\sqrt{2\pi(a-x)}}\left[1 + M_{1B}\left(1-\frac{x}{a}\right)^{\frac{1}{2}} + M_{2B}\left(1-\frac{x}{a}\right)^1 + M_{3B}\left(1-\frac{x}{a}\right)^{\frac{3}{2}}\right]$$

PARAMETERS:

$$M_{1B} = \frac{3\pi}{\sqrt{Q}}(5F_1 - 3F_0) - 8$$

$$M_{2B} = \frac{15\pi}{\sqrt{Q}}(2F_0 - 3F_1) + 15$$

$$M_{3B} = \frac{3\pi}{\sqrt{Q}}(10F_1 - 7F_0) - 8$$

where:

$$Q = \begin{cases} 1 + 1.464\left(\dfrac{a}{c}\right)^{1.65} & \text{for } 0 \le \dfrac{a}{c} \le 1.0 \\[4mm] \left[1 + 1.464\left(\dfrac{c}{a}\right)^{1.65}\right]\left(\dfrac{a}{c}\right)^{2} & \text{for } \dfrac{a}{c} > 1.0 \end{cases}$$

$$F_0 = \left[C_0 + C_1\left(\frac{a}{t}\right)^2 + C_2\left(\frac{a}{t}\right)^4 \right]\sqrt{\frac{a}{c}}$$

$$C_0 = 1.33469 - 0.29091\left(\frac{a}{c}\right) + 0.08125\left(\frac{a}{c}\right)^2$$

$$C_1 = 1.757673 - 1.5275\left(\frac{a}{c}\right) + 0.37185\left(\frac{a}{c}\right)^2$$

$$C_2 = 0.08429 + 0.4423\left(\frac{a}{c}\right) - 0.1894\left(\frac{a}{c}\right)^2$$

and

$$F_1 = \left[D_0 + D_1\left(\frac{a}{t}\right)^2 + D_2\left(\frac{a}{t}\right)^4 \right]\sqrt{\frac{a}{c}}$$

$$D_0 = 1.11855 - 0.2065\left(\frac{a}{c}\right) + 0.07817\left(\frac{a}{c}\right)^2$$

$$D_1 = 1.15312 - 0.98743\left(\frac{a}{c}\right) + 0.23315\left(\frac{a}{c}\right)^2$$

$$D_2 = 0.2246 - 0.4784\left(\frac{a}{c}\right) + 0.1864\left(\frac{a}{c}\right)^2$$

RANGE OF APPLICATION: $0 = a/t = 0.8$ and $0.6 = a \backslash c = 2.0$
ACCURACY: Better than 2% when compared to the reference FEM data.
REFERENCES:

- weight function:
Wang X., 1995, "Weight Functions for High Aspect Ratio Semielliptical Surface Cracks in Finite-Thickness Plates," University of Waterloo, to be published.

- reference data:
Shiratori M., Miyoshi T., Tanikawa K., 1986, "Analysis of Stress Intensity Factors for Surface Cracks Subjected to Arbitrarily Distributed Surface Stress (2nd Report, Analysis and Application of Influence Coefficients for Flat Plates with a Semielliptical Surface Crack)," *Trans. JSME*, Vol. 52, pp. 390-398.

Murakami Y., et al., 1992, *Stress Intensity Factors Handbook*, Vol. 3, Pergamon Press, pp. 588-590.
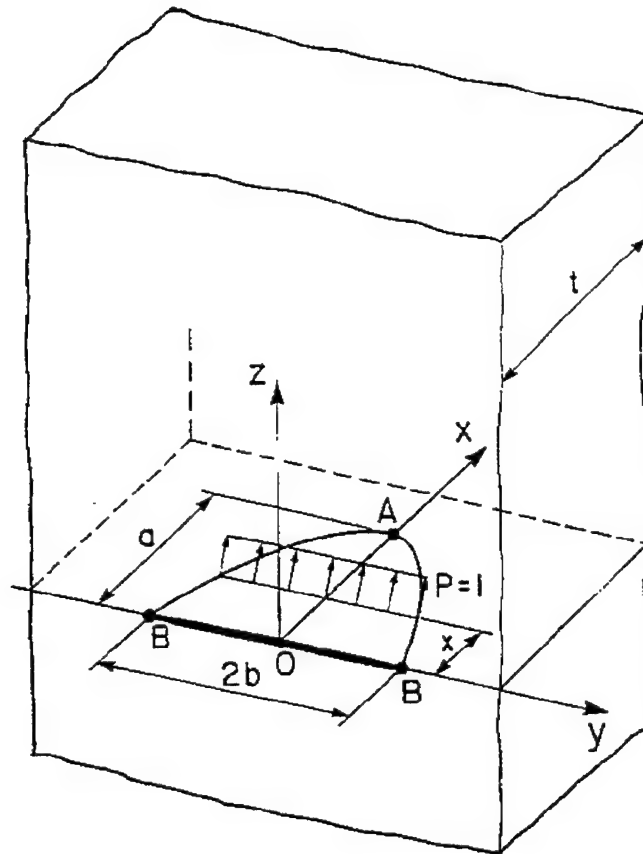
Figure 36. Deep Semielliptical Surface Crack in a Finite Thickness Plate.

Quarter-Elliptical Corner Crack in a Finite Thickness Plate

WEIGHT FUNCTION (Fig. 37) - Deepest Point A:

$$m_A(x,a) = \frac{2}{\sqrt{2\pi(a-x)}}\left[1 + M_{1A}\left(1-\frac{x}{a}\right)^{\frac{1}{2}} + M_{2A}\left(1-\frac{x}{a}\right)^{1} + M_{3A}\left(1-\frac{x}{a}\right)^{\frac{3}{2}}\right]$$

PARAMETERS:

$$M_{1A} = \frac{2\pi}{\sqrt{2Q}}(2Y_0 - 3Y_1) - \frac{24}{5}$$

$$M_{2A} = 3$$

$$M_{3A} = \frac{6\pi}{\sqrt{2Q}}(2Y_1 - Y_0) + \frac{8}{5}$$

where:

$$Q = 1 + 1.464\left(\frac{a}{c}\right)^{1.65}$$

$$Y_0 = A_0 + A_1\left(\frac{a}{t}\right) + A_2\left(\frac{a}{t}\right)^2 + A_3\left(\frac{a}{t}\right)^3 + A_4\left(\frac{a}{t}\right)^4$$

$$A_0 = 1.041 + 0.016\left(\frac{a}{c}\right) + 0.186\left(\frac{a}{c}\right)^2 - 0.111\left(\frac{a}{c}\right)^3$$

$$A_1 = -0.599 + 1.953\left(\frac{a}{c}\right) - 1.310\left(\frac{a}{c}\right)^2 - 0.028\left(\frac{a}{c}\right)^3$$

$$A_2 = 4.972 - 13.216\left(\frac{a}{c}\right) + 6.747\left(\frac{a}{c}\right)^2 + 1.918\left(\frac{a}{c}\right)^3$$

$$A_3 = -1.293 + 1.857\left(\frac{a}{c}\right) + 12.906\left(\frac{a}{c}\right)^2 - 13.441\left(\frac{a}{c}\right)^3$$

$$A_4 = -0.572 + 3.073\left(\frac{a}{c}\right) - 10.797\left(\frac{a}{c}\right)^2 + 8.393\left(\frac{a}{c}\right)^3$$

and

$$Y_1 = B_0 + B_1\left(\frac{a}{t}\right) + B_2\left(\frac{a}{t}\right)^2 + B_3\left(\frac{a}{t}\right)^3 + B_4\left(\frac{a}{t}\right)^4$$

$$B_0 = 0.500 - 0.323\left(\frac{a}{c}\right) + 0.213\left(\frac{a}{c}\right)^2 - 0.052\left(\frac{a}{c}\right)^3$$

$$B_1 = -0.507 + 1.373\left(\frac{a}{c}\right) - 0.740\left(\frac{a}{c}\right)^2 - 0.184\left(\frac{a}{c}\right)^3$$

$$B_2 = 3.468 - 9.028\left(\frac{a}{c}\right) + 6.349\left(\frac{a}{c}\right)^2 - 0.135\left(\frac{a}{c}\right)^3$$

$$B_3 = -1.359 + 1.731\left(\frac{a}{c}\right) + 5.357\left(\frac{a}{c}\right)^2 - 6.370\left(\frac{a}{c}\right)^3$$

$$B_4 = -0.162 + 2.977\left(\frac{a}{c}\right) - 8.250\left(\frac{a}{c}\right)^2 + 5.804\left(\frac{a}{c}\right)^3$$

WEIGHT FUNCTION (Figure 37) - Surface Point B

$$m_B(x,a) = \frac{2}{\sqrt{\pi x}}\left[1 + M_{1B}\left(\frac{x}{a}\right)^{\frac{1}{2}} + M_{2B}\left(\frac{x}{a}\right)^{1} + M_{3B}\left(\frac{x}{a}\right)^{\frac{3}{2}}\right]$$

PARAMETERS:

$$M_{1B} = \frac{3\pi}{\sqrt{Q}}(5F_1 - 3F_0) - 8$$

$$M_{2B} = \frac{15\pi}{\sqrt{Q}}(2F_0 - 3F_1) + 15$$

$$M_{3B} = \frac{3\pi}{\sqrt{Q}}(10F_1 - 7F_0) - 8$$

where:

$$Q = 1 + 1.464\left(\frac{a}{c}\right)^{1.65}$$

$$F_0 = \left[C_0 + C_1\left(\frac{a}{t}\right) + C_2\left(\frac{a}{t}\right)^2 + C_3\left(\frac{a}{t}\right)^3 + C_4\left(\frac{a}{t}\right)^4\right]\left(\frac{a}{c}\right)$$

$$C_0 = 3.340 - 4.495\left(\frac{a}{c}\right) + 3.016\left(\frac{a}{c}\right)^2 - 0.7278\left(\frac{a}{c}\right)^3$$

$$C_1 = 0.2318 - 0.2261\left(\frac{a}{c}\right) - 1.658\left(\frac{a}{c}\right)^2 + 1.504\left(\frac{a}{c}\right)^3$$

$$C_2 = 22.95 - 100.9\left(\frac{a}{c}\right) + 152.2\left(\frac{a}{c}\right)^2 - 72.92\left(\frac{a}{c}\right)^3$$

$$C_3 = -39.16 + 194.1\left(\frac{a}{c}\right) - 302.0\left(\frac{a}{c}\right)^2 + 145.9\left(\frac{a}{c}\right)^3$$

$$C_4 = 30.80 - 142.9\left(\frac{a}{c}\right) + 212.6\left(\frac{a}{c}\right)^2 - 99.92\left(\frac{a}{c}\right)^3$$

and

$$F_1 = \left[D_0 + D_1\left(\frac{a}{t}\right) + D_2\left(\frac{a}{t}\right)^2 + D_3\left(\frac{a}{t}\right)^3 + D_4\left(\frac{a}{t}\right)^4 \right]\left(\frac{a}{c}\right)$$

$$D_0 = 2.831 - 3.840\left(\frac{a}{c}\right) + 2.477\left(\frac{a}{c}\right)^2 - 0.511\left(\frac{a}{c}\right)^3$$

$$D_1 = 4.600 - 20.498\left(\frac{a}{c}\right) + 29.001\left(\frac{a}{c}\right)^2 - 13.226\left(\frac{a}{c}\right)^3$$

$$D_2 = -4.019 + 15.057\left(\frac{a}{c}\right) - 12.624\left(\frac{a}{c}\right)^2 + 2.677\left(\frac{a}{c}\right)^3$$

$$D_3 = 9.682 - 15.932\left(\frac{a}{c}\right) - 8.848\left(\frac{a}{c}\right)^2 + 13.910\left(\frac{a}{c}\right)^3$$

$$D_4 = -1.141 - 9.176\left(\frac{a}{c}\right) + 30.228\left(\frac{a}{c}\right)^2 - 19.195\left(\frac{a}{c}\right)^3$$

RANGE OF APPLICATION: $0 = a\backslash t = 0.8$ and $0.2 = a\backslash c = 1.0$
ACCURACY: Better than 1.5% when compared to the FEM data.
REFERENCES:

- weight function:
Zheng X. J., Glinka G., Dubey R. N., 1994, "Stress Intensity Factors and Weight Functions for a Corner Crack in a Finite Thickness Plate," *Engng. Fracture Mech.,*(to be published, 1996).

- reference data:
Shiratori M., Miyoshi T., 1985, "Analysis of Stress Intensity Factors for Surface Cracks Subjected to Arbitrarily Distributed Surface Stress (Analysis and Application of Data Base of Influence Coefficients K_{ij})," *Proc. Third Conf. Fract. Mech.*, Soc. Materials Science Japan, pp. 82-86.

Murakami Y., et al., 1992, *Stress Intensity Factors Handbook*, Vol. 3, Pergamon Press, pp. 591-597.

Raju I. S., Newman J. C., 1988, "Stress Intensity Factors for Corner Cracks in Rectangular Bars," in *Fracture Mechanics: Nineteenth Symposium, ASTM STP 969*, T.A.Cruse, ed., pp. 43-55.
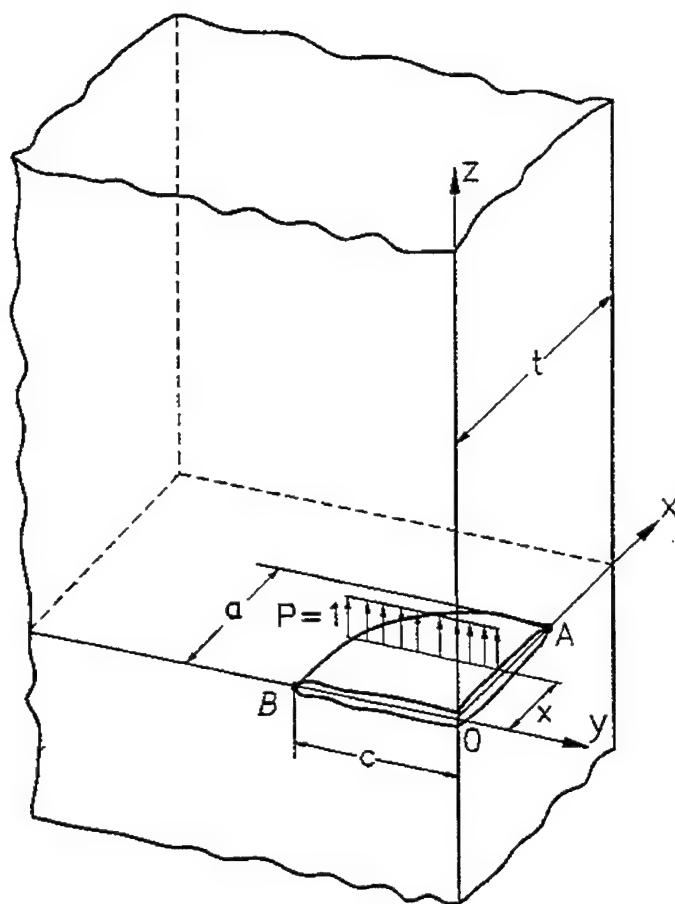
Figure 37. Quarter-Elliptical Corner Crack in a Finite Thickness Plate

Radial Edge Crack in a Circular Disk

WEIGHT FUNCTION (Figure 38):

$$m(x,a) = \frac{2}{\sqrt{2\pi(a-x)}}\left[1 + M_1\left(1-\frac{x}{a}\right)^{\frac{1}{2}} + M_2\left(1-\frac{x}{a}\right)^1 + M_3\left(1-\frac{x}{a}\right)^{\frac{3}{2}}\right]$$

PARAMETERS:

$$M_1 = \left[\begin{array}{l} -0.04732 + 0.49586\left(\dfrac{a}{D}\right) - 1.94141\left(\dfrac{a}{D}\right)^2 + 3.96175\left(\dfrac{a}{D}\right)^3 \\ -4.56109\left(\dfrac{a}{D}\right)^4 + 2.83026\left(\dfrac{a}{D}\right)^5 - 0.74080\left(\dfrac{a}{D}\right)^6 \end{array}\right] \exp\left[9.87969\left(\dfrac{a}{D}\right)\right]$$

$$M_2 = \exp\left[\begin{array}{l} -0.58602 + 8.48276\left(\dfrac{a}{D}\right) - 30.90993\left(\dfrac{a}{D}\right)^2 + 112.21153\left(\dfrac{a}{D}\right)^3 \\ -280.25303\left(\dfrac{a}{D}\right)^4 + 428.48183\left(\dfrac{a}{D}\right)^5 - 356.66155\left(\dfrac{a}{D}\right)^6 + 125.34267\left(\dfrac{a}{D}\right)^7 \end{array}\right]$$

$$M_3 = \exp\left[\begin{array}{l} -1.09836 + 3.06605\left(\dfrac{a}{D}\right) + 16.85709\left(\dfrac{a}{D}\right)^2 - 48.14897\left(\dfrac{a}{D}\right)^3 \\ +54.61627\left(\dfrac{a}{D}\right)^4 + 6.91042\left(\dfrac{a}{D}\right)^5 - 61.35817\left(\dfrac{a}{D}\right)^6 + 36.1270\left(\dfrac{a}{D}\right)^7 \end{array}\right]$$

RANGE OF APPLICATION: $0 < a/D < 0.9$.
ACCURACY: Better than 1.5% compared to the reference solution.
REFERENCES:

- weight function:
Kiciak A., 1995, University of Waterloo, to be published.

Glinka G., Shen G., 1991, "Universal Features of Weight Functions for Cracks in Mode I," *Engng. Fract. Mech.*, Vol. 40, No. 6, pp. 1135-1146 - this paper contains the original version of the weight function with coefficients M_i given in tabular form.

- reference data:
Wu X. R., Carlsson J. A., 1991, *Weight Functions and Stress Intensity Factor Solutions*, Pergamon Press.
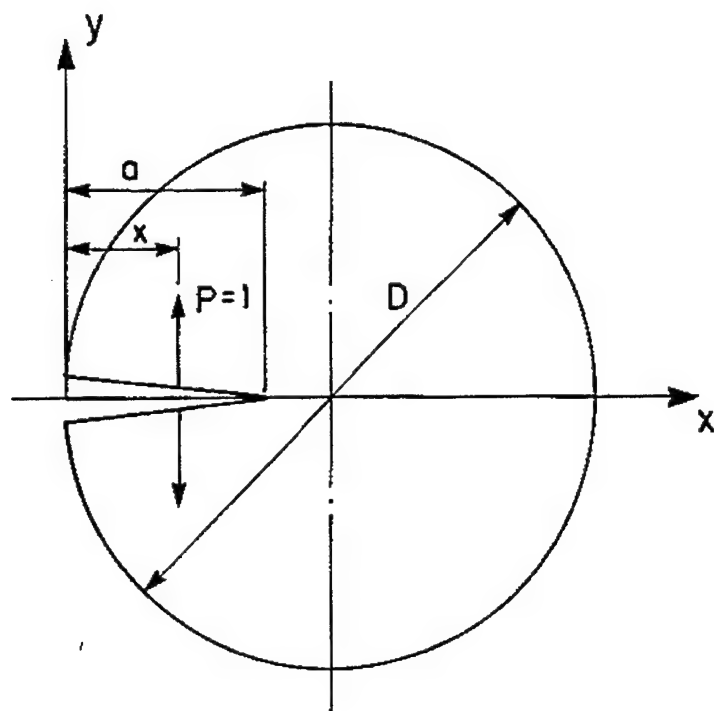
Figure 38. Radial Edge Crack in a Circular Disk

WEIGHT FUNCTIONS FOR CRACKS IN CYLINDERS

The weight functions are given in the form of expressions describing the M_i parameters as functions of crack dimensions and geometry of the cracked body. Given are the range of application, the accuracy and the source of the reference stress intensity factors for each set of parameters M_i including the generic geometry of the crack body. The geometry of a cylinder is characterized by the ratio of the external to internal radius, R_o/R_i.

Internal Axial Semielliptical Surface Crack in a Thick Cylinder ($R_o/R_i=2.0$)

WEIGHT FUNCTION (Figure 39) - Deepest Point A:

$$m_A(x,a) = \frac{2}{\sqrt{2\pi(a-x)}}\left[1 + M_{1A}\left(1-\frac{x}{a}\right)^{\frac{1}{2}} + M_{2A}\left(1-\frac{x}{a}\right)^{1} + M_{3A}\left(1-\frac{x}{a}\right)^{\frac{3}{2}}\right]$$

PARAMETERS:

$$M_{1A} = \frac{2\pi}{\sqrt{2Q}}\left(-Y_0 + 3Y_1\right) - \frac{24}{5}$$

$$M_{2A} = 3$$

$$M_{3A} = \frac{6\pi}{\sqrt{2Q}}\left(Y_0 - 2Y_1\right) + \frac{8}{5}$$

where:

$$Q = 1 + 1.464\left(\frac{a}{c}\right)^{1.65} \quad \text{and} \quad t = R_o - R_i$$

$$Y_0 = A_0 + A_1\left(\frac{a}{t}\right) + A_2\left(\frac{a}{t}\right)^2 + A_3\left(\frac{a}{t}\right)^4$$

$$A_0 = 1.12 - 0.207\left(\frac{a}{c}\right) - 0.153\left(\frac{a}{c}\right)^2 + 1.305\left(\frac{a}{c}\right)^3 - 2.007\left(\frac{a}{c}\right)^4 + 0.933\left(\frac{a}{c}\right)^5$$

$$A_1 = -0.111 - 7.205\left(\frac{a}{c}\right) + 36.455\left(\frac{a}{c}\right)^2 - 83.649\left(\frac{a}{c}\right)^3 + 89.741\left(\frac{a}{c}\right)^4 - 35.219\left(\frac{a}{c}\right)^5$$

$$A_2 = 1.498 + 20.265\left(\frac{a}{c}\right) - 132.935\left(\frac{a}{c}\right)^2 + 323.535\left(\frac{a}{c}\right)^3 - 343.920\left(\frac{a}{c}\right)^4 + 131.532\left(\frac{a}{c}\right)^5$$

$$A_3 = -0.140 + 18.828\left(\frac{a}{c}\right) - 85.243\left(\frac{a}{c}\right)^2 + 118.941\left(\frac{a}{c}\right)^3 - 52.084\left(\frac{a}{c}\right)^4$$

and

$$Y_1 = B_0 + B_1\left(\frac{a}{t}\right) + B_2\left(\frac{a}{t}\right)^2 + B_3\left(\frac{a}{t}\right)^3$$

$$B_0 = 0.687 - 0.377\left(\frac{a}{c}\right) + 3.617\left(\frac{a}{c}\right)^2 - 10.671\left(\frac{a}{c}\right)^3 + 12.482\left(\frac{a}{c}\right)^4 - 5.015\left(\frac{a}{c}\right)^5$$

$$B_1 = -0.163 - 1.496\left(\frac{a}{c}\right) - 7.725\left(\frac{a}{c}\right)^2 + 41.963\left(\frac{a}{c}\right)^3 + -56.282\left(\frac{a}{c}\right)^4 + 23.554\left(\frac{a}{c}\right)^5$$

$$B_2 = 0.821 + 7.481\left(\frac{a}{c}\right) - 33.313\left(\frac{a}{c}\right)^2 + 54.993\left(\frac{a}{c}\right)^3 - 44.961\left(\frac{a}{c}\right)^4 + 15.196\left(\frac{a}{c}\right)^5$$

$$B_3 = -0.087 + 3.742\left(\frac{a}{c}\right) - 20.172\left(\frac{a}{c}\right)^2 + 33.425\left(\frac{a}{c}\right)^3 - 16.841\left(\frac{a}{c}\right)^4$$

WEIGHT FUNCTION (Figure 39) - Surface Point B:

$$m_B(x,a) = \frac{2}{\sqrt{\pi x}}\left[1 + M_{1B}\left(\frac{x}{a}\right)^{\frac{1}{2}} + M_{2B}\left(\frac{x}{a}\right)^1 + M_{3B}\left(\frac{x}{a}\right)^{\frac{3}{2}}\right]$$

PARAMETERS

$$M_{1B} = \frac{3\pi}{\sqrt{Q}}(2F_0 - 5F_1) - 8$$

$$M_{2B} = \frac{15\pi}{\sqrt{Q}}(3F_1 - F_0) + 15$$

$$M_{3B} = \frac{3\pi}{\sqrt{Q}}(3F_0 - 10F_1) - 8$$

where:

$$Q = 1 + 1.464\left(\frac{a}{c}\right)^{1.65} \quad \text{and} \quad t = R_o - R_i$$

$$F_0 = \left[C_0 + C_1\left(\frac{a}{t}\right) + C_2\left(\frac{a}{t}\right)^2 + C_3\left(\frac{a}{t}\right)^4\right]\left(\frac{a}{c}\right)$$

$$C_0 = 5.923 - 20.55\left(\frac{a}{c}\right) + 36.937\left(\frac{a}{c}\right)^2 - 31.634\left(\frac{a}{c}\right)^3 + 10.37\left(\frac{a}{c}\right)^4$$

$$C_1 = -3.607 + 11.686\left(\frac{a}{c}\right) - 14.138\left(\frac{a}{c}\right)^2 + 9.935\left(\frac{a}{c}\right)^3 - 3.774\left(\frac{a}{c}\right)^4$$

$$C_2 = 19.14 - 72.902\left(\frac{a}{c}\right) + 112.643\left(\frac{a}{c}\right)^2 - 86.904\left(\frac{a}{c}\right)^3 + 28.149\left(\frac{a}{c}\right)^4$$

$$C_3 = 9.586 - 64.389\left(\frac{a}{c}\right) + 151.449\left(\frac{a}{c}\right)^2 - 144.822\left(\frac{a}{c}\right)^3 + 48.124\left(\frac{a}{c}\right)^4$$

and

$$F_1 = \left[D_0 + D_1\left(\frac{a}{t}\right) + D_2\left(\frac{a}{t}\right)^2 + D_3\left(\frac{a}{t}\right)^4\right]\left(\frac{a}{c}\right)$$

$$D_0 = 0.687 - 1.821\left(\frac{a}{c}\right) + 2.718\left(\frac{a}{c}\right)^2 - 1.981\left(\frac{a}{c}\right)^3 + 0.567\left(\frac{a}{c}\right)^4$$

$$D_1 = -1.797 + 9.399\left(\frac{a}{c}\right) - 19.195\left(\frac{a}{c}\right)^2 + 17.881\left(\frac{a}{c}\right)^3 - 6.244\left(\frac{a}{c}\right)^4$$

$$D_2 = 8.504 - 42.608\left(\frac{a}{c}\right) + 87.828\left(\frac{a}{c}\right)^2 - 82.735\left(\frac{a}{c}\right)^3 + 29.055\left(\frac{a}{c}\right)^4$$

$$D_3 = -0.666 + 6.54\left(\frac{a}{c}\right) - 21.603\left(\frac{a}{c}\right)^2 + 27.036\left(\frac{a}{c}\right)^3 - 11.326\left(\frac{a}{c}\right)^4$$

RANGE OF APPLICATION: $R_0/R_i = 2.0$, $0 = a/t = 0.8$, $a/c = 0$ and $0.2 = a/c = 1.0$
ACCURACY: Better than 3% when compared to the FEM data.
REFERENCES:

- *weight function:*
Zheng X. J., Glinka G., 1995, "Weight Functions and Stress Intensity Factors for Longitudinal Semi-Elliptical Cracks in Thick-Wall Cylinders," *J. Press. Vess.Technol.*, ASME, vol. 117, 1995, pp. 383 - 389

- *reference data:*
Mettu S. R., Raju I. S., Forman R. G., 1988, "Stress Intensity Factors for Part-Through Surface Cracks in Hollow Cylinders," NASA Technical Report, No. JSC 25685 LESC 30124.

Andrasic C. P., Parker A. P., 1984, "Dimensionless Stress Intensity Factors for Cracked Thick Cylinder Under Polynomial Crack Face Loading," *Engng. Fract. Mech.*, Vol. 19, 1984, pp. 187-193.

Murakami Y., et al., 1986, *Stress Intensity Factor Handbook*, Vol. 2, Pergamon Press, pp. 309-317.
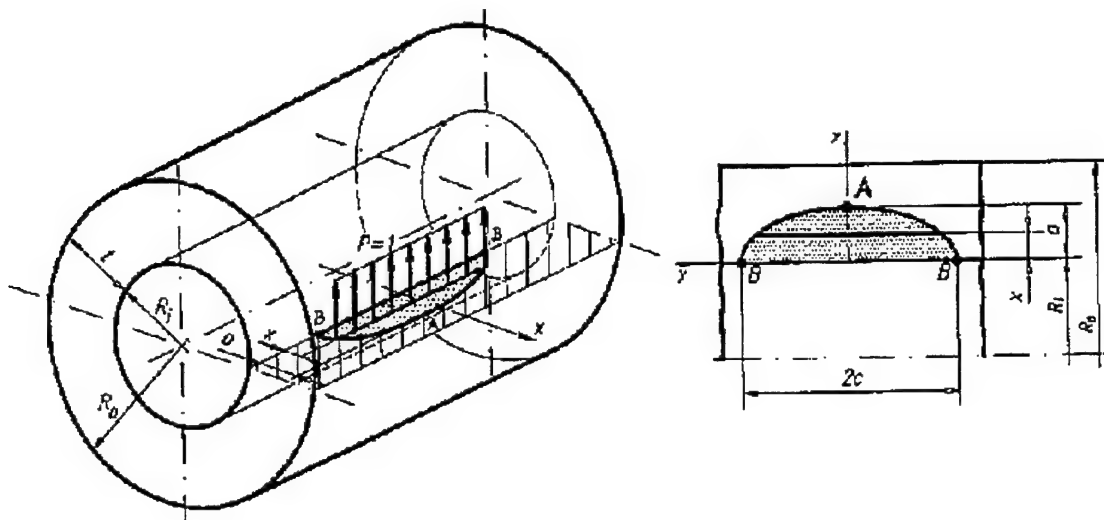
Figure 39. Internal Axial Semielliptical Surface Crack in a Thick Cylinder

Internal Axial Semielliptical Surface Crack in a Thick Cylinder (R_o/R_i=1.5)

WEIGHT FUNCTION (Figure 39) - Deepest Point A:

$$m_A(x,a) = \frac{2}{\sqrt{2\pi(a-x)}}\left[1 + M_{1A}\left(1-\frac{x}{a}\right)^{\frac{1}{2}} + M_{2A}\left(1-\frac{x}{a}\right)^{1} + M_{3A}\left(1-\frac{x}{a}\right)^{\frac{3}{2}}\right]$$

PARAMETERS:

$$M_{1A} = \frac{2\pi}{\sqrt{2Q}}(-Y_0 + 3Y_1) - \frac{24}{5}$$

$$M_{2A} = 3$$

$$M_{3A} = \frac{6\pi}{\sqrt{2Q}}(Y_0 - 2Y_1) + \frac{8}{5}$$

where:

$$Q = 1 + 1.464\left(\frac{a}{c}\right)^{1.65} \quad\text{and}\quad t = R_o - R_i$$

$$Y_0 = A_0 + A_1\left(\frac{a}{t}\right) + A_2\left(\frac{a}{t}\right)^2 + A_3\left(\frac{a}{t}\right)^4$$

$$A_0 = 1.044 + 0.07\exp\left[-5.051\left(\frac{a}{c}\right)\right]$$

$$A_1 = -0.433 + 0.665\exp\left[-3.393\left(\frac{a}{c}\right)\right]$$

$$A_2 = 0.711 + 1.161\exp\left[-3.386\left(\frac{a}{c}\right)\right]$$

$$A_3 = -0.179 + 1.46\exp\left[-4.165\left(\frac{a}{c}\right)\right]$$

and

$$Y_1 = B_0 + B_1\left(\frac{a}{t}\right) + B_2\left(\frac{a}{t}\right)^2 + B_3\left(\frac{a}{t}\right)^3$$

$$B_0 = 2.825 - 2.16\exp\left[-0.035\left(\frac{a}{c}\right)\right]$$

$$B_1 = -0.225 + 0.265\exp\left[-5.574\left(\frac{a}{c}\right)\right]$$

$$B_2 = 0.307 + 0.753\exp\left[-4.025\left(\frac{a}{c}\right)\right]$$

$$B_3 = 1.398 - 1.284\exp\left[0.079\left(\frac{a}{c}\right)\right]$$

WEIGHT FUNCTION (Figure 39) - Surface Point B:

$$m_B(x,a) = \frac{2}{\sqrt{\pi x}}\left[1 + M_{1B}\left(\frac{x}{a}\right)^{\frac{1}{2}} + M_{2B}\left(\frac{x}{a}\right)^1 + M_{3B}\left(\frac{x}{a}\right)^{\frac{3}{2}}\right]$$

PARAMETERS:

$$M_{1B} = \frac{3\pi}{\sqrt{Q}}\left(2F_0 - 5F_1\right) - 8$$

$$M_{2B} = \frac{15\pi}{\sqrt{Q}}\left(3F_1 - F_0\right) + 15$$

$$M_{3B} = \frac{3\pi}{\sqrt{Q}}\left(3F_0 - 10F_1\right) - 8$$

where:

$$Q = 1 + 1.464\left(\frac{a}{c}\right)^{1.65} \quad \text{and} \quad t = R_o - R_i$$

$$F_0 = \left[C_0 + C_1\left(\frac{a}{t}\right) + C_2\left(\frac{a}{t}\right)^2 + C_3\left(\frac{a}{t}\right)^4\right]\left(\frac{a}{c}\right)$$

$$C_0 = 0.972 + 5.163\exp\left[-5.061\left(\frac{a}{c}\right) + 1.568\left(\frac{a}{c}\right)^2\right]$$

$$C_1 = -0.199 - 10.239\exp\left[-46.053\left(\frac{a}{c}\right) - 4.009\left(\frac{a}{c}\right)^2\right]$$

$$C_2 = 0.119 + 8.784\exp\left[-4.081\left(\frac{a}{c}\right) + 1.092\left(\frac{a}{c}\right)^2\right]$$

$$C_3 = -0.104 + 28.133\exp\left[-9.959\left(\frac{a}{c}\right) - 9.817\left(\frac{a}{c}\right)^2\right]$$

and

$$F_1 = \left[D_0 + D_1\left(\frac{a}{t}\right) + D_2\left(\frac{a}{t}\right)^2 + D_3\left(\frac{a}{t}\right)^4\right]\left(\frac{a}{c}\right)$$

$$D_0 = 1.033 - 4.842\left(\frac{a}{c}\right) + 9.708\left(\frac{a}{c}\right)^2 - 8.397\left(\frac{a}{c}\right)^3 + 2.690\left(\frac{a}{c}\right)^4$$

$$D_1 = -3.448 + 24.231\left(\frac{a}{c}\right) - 50.221\left(\frac{a}{c}\right)^2 + 42.498\left(\frac{a}{c}\right)^3 - 13.099\left(\frac{a}{c}\right)^4$$

$$D_2 = 6.535 - 30.622\left(\frac{a}{c}\right) + 45.644\left(\frac{a}{c}\right)^2 - 25.05\left(\frac{a}{c}\right)^3 + 3.636\left(\frac{a}{c}\right)^4$$

$$D_3 = 2.243 - 21.677\left(\frac{a}{c}\right) + 65.546\left(\frac{a}{c}\right)^2 - 76.555\left(\frac{a}{c}\right)^3 + 30.433\left(\frac{a}{c}\right)^4$$

RANGE OF APPLICATION: $R_0/R_i = 1.5$, $0 = a/t = 0.8$, $a/c = 0$ and $0.2 = a/c = 1.0$
ACCURACY: Better than 3% when compared to the FEM data.
REFERENCES:

- *weight function:*
Zheng X. J., Kiciak A., Glinka G., 1996, "Determination of Weight Functions and Stress Intensity Factors for Semielliptical Cracks in Thick-wall Cylinders," *Nucl. Engng. Design*, to be published.

- reference data:

Mettu S. R., Raju I. S., Forman R. G., 1988, "Stress Intensity Factors for Part-Through Surface Cracks in Hollow Cylinders," NASA Technical Report, No. JSC 25685 LESC 30124.

Andrasic C. P., Parker A. P., 1984, "Dimensionless Stress Intensity Factors for Cracked Thick Cylinder Under Polynomial Crack Face Loading," *Engng. Fract. Mech.*, Vol. 19, 1984, pp. 187-193.

Murakami Y., et al., 1986, *Stress Intensity Factor Handbook*, Vol. 2, Pergamon Press, pp. 309-317.

Internal Axial Semielliptical Surface Crack in a Thick Cylinder (R_o/R_i=1.25)

WEIGHT FUNCTION (Figure 39) – Deepest Point A:

$$m_A(x,a) = \frac{2}{\sqrt{2\pi(a-x)}}\left[1 + M_{1A}\left(1-\frac{x}{a}\right)^{\frac{1}{2}} + M_{2A}\left(1-\frac{x}{a}\right)^{1} + M_{3A}\left(1-\frac{x}{a}\right)^{\frac{3}{2}}\right]$$

PARAMETERS:

$$M_{1A} = \frac{2\pi}{\sqrt{2Q}}(-Y_0 + 3Y_1) - \frac{24}{5}$$

$$M_{2A} = 3$$

$$M_{3A} = \frac{6\pi}{\sqrt{2Q}}(Y_0 - 2Y_1) + \frac{8}{5}$$

where:

$$Q = 1 + 1.464\left(\frac{a}{c}\right)^{1.65} \quad \text{and} \quad t = R_o - R_i$$

$$Y_0 = A_0 + A_1\left(\frac{a}{t}\right) + A_2\left(\frac{a}{t}\right)^2 + A_3\left(\frac{a}{t}\right)^4$$

$$A_0 = 1.010 + 0.0998\exp\left[-13.15\left(\frac{a}{c}\right)\right]$$

$$A_1 = 0.055 + 0.366\exp\left[-31.17\left(\frac{a}{c}\right)\right]$$

$$A_2 = -0.057 + 3.269\exp\left[-3.859\left(\frac{a}{c}\right)\right]$$

$$A_3 = -0.149 + 0.061\exp\left[1.354\left(\frac{a}{c}\right)\right]$$

and

$$Y_1 = B_0 + B_1\left(\frac{a}{t}\right) + B_2\left(\frac{a}{t}\right)^2 + B_3\left(\frac{a}{t}\right)^3$$

$$B_0 = 6.594 - 5.944\exp\left[-0.012\left(\frac{a}{c}\right)\right]$$

$$B_1 = -0.136 + 0.436\exp\left[-8.663\left(\frac{a}{c}\right)\right]$$

$$B_2 = 0.269 + 0.787\exp\left[-4.562\left(\frac{a}{c}\right)\right]$$

$$B_3 = 1.552 - 1.538\exp\left[0.0434\left(\frac{a}{c}\right)\right]$$

WEIGHT FUNCTION (Figure 39) - Surface Point B:

$$m_B(x,a) = \frac{2}{\sqrt{\pi x}}\left[1 + M_{1B}\left(\frac{x}{a}\right)^{\frac{1}{2}} + M_{2B}\left(\frac{x}{a}\right)^1 + M_{3B}\left(\frac{x}{a}\right)^{\frac{3}{2}}\right]$$

PARAMETERS:

$$M_{1B} = \frac{3\pi}{\sqrt{Q}}(2F_0 - 5F_1) - 8$$

$$M_{2B} = \frac{15\pi}{\sqrt{Q}}(3F_1 - F_0) + 15$$

$$M_{3B} = \frac{3\pi}{\sqrt{Q}}(3F_0 - 10F_1) - 8$$

where:

$$Q = 1 + 1.464 \left(\frac{a}{c} \right)^{1.65} \quad \text{and} \quad t = R_o - R_i$$

$$F_0 = \left[C_0 + C_1 \left(\frac{a}{t} \right) + C_2 \left(\frac{a}{t} \right)^2 + C_3 \left(\frac{a}{t} \right)^4 \right] \left(\frac{a}{c} \right)$$

$$C_0 = 5.566 - 19.583 \left(\frac{a}{c} \right) + 37.335 \left(\frac{a}{c} \right)^2 - 33.705 \left(\frac{a}{c} \right)^3 + 11.507 \left(\frac{a}{c} \right)^4$$

$$C_1 = -1.75 + 9.514 \left(\frac{a}{c} \right) - 16.618 \left(\frac{a}{c} \right)^2 + 10.44 \left(\frac{a}{c} \right)^3 - 1.616 \left(\frac{a}{c} \right)^4$$

$$C_2 = 12.497 - 49.067 \left(\frac{a}{c} \right) + 72.59 \left(\frac{a}{c} \right)^2 - 45.216 \left(\frac{a}{c} \right)^3 + 9.55 \left(\frac{a}{c} \right)^4$$

$$C_3 = 3.468 - 29.49 \left(\frac{a}{c} \right) + 83.789 \left(\frac{a}{c} \right)^2 - 93.289 \left(\frac{a}{c} \right)^3 + 35.507 \left(\frac{a}{c} \right)^4$$

and

$$F_1 = \left[D_0 + D_1 \left(\frac{a}{t} \right) + D_2 \left(\frac{a}{t} \right)^2 + D_3 \left(\frac{a}{t} \right)^4 \right] \left(\frac{a}{c} \right)$$

$$D_0 = 0.486 - 0.879 \left(\frac{a}{c} \right) + 1.161 \left(\frac{a}{c} \right)^2 - 0.793 \left(\frac{a}{c} \right)^3 + 0.212 \left(\frac{a}{c} \right)^4$$

$$D_1 = -0.533 + 2.626 \left(\frac{a}{c} \right) - 3.412 \left(\frac{a}{c} \right)^2 + 0.999 \left(\frac{a}{c} \right)^3 + 0.333 \left(\frac{a}{c} \right)^4$$

$$D_2 = 4.116 - 15.985 \left(\frac{a}{c} \right) + 22.358 \left(\frac{a}{c} \right)^2 - 12.235 \left(\frac{a}{c} \right)^3 + 1.826 \left(\frac{a}{c} \right)^4$$

$$D_3 = 0.569 - 6.605 \left(\frac{a}{c} \right) + 21.548 \left(\frac{a}{c} \right)^2 - 26.37 \left(\frac{a}{c} \right)^3 + 10.853 \left(\frac{a}{c} \right)^4$$

RANGE OF APPLICATION: $R_0/R_i = 1.25$, $0 = a/t = 0.8$, $a/c = 0$ and $0.2 = a/c = 1.0$
ACCURACY: Better than 3% when compared to the FEM data.
REFERENCES:

- weight function:
Zheng X. J., Glinka G., Dubey R. N., 1995, "Calculation of Stress Intensity Factors for Semielliptical Cracks in a Thick-Wall Cylinder," *Int. J.Pres.Ves. & Piping*, Vol. 62, pp. 249-258.

- reference data:

Mettu S. R., Raju I. S., Forman R. G., 1988, "Stress Intensity Factors for Part-Through Surface Cracks in Hollow Cylinders," NASA Technical Report, No. JSC 25685 LESC 30124.

Andrasic C. P., Parker A. P., 1984, "Dimensionless Stress Intensity Factors for Cracked Thick Cylinder Under Polynomial Crack Face Loading," *Engng. Fract. Mech.*, Vol. 19, 1984, pp. 187-193.

Murakami Y., et al., 1986, *Stress Intensity Factor Handbook*, Vol. 2, Pergamon Press, pp. 309-317.

Internal Axial Semielliptical Surface Crack in a Thick Cylinder ($R_o/R_i=1.1$)

WEIGHT FUNCTION (Figure 39) - Deepest Point A:

$$m_A(x,a) = \frac{2}{\sqrt{2\pi(a-x)}}\left[1 + M_{1A}\left(1-\frac{x}{a}\right)^{\frac{1}{2}} + M_{2A}\left(1-\frac{x}{a}\right)^{1} + M_{3A}\left(1-\frac{x}{a}\right)^{\frac{3}{2}}\right]$$

PARAMETERS:

$$M_{1A} = \frac{2\pi}{\sqrt{2Q}}(2Y_0 + 3Y_1) - \frac{24}{5}$$

$$M_{2A} = 3$$

$$M_{3A} = \frac{6\pi}{\sqrt{2Q}}(2Y_1 - Y_0) + \frac{8}{5}$$

where:

$$Q = 1 + 1.464\left(\frac{a}{c}\right)^{1.65} \quad \text{and} \quad t = R_o - R_i$$

$$Y_0 = A_0 + A_1\left(\frac{a}{t}\right)^2 + A_2\left(\frac{a}{t}\right)^4$$

$$A_0 = 1.1449 - 0.6699\left(\frac{a}{c}\right) + 1.0464\left(\frac{a}{c}\right)^2 - 0.5202\left(\frac{a}{c}\right)^3$$

$$A_1 = 3.84 - 10.531\left(\frac{a}{c}\right) + 6.931\left(\frac{a}{c}\right)^2$$

$$A_2 = -8.519 + 20.456\left(\frac{a}{c}\right) - 13.027\left(\frac{a}{c}\right)^2 + \frac{1}{0.061 + \left(\frac{a}{c}\right)^{0.983}}$$

and

113

$$Y_1 = B_0 + B_1 \left(\frac{a}{t}\right)^2 + B_2 \left(\frac{a}{t}\right)^4$$

$$B_0 = 0.4732 - 0.4967 \left(\frac{a}{c}\right) + 0.7576 \left(\frac{a}{c}\right)^2 - 0.4417 \left(\frac{a}{c}\right)^3$$

$$B_1 = 2.415 - 6.901 \left(\frac{a}{c}\right) + 5.928 \left(\frac{a}{c}\right)^2 - 1.291 \left(\frac{a}{c}\right)^3$$

$$B_2 = -6.251 + 13.282 \left(\frac{a}{c}\right) - 8.097 \left(\frac{a}{c}\right)^2 + \frac{1}{0.090 + \left(\frac{a}{c}\right)^{0.92}}$$

WEIGHT FUNCTION (Figure 39) - Surface Point B:

$$m_B(x,a) = \frac{2}{\sqrt{\pi x}} \left[1 + M_{1B} \left(\frac{x}{a}\right)^{\frac{1}{2}} + M_{2B} \left(\frac{x}{a}\right)^1 + M_{3B} \left(\frac{x}{a}\right)^{\frac{3}{2}} \right]$$

PARAMETERS:

$$M_{1B} = \frac{3\pi}{\sqrt{Q}} (5F_1 - 3F_0) - 8$$

$$M_{2B} = \frac{15\pi}{\sqrt{Q}} (2F_0 - 3F_1) + 15$$

$$M_{3B} = \frac{3\pi}{\sqrt{Q}} (10F_1 - 7F_0) - 8$$

where:

$$Q = 1 + 1.464\left(\frac{a}{c}\right)^{1.65} \quad \text{and} \quad t = R_o - R_i$$

$$F_0 = \left[C_0 + C_1\left(\frac{a}{t}\right)^2 + C_2\left(\frac{a}{t}\right)^4 \right]\sqrt{\frac{a}{c}}$$

$$C_0 = 1.2959 - 0.2935\left(\frac{a}{c}\right) + 0.1203\left(\frac{a}{c}\right)^2$$

$$C_1 = 0.1256 + 27.96\left(\frac{a}{c}\right) - 143.547\left(\frac{a}{c}\right)^2 + 293.879\left(\frac{a}{c}\right)^3 - 270.492\left(\frac{a}{c}\right)^4 + 92.502\left(\frac{a}{c}\right)^5$$

$$C_2 = -2.065 + 1.15\left(\frac{a}{c}\right) + \frac{1}{0.2 + \left(\frac{a}{c}\right)^{1.05}}$$

and

$$F_1 = \left[D_0 + D_1\left(\frac{a}{t}\right)^2 + D_2\left(\frac{a}{t}\right)^4 \right]\sqrt{\frac{a}{c}}$$

$$D_0 = 1.2519 - 0.8104\left(\frac{a}{c}\right) + 0.4901\left(\frac{a}{c}\right)^2$$

$$D_1 = 0.3311 + 15.433\left(\frac{a}{c}\right) - 81.361\left(\frac{a}{c}\right)^2 + 167.357\left(\frac{a}{c}\right)^3 - 153.789\left(\frac{a}{c}\right)^4 + 52.309\left(\frac{a}{c}\right)^5$$

$$D_2 = -1.879 + 1.087\left(\frac{a}{c}\right) + \frac{1}{0.299 + \left(\frac{a}{c}\right)^{1.05}}$$

RANGE OF APPLICATION: $R_0/R_i = 1.1$, $0 = a/t = 0.8$, and $0 = a/c = 1.0$
ACCURACY: Better than 5% when compared to the FEM data.
REFERENCES:

- weight function:
<u>Wang X. J., Lambert S. B.</u>, 1996, "Stress Intensity Factors and Weight Functions for Longitudinal Semielliptical Surface Cracks in Thin Pipes," *Int. J.Pres.Ves. & Piping*, Vol. 65, pp. 75 -87.

<u>Shen. G., Liebster T. D., Glinka G.</u> ,1993, "Calculation of Stress Intensity Factors for Cracks in Pipes," *Proc. of the 12th Int. Conf. on Offshore Mech. and Arctic Engng., ASME,* M. Salama et al., ed., Vol. III-B, *Materials Engineering,* pp.847-854. (this paper contains the older version of the weight function, limited to $0 = a/t = 0.8$ and $0.2 = a/c = 1.0$)

- reference data:

Raju I. S., Newman J. C., 1982, "Stress Intensity Factors for Internal and External Surface Cracks in Cylindrical Vessels," *J. Press. Ves. Technol.*, Vol. 104, pp. 293-298.

Andrasic C. P., Parker A. P., 1984, "Dimensionless Stress Intensity Factors for Cracked Thick Cylinder Under Polynomial Crack Face Loading," *Engng. Fract. Mech.*, Vol. 19, 1984, pp. 187-193.

External Axial Semielliptical Surface Crack in a Thick Cylinder (R_o/R_i=2.0)

WEIGHT FUNCTION (Figure 40) - Deepest Point A:

$$m_A(x,a) = \frac{2}{\sqrt{2\pi(a-x)}}\left[1 + M_{1A}\left(1-\frac{x}{a}\right)^{\frac{1}{2}} + M_{2A}\left(1-\frac{x}{a}\right)^{1} + M_{3A}\left(1-\frac{x}{a}\right)^{\frac{3}{2}}\right]$$

PARAMETERS:

$$M_{1A} = \frac{2\pi}{\sqrt{2Q}}(-Y_0 + 3Y_1) - \frac{24}{5}$$

$$M_{2A} = 3$$

$$M_{3A} = \frac{6\pi}{\sqrt{2Q}}(Y_0 - 2Y_1) + \frac{8}{5}$$

where:

$$Q = 1 + 1.464\left(\frac{a}{c}\right)^{1.65} \quad \text{and} \quad t = R_o - R_i$$

$$Y_0 = A_0 + A_1\left(\frac{a}{t}\right) + A_2\left(\frac{a}{t}\right)^2 + A_3\left(\frac{a}{t}\right)^4$$

$$A_0 = 0.98463 + 0.10409\exp\left[11.93568\left(\frac{a}{c}\right) - 44.74122\left(\frac{a}{c}\right)^2 + 53.45540\left(\frac{a}{c}\right)^3 - 21.48712\left(\frac{a}{c}\right)^4\right]$$

$$A_1 = 0.02208 - 0.04469\exp\left[35.69496\left(\frac{a}{c}\right) - 138.51103\left(\frac{a}{c}\right)^2 + 185.87345\left(\frac{a}{c}\right)^3 - 85.19922\left(\frac{a}{c}\right)^4\right]$$

$$A_2 = 0.41663 + 0.41917\exp\left[22.34798\left(\frac{a}{c}\right) - 87.48907\left(\frac{a}{c}\right)^2 + 118.30990\left(\frac{a}{c}\right)^3 - 55.88622\left(\frac{a}{c}\right)^4\right]$$

$$A_3 = -0.07482 + 17.78423\exp\left[-23.84462\left(\frac{a}{c}\right) + 71.77065\left(\frac{a}{c}\right)^2 - 118.12933\left(\frac{a}{c}\right)^3 + 63.64254\left(\frac{a}{c}\right)^4\right]$$

and

$$Y_1 = B_0 + B_1\left(\frac{a}{t}\right) + B_2\left(\frac{a}{t}\right)^2 + B_3\left(\frac{a}{t}\right)^4$$

$$B_0 = 0.71344 + 0.00525\exp\left[25.42681\left(\frac{a}{c}\right) - 82.30859\left(\frac{a}{c}\right)^2 + 39.63312\left(\frac{a}{c}\right)^3 + 16.09569\left(\frac{a}{c}\right)^4\right]$$

$$B_1 = 0.02433 - 0.08062\exp\left[24.45619\left(\frac{a}{c}\right) - 103.67649\left(\frac{a}{c}\right)^2 + 158.27997\left(\frac{a}{c}\right)^3 - 87.15246\left(\frac{a}{c}\right)^4\right]$$

$$B_2 = 0.12875 + 0.46420\exp\left[14.79057\left(\frac{a}{c}\right) - 66.68409\left(\frac{a}{c}\right)^2 + 103.18837\left(\frac{a}{c}\right)^3 - 58.96618\left(\frac{a}{c}\right)^4\right]$$

$$B_3 = 1.00553 - 8.68986\left(\frac{a}{c}\right) + 35.59049\left(\frac{a}{c}\right)^2 - 85.96909\left(\frac{a}{c}\right)^3 + 118.96622\left(\frac{a}{c}\right)^4 - 84.66299\left(\frac{a}{c}\right)^5$$
$$+ 23.75335\left(\frac{a}{c}\right)^6$$

WEIGHT FUNCTION (Figure 40) - Surface Point B:

$$m_B(x,a) = \frac{2}{\sqrt{\pi x}}\left[1 + M_{1B}\left(\frac{x}{a}\right)^{\frac{1}{2}} + M_{2B}\left(\frac{x}{a}\right)^1 + M_{3B}\left(\frac{x}{a}\right)^{\frac{3}{2}}\right]$$

PARAMETERS:

$$M_{1B} = \frac{3\pi}{\sqrt{Q}}\left(2F_0 - 5F_1\right) - 8$$

$$M_{2B} = \frac{15\pi}{\sqrt{Q}}\left(3F_1 - F_0\right) + 15$$

$$M_{3B} = \frac{3\pi}{\sqrt{Q}}\left(3F_0 - 10F_1\right) - 8$$

where:

$$F_0 = C_0 + C_1\left(\frac{a}{t}\right) + C_2\left(\frac{a}{t}\right)^2 + C_3\left(\frac{a}{t}\right)^4 + C_4\left(\frac{a}{t}\right)^5$$

$$C_0 = 1.40290\left\{1 - \exp\left[-6.93070\left(\frac{a}{c}\right) + 21.48633\left(\frac{a}{c}\right)^2 - 36.14294\left(\frac{a}{c}\right)^3 + 28.68609\left(\frac{a}{c}\right)^4 - 8.80402\left(\frac{a}{c}\right)^5\right]\right\}$$

$$C_1 = -15.12461\left(\frac{a}{c}\right)\left[1 - 1.17520\left(\frac{a}{c}\right)\right]\exp\left[-3.64659\left(\frac{a}{c}\right) - 5.78270\left(\frac{a}{c}\right)^2 + 13.55459\left(\frac{a}{c}\right)^3 - 6.78266\left(\frac{a}{c}\right)^4\right]$$

$$C_2 = 1.11589\left\{1 - \exp\left[-0.60488\left(\frac{a}{c}\right) - 9.42291\left(\frac{a}{c}\right)^2 + 17.10918\left(\frac{a}{c}\right)^3 - 7.51091\left(\frac{a}{c}\right)^4\right]\right\}$$

$$C_3 = 55.90204\left(\frac{a}{c}\right)\left[1 + 2.086702\left(\frac{a}{c}\right)\right]\exp\left[-10.21823\left(\frac{a}{c}\right) + 8.20568\left(\frac{a}{c}\right)^2 - 7.52675\left(\frac{a}{c}\right)^3 + 2.66400\left(\frac{a}{c}\right)^4\right]$$

$$C_4 = -16.95222\left(\frac{a}{c}\right)\left[1 - 0.88925\left(\frac{a}{c}\right)\right]\exp\left[-9.87203\left(\frac{a}{c}\right) + 19.30584\left(\frac{a}{c}\right)^2 - 26.66380\left(\frac{a}{c}\right)^3 + 14.35426\left(\frac{a}{c}\right)^4\right]$$

and

$$F_1 = D_0 + D_1\left(\frac{a}{t}\right) + D_2\left(\frac{a}{t}\right)^2$$

$$D_0 = 0.20478\left\{1 - \exp\left[-11.38873\left(\frac{a}{c}\right) + 28.07640\left(\frac{a}{c}\right)^2 - 30.62707\left(\frac{a}{c}\right)^3 + 9.86369\left(\frac{a}{c}\right)^4\right]\right\}$$

$$D_1 = -9.73349\left(\frac{a}{c}\right)\left[1 - 1.09108\left(\frac{a}{c}\right)\right]\exp\left[-4.22628\left(\frac{a}{c}\right) - 4.99914\left(\frac{a}{c}\right)^2 + 10.82767\left(\frac{a}{c}\right)^3 - 4.84826\left(\frac{a}{c}\right)^4\right]$$

$$D_2 = 14.67302\left(\frac{a}{c}\right)\left[1 - 0.90366\left(\frac{a}{c}\right)\right]\exp\left[-5.27930\left(\frac{a}{c}\right) + 1.71158\left(\frac{a}{c}\right)^2 + 1.33890\left(\frac{a}{c}\right)^3\right]$$

RANGE OF APPLICATION: $R_0/R_i = 2.0$, $0 = a/t = 1.0$, $a/c = 0$ and $0.2 = a/c = 1.0$
ACCURACY: Better than 3% when compared to the FEM data.
REFERENCES:

- weight function:

Kiciak A., Glinka G., Burns D. J., 1996, "Weight Functions and Stress Intensity Factors for Longitudinal Semielliptical Cracks in Thick-wall Cylinders," *J. Press. Vess. Technol.*, ASME (to be published)

- reference data:

Mettu S. R., Raju I. S., Forman R. G., 1988, "Stress Intensity Factors for Part-Through Surface Cracks in Hollow Cylinders," NASA Technical Report, No. JSC 25685 LESC 30124.

Andrasic C. P., Parker A. P., 1984, "Dimensionless Stress Intensity Factors for Cracked Thick Cylinder Under Polynomial Crack Face Loading," *Engng. Fract. Mech.*, Vol. 19, 1984, pp. 187-193.

Murakami Y., et al., 1986, *Stress Intensity Factor Handbook*, Vol. 2, Pergamon Press, pp. 309-317.
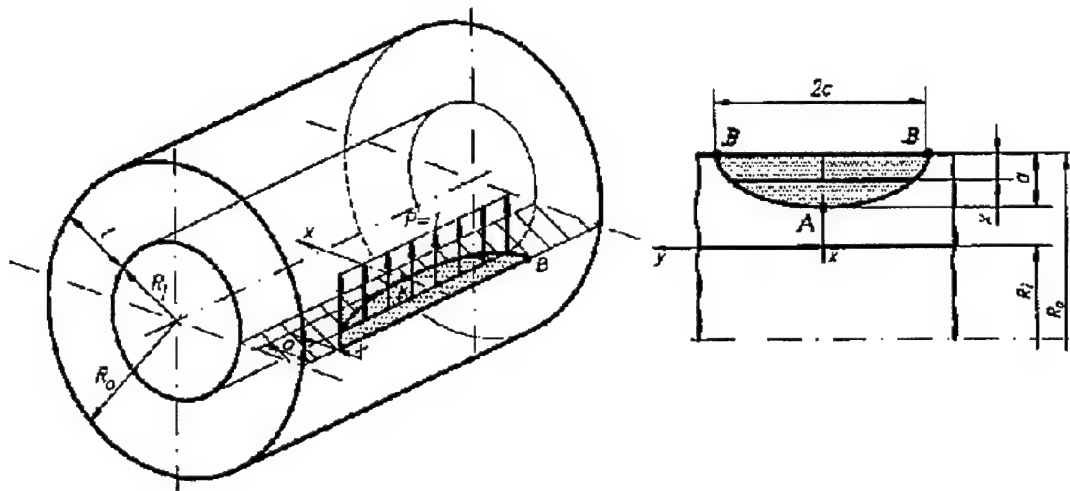
Figure 40. External Axial Semielliptical Surface Crack in a Thick Cylinder

External Axial Semielliptical Surface Crack in a Thick Cylinder ($R_o/R_i = 1.5$)

WEIGHT FUNCTION (Figure 40) - Deepest Point A:

$$m_A(x,a) = \frac{2}{\sqrt{2\pi(a-x)}}\left[1 + M_{1A}\left(1-\frac{x}{a}\right)^{\frac{1}{2}} + M_{2A}\left(1-\frac{x}{a}\right)^{1} + M_{3A}\left(1-\frac{x}{a}\right)^{\frac{3}{2}}\right]$$

PARAMETERS:

$$M_{1A} = \frac{2\pi}{\sqrt{2Q}}(-Y_0 + 3Y_1) - \frac{24}{5}$$

$$M_{2A} = 3$$

$$M_{3A} = \frac{6\pi}{\sqrt{2Q}}(Y_0 - 2Y_1) + \frac{8}{5}$$

where:

$$Q = 1 + 1.464 \left(\frac{a}{c} \right)^{1.65} \quad \text{and} \quad t = R_o - R_i$$

$$Y_0 = A_0 + A_1 \left(\frac{a}{t} \right) + A_2 \left(\frac{a}{t} \right)^2 + A_3 \left(\frac{a}{t} \right)^4$$

$$A_0 = 0.69716 + \exp\left[\begin{array}{l} -0.85208 + 0.14072\left(\frac{a}{c} \right) - 1.88533\left(\frac{a}{c} \right)^2 + 2.38695\left(\frac{a}{c} \right)^3 \\ -0.92014\left(\frac{a}{c} \right)^4 \end{array} \right]$$

$$A_1 = 0.83400 - \exp\left[\begin{array}{l} -1.89775 + 21.36041\left(\frac{a}{c} \right) - 84.13521\left(\frac{a}{c} \right)^2 + 142.22714\left(\frac{a}{c} \right)^3 \\ -109.84164\left(\frac{a}{c} \right)^4 + 32.02799\left(\frac{a}{c} \right)^5 \end{array} \right]$$

$$A_2 = 0.25833 + \exp\left[\begin{array}{l} 0.38467 + 3.46411\left(\frac{a}{c} \right) - 3.41241\left(\frac{a}{c} \right)^2 + 28.40776\left(\frac{a}{c} \right)^3 \\ +23.50662\left(\frac{a}{c} \right)^4 \end{array} \right]$$

$$A_3 = -0.024225 + \exp\left[\begin{array}{l} 0.18341 + 12.66325\left(\frac{a}{c} \right) - 148.59759\left(\frac{a}{c} \right)^2 + 400.31551\left(\frac{a}{c} \right)^3 \\ -419.88103\left(\frac{a}{c} \right)^4 + 150.43104\left(\frac{a}{c} \right)^5 \end{array} \right]$$

and

$$Y_1 = B_0 + B_1\left(\frac{a}{t}\right) + B_2\left(\frac{a}{t}\right)^2 + B_3\left(\frac{a}{t}\right)^4$$

$$B_0 = 0.22856 + \exp\left[\begin{array}{l} -0.78477 + 0.07367\left(\frac{a}{c}\right) - 0.19984\left(\frac{a}{c}\right)^2 - 0.04996\left(\frac{a}{c}\right)^3 \\ -0.25050\left(\frac{a}{c}\right)^4 \end{array}\right]$$

$$B_1 = 0.43259 - \exp\left[\begin{array}{l} -2.27787 + 20.51173\left(\frac{a}{c}\right) - 84.19018\left(\frac{a}{c}\right)^2 + 154.08510\left(\frac{a}{c}\right)^3 \\ -132.35299\left(\frac{a}{c}\right)^4 + 43.43167\left(\frac{a}{c}\right)^5 \end{array}\right]$$

$$B_2 = 0.14247 + \exp\left[\begin{array}{l} -1.11085 + 13.46249\left(\frac{a}{c}\right) - 55.49509\left(\frac{a}{c}\right)^2 + 74.92487\left(\frac{a}{c}\right)^3 \\ -37.080007\left(\frac{a}{c}\right)^4 \end{array}\right]$$

$$B_3 = -0.02704 + \exp\left[\begin{array}{l} -0.44818 - 0.17795\left(\frac{a}{c}\right) - 53.30479\left(\frac{a}{c}\right)^2 + 25.51119\left(\frac{a}{c}\right)^3 \\ +24.67589\left(\frac{a}{c}\right)^4 \end{array}\right]$$

WEIGHT FUNCTION (Figure 40) - Surface Point B:

$$m_B(x,a) = \frac{2}{\sqrt{\pi x}}\left[1 + M_{1B}\left(\frac{x}{a}\right)^{\frac{1}{2}} + M_{2B}\left(\frac{x}{a}\right)^1 + M_{3B}\left(\frac{x}{a}\right)^{\frac{3}{2}}\right]$$

PARAMETERS:

$$M_{1B} = \frac{3\pi}{\sqrt{Q}}(2F_0 - 5F_1) - 8$$

$$M_{2B} = \frac{15\pi}{\sqrt{Q}}(3F_1 - F_0) + 15$$

$$M_{3B} = \frac{3\pi}{\sqrt{Q}}(3F_0 - 10F_1) - 8$$

where:

$$Q = 1 + 1.464\left(\frac{a}{c}\right)^{1.65} \quad \text{and} \quad t = R_o - R_i$$

$$F_0 = C_0 + C_1\left(\frac{a}{t}\right) + C_2\left(\frac{a}{t}\right)^2 + C_3\left(\frac{a}{t}\right)^4$$

$$C_0 = 0.69519\left\{1 + 0.31674\left(\frac{a}{c}\right) + 0.34206\left(\frac{a}{c}\right)^2 - \exp\left[-29.87363\left(\frac{a}{c}\right) + 139.14830\left(\frac{a}{c}\right)^2 - 382.37581\left(\frac{a}{c}\right)^3\right]\right\}$$

$$C_1 = -\left(\frac{a}{c}\right)\left[55.208999 - 68.89759\left(\frac{a}{c}\right)\right]\exp\left[-16.47111\left(\frac{a}{c}\right) + 38.49788\left(\frac{a}{c}\right)^2 - 55.27126\left(\frac{a}{c}\right)^3 + 27.25396\left(\frac{a}{c}\right)^4\right]$$

$$C_2 = 2.70539\left\{1 - 1.50789\left(\frac{a}{c}\right) + 0.72855\left(\frac{a}{c}\right)^2 - \exp\left[-23.29526\left(\frac{a}{c}\right) + 84.84981\left(\frac{a}{c}\right)^2 - 144.62398\left(\frac{a}{c}\right)^3\right]\right\}$$

$$C_3 = \left(\frac{a}{c}\right)\left[27.52544 - 14.91620\left(\frac{a}{c}\right) - 12.89888\left(\frac{a}{c}\right)^2\right]\exp\left[-17.21310\left(\frac{a}{c}\right) + 21.22175\left(\frac{a}{c}\right)^2 - 7.53042\left(\frac{a}{c}\right)^3\right]$$

and

$$F_1 = D_0 + D_1\left(\frac{a}{t}\right) + D_2\left(\frac{a}{t}\right)^2 + D_3\left(\frac{a}{t}\right)^4$$

$$D_0 = 0.09646\left\{1 + 1.51333\left(\frac{a}{c}\right) - 1.27723\left(\frac{a}{c}\right)^2 + 0.79576\left(\frac{a}{c}\right)^3 - \exp\left[-27.55715\left(\frac{a}{c}\right)\right]\right\}$$

$$D_1 = -0.66304\left(\frac{a}{c}\right)\left\{1 - \exp\left[-11.75502\left(\frac{a}{c}\right)\right]\right\}\left[1 - 2.30088\left(\frac{a}{c}\right) + 0.66328\left(\frac{a}{c}\right)^2 + 0.58371\left(\frac{a}{c}\right)^3\right]$$

$$D_2 = 2.07021\left\{1 - \exp\left[-3.57311\left(\frac{a}{c}\right)\right]\right\}\left[1 - 2.31235\left(\frac{a}{c}\right) + 1.38520\left(\frac{a}{c}\right)^2\right]$$

$$D_3 = \left[0.23183 - 2.02421\left(\frac{a}{c}\right) + 4.64517\left(\frac{a}{c}\right)^2 - 2.861145\left(\frac{a}{c}\right)^3\right]\left\{1 - \exp\left[-52.19501\left(\frac{a}{c}\right)^{0.25}\right]\right\}$$

RANGE OF APPLICATION: $R_0/R_i = 1.5$, $0 = a/t = 1.0$, $a/c = 0$ and $0.2 = a/c = 1.0$
ACCURACY: Better than 3% when compared to the FEM data.
REFERENCES:

- weight function:
Kiciak A., Glinka G., Burns D. J., 1996, University of Waterloo, to be published.

- reference data:
Mettu S. R., Raju I. S., Forman R. G., 1988, "Stress Intensity Factors for Part-Through Surface Cracks in Hollow Cylinders," NASA Technical Report, No. JSC 25685 LESC 30124.

Andrasic C. P., Parker A. P., 1984, "Dimensionless Stress Intensity Factors for Cracked Thick Cylinder Under Polynomial Crack Face Loading," *Engng. Fract. Mech.*, Vol. 19, 1984, pp. 187-193.

Murakami Y., et al., 1986, *Stress Intensity Factor Handbook*, Vol. 2, Pergamon Press, pp. 309-317.

External Axial Semielliptical Surface Crack in a Thick Cylinder (R_o/R_i=1.25)

WEIGHT FUNCTION (Figure 40) - Deepest Point A:

$$m_A(x,a) = \frac{2}{\sqrt{2\pi(a-x)}}\left[1 + M_{1A}\left(1-\frac{x}{a}\right)^{\frac{1}{2}} + M_{2A}\left(1-\frac{x}{a}\right)^1 + M_{3A}\left(1-\frac{x}{a}\right)^{\frac{3}{2}}\right]$$

PARAMETERS:

$$M_{1A} = \frac{2\pi}{\sqrt{2Q}}\left(-Y_0 + 3Y_1\right) - \frac{24}{5}$$

$$M_{2A} = 3$$

$$M_{3A} = \frac{6\pi}{\sqrt{2Q}}\left(Y_0 - 2Y_1\right) + \frac{8}{5}$$

where:

$$Q = 1 + 1.464\left(\frac{a}{c}\right)^{1.65} \quad \text{and} \quad t = R_o - R_i$$

$$Y_0 = A_0 + A_1\left(\frac{a}{t}\right) + A_2\left(\frac{a}{t}\right)^2 + A_3\left(\frac{a}{t}\right)^4$$

$$A_0 = 0.94235 + \exp\left[-1.68499 - 8.56013\left(\frac{a}{c}\right) + 23.08395\left(\frac{a}{c}\right)^2 - 26.59266\left(\frac{a}{c}\right)^3 + 10.62456\left(\frac{a}{c}\right)^4\right]$$

$$A_1 = -0.38656 + \exp\left[-0.82502 + 4.66494\left(\frac{a}{c}\right) - 12.06481\left(\frac{a}{c}\right)^2 + 11.96283\left(\frac{a}{c}\right)^3 - 4.23850\left(\frac{a}{c}\right)^4\right]$$

$$A_2 = -0.57088 + \exp\left[1.58221 - 3.16636\left(\frac{a}{c}\right) - 4.515307\left(\frac{a}{c}\right)^2 + 11.48057\left(\frac{a}{c}\right)^3 - 5.95069\left(\frac{a}{c}\right)^4\right]$$

$$A_3 = 0.19498 - \exp\left[\begin{array}{l} -15.94324 + 112.58315\left(\frac{a}{c}\right) - 340.20961\left(\frac{a}{c}\right)^2 + 497.99358\left(\frac{a}{c}\right)^3 \\ -354.74017\left(\frac{a}{c}\right)^4 + 98.71664\left(\frac{a}{c}\right)^5 \end{array}\right]$$

and

$$Y_1 = B_0 + B_1\left(\frac{a}{t}\right) + B_2\left(\frac{a}{t}\right)^2 + B_3\left(\frac{a}{t}\right)^3 + B_4\left(\frac{a}{t}\right)^4$$

$$B_0 = 050249 + \exp\left[\begin{array}{l} -1.71519 - 2.14909\left(\dfrac{a}{c}\right) + 7.58393\left(\dfrac{a}{c}\right)^2 - 10.00652\left(\dfrac{a}{c}\right)^3 \\[2ex] + 4.71914\left(\dfrac{a}{c}\right)^4 \end{array}\right]$$

$$B_1 = 1.53122 - \exp\left[\begin{array}{l} 0.31448 + 0.59120\left(\dfrac{a}{c}\right) - 2.21570\left(\dfrac{a}{c}\right)^2 + 3.08396\left(\dfrac{a}{c}\right)^3 \\[2ex] -1.37007\left(\dfrac{a}{c}\right)^4 \end{array}\right]$$

$$B_2 = 0.04652 + \exp\left[0.04497 - 3.84029\left(\dfrac{a}{c}\right) - 1.32259\left(\dfrac{a}{c}\right)^2\right]$$

$$B_3 = 0.02569 + \exp\left[\begin{array}{l} -0.55548 + 0.88270\left(\dfrac{a}{c}\right) - 13.45912\left(\dfrac{a}{c}\right)^2 - 2.45236\left(\dfrac{a}{c}\right)^3 \\[2ex] + 8.50684\left(\dfrac{a}{c}\right)^4 \end{array}\right]$$

$$B_4 = -0.01828 - \exp\left[\begin{array}{l} -2.10419 + 7.85207\left(\dfrac{a}{c}\right) - 33.70843\left(\dfrac{a}{c}\right)^2 + 25.85419\left(\dfrac{a}{c}\right)^3 \\[2ex] -4.64059\left(\dfrac{a}{c}\right)^4 \end{array}\right]$$

WEIGHT FUNCTION (Figure 40) - Surface Point B:

$$m_B(x,a) = \frac{2}{\sqrt{\pi x}}\left[1 + M_{1B}\left(\frac{x}{a}\right)^{\frac{1}{2}} + M_{2B}\left(\frac{x}{a}\right)^1 + M_{3B}\left(\frac{x}{a}\right)^{\frac{3}{2}}\right]$$

PARAMETERS:

$$M_{1B} = \frac{3\pi}{\sqrt{Q}}\left(2F_0 - 5F_1\right) - 8$$

$$M_{2B} = \frac{15\pi}{\sqrt{Q}}\left(3F_1 - F_0\right) + 15$$

$$M_{3B} = \frac{3\pi}{\sqrt{Q}}\left(3F_0 - 10F_1\right) - 8$$

where:

$$Q = 1 + 1.464\left(\frac{a}{c}\right)^{1.65} \qquad \text{and} \qquad t = R_o - R_i$$

$$F_0 = C_0 + C_1\left(\frac{a}{t}\right) + C_2\left(\frac{a}{t}\right)^2 + C_3\left(\frac{a}{t}\right)^4$$

$$C_0 = 0.47251\left\{1 + 1.58454\left(\frac{a}{c}\right) - 0.19842\left(\frac{a}{c}\right)^2 - \exp\left[-14.02505\left(\frac{a}{c}\right)\right]\right\}$$

$$C_1 = -0.22958\left\{1 - 2.79131\left(\frac{a}{c}\right) + 1.47068\left(\frac{a}{c}\right)^2 - \exp\left[-14.11736\left(\frac{a}{c}\right)\right]\right\}$$

$$C_2 = 1.80687\left\{1 - 1.27898\left(\frac{a}{c}\right) + 0.55332\left(\frac{a}{c}\right)^2 - \exp\left[-11.39742\left(\frac{a}{c}\right) + 34.86421\left(\frac{a}{c}\right)^2 - 78.88988\left(\frac{a}{c}\right)^3\right]\right\}$$

$$C_3 = 0.24024\left\{1 - 2.08060\left(\frac{a}{c}\right) + 1.01701\left(\frac{a}{c}\right)^2 - \exp\left[-3.18934\left(\frac{a}{c}\right) - 3.79275\left(\frac{a}{c}\right)^2\right]\right\}$$

and

128

$$F_1 = D_0 + D_1\left(\frac{a}{t}\right) + D_2\left(\frac{a}{t}\right)^2 + D_3\left(\frac{a}{t}\right)^4$$

$$D_0 = 0.12603\left\{1 + 0.54116\left(\frac{a}{c}\right) - \exp\left[-3.19737\left(\frac{a}{c}\right)\right]\right\}$$

$$D_1 = -0.15562\left\{\left[1 - 2.30358\left(\frac{a}{c}\right) + 1.03870\left(\frac{a}{c}\right)^2 - \exp\left[-5.24795\left(\frac{a}{c}\right) + 2.35842\left(\frac{a}{c}\right)^2\right]\right]\right\}$$

$$D_2 = 2.17158\left\{1 - \exp\left[-1.21697\left(\frac{a}{c}\right)\right]\right\}\left[1 - 1.89058\left(\frac{a}{c}\right) + 0.96829\left(\frac{a}{c}\right)^2\right]$$

$$D_3 = \left(\frac{a}{c}\right)\left[\begin{array}{l}1.08880 - 12.47981\left(\frac{a}{c}\right) + 46.80652\left(\frac{a}{c}\right)^2 - 77.95158\left(\frac{a}{c}\right)^3 \\ + 60.62440\left(\frac{a}{c}\right)^4 - 18.09600\left(\frac{a}{c}\right)^5\end{array}\right]$$

RANGE OF APPLICATION: $R_0/R_i = 1.25$, $0 = a/t = 1.0$, $a/c = 0$ and $0.2 = a/c = 1.0$
ACCURACY: Better than 3% when compared to the FEM data.
REFERENCES:

- weight function:
Kiciak A., Glinka G., Burns D. J., 1996, University of Waterloo, to be published.

- reference data:
Mettu S. R., Raju I. S., Forman R. G., 1988, "Stress Intensity Factors for Part-Through Surface Cracks in Hollow Cylinders," NASA Technical Report, No. JSC 25685 LESC 30124.

Andrasic C. P., Parker A. P., 1984, "Dimensionless Stress Intensity Factors for Cracked Thick Cylinder Under Polynomial Crack Face Loading," *Engng. Fract. Mech.*, Vol. 19, 1984, pp. 187-193.

Murakami Y., et al., 1986, *Stress Intensity Factor Handbook*, Vol. 2, Pergamon Press, pp. 309-317.

External Axial Semielliptical Surface Crack in a Thick Cylinder (R_o/R_i=1.1)

WEIGHT FUNCTION (Figure 40) - Deepest Point A:

$$m_A(x,a) = \frac{2}{\sqrt{2\pi(a-x)}}\left[1 + M_{1A}\left(1-\frac{x}{a}\right)^{\frac{1}{2}} + M_{2A}\left(1-\frac{x}{a}\right)^{1} + M_{3A}\left(1-\frac{x}{a}\right)^{\frac{3}{2}}\right]$$

PARAMETERS:

$$M_{1A} = \frac{2\pi}{\sqrt{2Q}}(2Y_0 - 3Y_1) - \frac{24}{5}$$

$$M_{2A} = 3$$

$$M_{3A} = \frac{6\pi}{\sqrt{2Q}}(2Y_1 - Y_0) + \frac{8}{5}$$

where:

$$Q = 1 + 1.464\left(\frac{a}{c}\right)^{1.65} \quad \text{and} \quad t = R_o - R_i$$

$$Y_0 = A_0 + A_1\left(\frac{a}{t}\right)^2 + A_2\left(\frac{a}{t}\right)^4$$

$$A_0 = 1.1492 - 0.4322\left(\frac{a}{c}\right) + 0.2984\left(\frac{a}{c}\right)^2$$

$$A_1 = 4.00 - 8.98\left(\frac{a}{c}\right) + 5.29\left(\frac{a}{c}\right)^2$$

$$A_2 = -7.44 + 14.559\left(\frac{a}{c}\right) - 8.305\left(\frac{a}{c}\right)^2 + \frac{1}{0.066 + \left(\frac{a}{c}\right)^{1.094}}$$

and

$$Y_1 = B_0 + B_1\left(\frac{a}{t}\right)^2 + B_2\left(\frac{a}{t}\right)^4$$

$$B_0 = 0.4840 - 0.5211\left(\frac{a}{c}\right) + 0.788\left(\frac{a}{c}\right)^2 - 0.453\left(\frac{a}{c}\right)^3$$

$$B_1 = 2.4478 - 5.0937\left(\frac{a}{c}\right) + 2.850\left(\frac{a}{c}\right)^2$$

$$B_2 = -5.69 + 9.653\left(\frac{a}{c}\right) - 5.062\left(\frac{a}{c}\right)^2 + \frac{1}{0.097 + \left(\dfrac{a}{c}\right)^{1.006}}$$

WEIGHT FUNCTION (Figure 40) - Surface Point B:

$$m_B(x,a) = \frac{2}{\sqrt{\pi x}}\left[1 + M_{1B}\left(\frac{x}{a}\right)^{\frac{1}{2}} + M_{2B}\left(\frac{x}{a}\right)^1 + M_{3B}\left(\frac{x}{a}\right)^{\frac{3}{2}}\right]$$

PARAMETERS:

$$M_{1B} = \frac{3\pi}{\sqrt{Q}}(5F_1 - 3F_0) - 8$$

$$M_{2B} = \frac{15\pi}{\sqrt{Q}}(2F_0 - 3F_1) + 15$$

$$M_{3B} = \frac{3\pi}{\sqrt{Q}}(10F_1 - 7F_0) - 8$$

where:

$$Q = 1 + 1.464 \left(\frac{a}{c} \right)^{1.65} \quad \text{and} \quad t = R_o - R_i$$

$$F_0 = \left[C_0 + C_1 \left(\frac{a}{t} \right)^2 + C_2 \left(\frac{a}{t} \right)^4 \right] \sqrt{\frac{a}{c}}$$

$$C_0 = 1.2964 - 0.2532 \left(\frac{a}{c} \right) + 0.0895 \left(\frac{a}{c} \right)^2$$

$$C_1 = -0.1110 + 25.953 \left(\frac{a}{c} \right) - 115.107 \left(\frac{a}{c} \right)^2 + 210.832 \left(\frac{a}{c} \right)^3 - 177.848 \left(\frac{a}{c} \right)^4 + 56.8339 \left(\frac{a}{c} \right)^5$$

$$C_2 = 1.405 - 3.746 \left(\frac{a}{c} \right) + 2.262 \left(\frac{a}{c} \right)^2$$

and

$$F_1 = \left[D_0 + D_1 \left(\frac{a}{t} \right)^2 + D_2 \left(\frac{a}{t} \right)^4 \right] \sqrt{\frac{a}{c}}$$

$$D_0 = 1.2531 - 0.7814 \left(\frac{a}{c} \right) + 0.4668 \left(\frac{a}{c} \right)^2$$

$$D_1 = 0.2128 + 14.4065 \left(\frac{a}{c} \right) - 67.574 \left(\frac{a}{c} \right)^2 + 129.93 \left(\frac{a}{c} \right)^3 - 115.252 \left(\frac{a}{c} \right)^4 + 38.6732 \left(\frac{a}{c} \right)^5$$

$$D_2 = 0.7704 - 1.3817 \left(\frac{a}{c} \right) + 0.58529 \left(\frac{a}{c} \right)^2$$

RANGE OF APPLICATION: $R_0/R_i = 1.1$, $0 = a/t = 1.0$, and $0 = a/c = 1.0$
ACCURACY: Better than 5% when compared to the FEM data.
REFERENCES:

- weight function:
Wang X. J., Lambert S. B., 1996, "Stress Intensity Factors and Weight Functions for Longitudinal Semielliptical Surface Cracks in Thin Pipes," *Int. J.Pres.Ves. & Piping*, Vol. 65, pp 75-87.

- reference data:
Raju I. S., Newman J. C., 1982, "Stress Intensity Factors for Internal and External Surface Cracks in Cylindrical Vessels," *J. Press. Ves. Technol.*, Vol. 104, pp. 293-298.

Andrasic C. P.. Parker A. P., 1984, "Dimensionless Stress Intensity Factors for Cracked Thick Cylinder Under Polynomial Crack Face Loading," *Engng. Fract. Mech.*, Vol. 19, 1984, pp. 187-193.